Thermodynamic Model for High Temperature Corrosion Applications: The (NaCl + Na2CO3 + Na2SO4 + Na2S2O7 + Na2CrO4 + Na2Cr2O7 + Na2MoO4 + Na2Mo2O7 + Na2O + KCl + K2CO3 + K2SO4 + K2S2O7 + K2CrO4 + K2Cr2O7 + K2MoO4 + K2Mo2O7 + K2O) System

Benalia, Sara; Tesfaye, Fiseha; Lindberg, Daniel; Hupa, Leena; Chartrand, Patrice; Robelin, Christian

Published in:
Industrial & Engineering Chemistry Research

DOI:
10.1021/acs.iecr.3c02295

E-pub ahead of print: 04/12/2023

Document Version
Accepted author manuscript

Document License
CC BY-NC-ND

A Thermodynamic Model for High Temperature Corrosion Applications : The ($NaCl + Na_2CO_3 + Na_2SO_4 + Na_2S_2O_7 + Na_2CrO_4 + Na_2Cr_2O_7 + Na_2MoO_4 + Na_2Mo_2O_7 + Na_2O + KCl + K_2CO_3 + K_2SO_4 + K_2S_2O_7 + K_2CrO_4 + K_2Cr_2O_7 + K_2MoO_4 + K_2Mo_2O_7 + K_2O$) System

Sara Benalia[a,b], Fiseha Tesfaye[b,c], Daniel Lindberg[d], Leena Hupa[b], Patrice Chartrand[a], Christian Robelin[a,*]

[a] Centre for Research in Computational Thermochemistry (CRCT), Department of Chemical Engineering, Polytechnique Montréal, Box 6079, Station Downtown, Montréal (Quebec), Canada, H3C 3A7

[b] Johan Gadolin Process Chemistry Centre, Laboratory of Molecular Science and Engineering, Åbo Akademi University, Henrikinkatu 2, FI-20500 Turku, Finland

[c] Metso Outotec Metals Oy, Rauhalanpuisto 9, PO Box 1000, FI-02231 Espoo, Finland

[d] Aalto University, School of Chemical Engineering, Department of Chemical and Metallurgical Engineering, FI-00076 Aalto, Finland

Abstract

A thermodynamic model has been developed for the condensed phases of the salt system ($NaCl + Na_2CO_3 + Na_2SO_4 + Na_2S_2O_7 + Na_2CrO_4 + Na_2Cr_2O_7 + Na_2MoO_4 + Na_2Mo_2O_7 + Na_2O + KCl + K_2CO_3 + K_2SO_4 + K_2S_2O_7 + K_2CrO_4 + K_2Cr_2O_7 + K_2MoO_4 + K_2Mo_2O_7 + K_2O$) (diluted in free oxides), which is most often involved in combustion processes for energy production. This model is relevant in particular for the solid deposits formed

in steel and stainless steel installations containing Ni, Cr, Mo, W, and V as alloying elements, and permits the accurate prediction of thermodynamic properties and phase equilibria in the multicomponent system. The ($NaCl + Na_2CO_3 + Na_2SO_4 + Na_2S_2O_7 + Na_2CrO_4 + Na_2Cr_2O_7 + Na_2O + KCl + K_2CO_3 + K_2SO_4 + K_2S_2O_7 + K_2CrO_4 + K_2Cr_2O_7 + K_2O$) sub-system was critically evaluated in previous papers. In the present work, Na_2MoO_4, K_2MoO_4, $Na_2Mo_2O_7$, and $K_2Mo_2O_7$ have been added to the previously developed thermodynamic model. The available phase diagram and thermodynamic data have been critically evaluated, and model parameters have been obtained. The Modified Quasichemical Model in the Quadruplet Approximation was used for both the liquid solution and the high-temperature hexagonal solid solution ($Na_2CO_3 + Na_2SO_4 + Na_2CrO_4 + Na_2MoO_4 + K_2CO_3 + K_2SO_4 + K_2CrO_4 + [K_2MoO_4]$), whereas the Compound Energy Formalism (CEF) was used for all other solid solutions.

Due to the lack of data, several common-ion binary sub-systems have been investigated in this work at different compositions by DSC-TGA. In addition, the non-stoichiometric molybdenum-glaserite phase has been studied at the composition (35 mol% Na_2MoO_4 + 65 mol% K_2MoO_4) using SEM-EDS and DSC-TGA, after annealing at 400°C for four weeks.

Keywords: Thermodynamic modeling; Phase diagrams; Alkali molybdates; Alkali dimolybdates; DSC-TGA

*Corresponding author (E-mail address: christian.robelin@polymtl.ca)

1. Introduction

Hot corrosion in steels and stainless steels consisting of the alloying elements Ni, Cr, Mo, W, and V refers to accelerated oxidation occurring at high temperatures (from 600 to 950°C) [1-3] in the presence of combustion gases (N_2, CO_2, CO, O_2, H_2O, etc.) containing contaminants (SO_2, Cl_2, S_2, HCl, etc.), and corrosive products (Na_2O, K_2O, NaOH, KOH, NaCl, KCl, etc.). [4, 5] Typical corrosion temperatures for some combustion processes, such

as black liquor combustion, are of the order of 500°C. The threshold for these temperatures depends on the lowest melting temperature of the ashes produced.

Hot corrosion is an accelerated attack associated with corrosive deposits accumulating on the plant walls, specifically NaCl, KCl, Na_2CO_3, K_2CO_3, Na_2SO_4, K_2SO_4,[1, 4, 6-8] Na_2CrO_4 and K_2CrO_4 [4, 9, 10] salts. Further salts are known to promote corrosion, such as Na_2MoO_4 and K_2MoO_4 [4, 10, 11] in the solid or liquid form and can dissolve into the previously mentioned salts.

According to Misra's investigation, [12] MoO_3 flux created at the interface between the metal and the scale initiates catastrophic corrosion in molybdenum-containing superalloys. [12] The transformation of Na_2SO_4 into Na_2CrO_4 can occur long before the onset of catastrophic corrosion, which is accompanied by the conversion of Na_2CrO_4 to Na_2MoO_4. A mixture of Na_2MoO_4 and MoO_3 has been attributed to this kind of catastrophic corrosion. [12]

Peters et al. [13] previously reported the oxidation of Na_2SO_4/Na_2MoO_4-coated samples, for which a Na_2SO_4-coated (Ni-15% Cr) alloy exhibited a severe corrosion behavior in the same reaction chamber as the Ni-15Cr-Mo alloys. That is, MoO_3 was dissolving in the salt layer and was then carried into the vapor phase according to the reaction $Na_2SO_4 + MoO_3 = Na_2MoO_4 + SO_3$.

An accurate thermodynamic model is available for the condensed phases of the ($NaCl + Na_2CO_3 + Na_2SO_4 + Na_2S_2O_7 + Na_2CrO_4 + Na_2Cr_2O_7 + Na_2O + KCl + K_2CO_3 + K_2SO_4 + K_2S_2O_7 + K_2CrO_4 + K_2Cr_2O_7 + K_2O$) system (diluted in free oxides). The chromium-free version was originally developed by Lindberg et al. [14, 15] and then extended in our previous study. [16] The present paper describes the addition of molybdates (Na_2MoO_4 and K_2MoO_4) and dimolybdates ($Na_2Mo_2O_7$ and $K_2Mo_2O_7$) to our existing model. In our previous works, [4, 17] an assessment of the thermodynamic properties (standard enthalpy of formation $\Delta H^{\circ}_{298.15\,K}$ from the elements in their stable standard state at 298.15K and 1 atm, absolute (third law) entropy $S^{\circ}_{298.15\,K}$ referenced at 298.15K and 1 atm, and heat capacity C_P as a function of temperature) was performed for Na_2MoO_4, K_2MoO_4, $Na_2Mo_2O_7$ and $K_2Mo_2O_7$. Also, extensive information on the crystal structures of all allotropes of these four compounds was obtained from the literature, making it easier to identify possible solid solutions forming with other considered salts.

In the liquid solution of the ($NaCl + Na_2CO_3 + Na_2SO_4 + Na_2S_2O_7 + Na_2CrO_4 + Na_2Cr_2O_7$

+ Na_2MoO_4 + $Na_2Mo_2O_7$ + Na_2O + KCl + K_2CO_3 + K_2SO_4 + $K_2S_2O_7$ + K_2CrO_4 + $K_2Cr_2O_7$ + K_2MoO_4 + $K_2Mo_2O_7$ + K_2O) system described in the present article, free oxides are present in dilute amounts since reactions of the type $2\ A_2MO_4 = A_2M_2O_7 + A_2O$ (where A = Na, K and M = Cr, Mo) are very limited up to above the liquidus temperatures. [17]

The developed thermodynamic model has been calibrated using the CALPHAD approach (CALculation of PHAse Diagrams), based on the available thermodynamic and phase equilibrium data from the literature, and also on our differential scanning calorimetry (DSC)-thermogravimetric analysis (TGA) measurements at several compositions in the following common-ion binary sub-systems : (Na_2CO_3 + Na_2MoO_4), (Na_2SO_4 + Na_2MoO_4), (K_2SO_4 + K_2MoO_4), (Na_2CrO_4 + Na_2MoO_4), (K_2CrO_4 + K_2MoO_4), and (Na_2MoO_4 + K_2MoO_4).

Phase diagram data were very limited for Na_2MoO_4- and K_2MoO_4-containing common-cation ternary sub-systems, reciprocal ternary sub-systems (that is, systems with Na, K, and two anions), and higher order sub-systems. As will be discussed later, such data were only available for the (Na_2SO_4 + Na_2CrO_4 + Na_2MoO_4) and Na, K // Cl, MoO_4 sub-systems. The liquid solution exhibits small deviations from ideality. Hence, predictions in the entire multicomponent system (NaCl + Na_2CO_3 + Na_2SO_4 + $Na_2S_2O_7$ + Na_2CrO_4 + $Na_2Cr_2O_7$ + Na_2MoO_4 + $Na_2Mo_2O_7$ + Na_2O + KCl + K_2CO_3 + K_2SO_4 + $K_2S_2O_7$ + K_2CrO_4 + $K_2Cr_2O_7$ + K_2MoO_4 + $K_2Mo_2O_7$ + K_2O) (diluted in free oxides) are expected to be reasonably accurate. All calculations and optimizations have been conducted using the FactSage thermochemical software. [18]

2. Thermodynamic data, crystal structures and space groups for the pure compounds

Thermodynamic data ($\Delta H^{\circ}_{298.15\ K}$, $S^{\circ}_{298.15\ K}$, and C_P) for the condensed pure compounds of the (NaCl + Na_2CO_3 + Na_2SO_4 + $Na_2S_2O_7$ + Na_2CrO_4 + $Na_2Cr_2O_7$ + Na_2MoO_4 + $Na_2Mo_2O_7$ + Na_2O + KCl + K_2CO_3 + K_2SO_4 + $K_2S_2O_7$ + K_2CrO_4 + $K_2Cr_2O_7$ +

$K_2MoO_4 + K_2Mo_2O_7 + K_2O$) system were previously selected in references [4, 14, 17, 19, 20] and were directly used in the present study. The thermodynamic data for NaCl and KCl have been evaluated by Chartrand and Pelton. [19] Assessments of the thermodynamic properties of Na_2CO_3, Na_2SO_4, K_2CO_3, K_2SO_4, $Na_2S_2O_7$ and $K_2S_2O_7$ have been conducted by Lindberg et al. [14, 20] The thermodynamic data for Na_2CrO_4, K_2CrO_4, $Na_2Cr_2O_7$, $K_2Cr_2O_7$, Na_2MoO_4, K_2MoO_4, $Na_2Mo_2O_7$, and $K_2Mo_2O_7$ were taken directly from our previous works. [4, 17] Finally, the thermodynamic properties of Na_2O and K_2O were taken directly from the FToxid database in FactSage. [18] For every solid compound, the most probable crystal structure and space group were discussed previously based on the available information from the literature.

A summary of the crystal structures and space groups of all relevant pure salt compounds is displayed in Table 1. Note that new information taken from [4, 17] is presented only for Na_2MoO_4, $Na_2Mo_2O_7$, K_2MoO_4, and $K_2Mo_2O_7$. For all other solid compounds, the corresponding information was given previously, [16] and is repeated here for the sake of clarity.

The thermodynamic data for the condensed pure compounds optimized in the present study are given in Table 2.

Table 1: Crystal structures and space groups of all relevant pure salt compounds

Pure compound	Allotrope	Crystal structure	Space group	Pearson Symbol / Phase Prototype	Reference
NaCl	NaCl	Cubic	$Fm\bar{3}m$ (225)	cF8 / NaCl	FactSage (FTsalt database) [18]

KCl	KCl	Cubic	$Fm\bar{3}m$ (225)	cF8 / NaCl	FactSage (FTsalt database) [18, 21]
Na_2CO_3	$Na_2CO_3(S_1)$	Monoclinic	C2/m (12)	mS24 / γ-Na_2CO_3-a	
	$Na_2CO_3(S_2)$	Monoclinic	C2/m (12)	mS24 / β-Na_2CO_3-b	
	$Na_2CO_3(S_3)$	Hexagonal	$P6_3/mmc$ (194)	hP22 / K_2SO_4	
K_2CO_3	$K_2CO_3(S_1)$	Monoclinic	$P2_1/c$ (14)	mP24 / K_2CO_3	FactSage (FTsalt database) [18]
	$K_2CO_3(S_2)$	Hexagonal	$P6_3/mmc$ (194)	hP22 / K_2SO_4	
Na_2SO_4	$Na_2SO_4(S_3)$	Orthorhombic	Fddd (70)	oF56 / Na_2SO_4	FactSage (FTsalt database) [18, 14]
	$Na_2SO_4(S_1)$	Orthorhombic	Cmcm (63)	oS28 / Na_2CrO_4	
	$Na_2SO_4(S_2)$	Hexagonal	$P6_3/mmc$ (194)	hP22 / K_2SO_4	
$Na_2S_2O_7$	$Na_2S_2O_7$	Triclinic	$P\bar{1}$ (2)	aP22 / $Cd_2P_2O_7$	FactSage (FTsalt database) [18, 22, 23]
K_2SO_4	$K_2SO_4(S_1)$	Orthorhombic	Pnma (62)	oP28 / K_2SO_4	FactSage (FTsalt database) [18, 14]
	$K_2SO_4(S_2)$	Hexagonal	$P6_3/mmc$ (194)	hP22 / K_2SO_4	
$K_2S_2O_7$	$K_2S_2O_7(S_1)$	Monoclinic	C2/c (15)	mS44 / $K_2S_2O_7$	FactSage (FTsalt database) [18, 22]
	$K_2S_2O_7(S_2)$	-	-	-	
Na_2CrO_4	$Na_2CrO_4(S_1)$	Orthorhombic	Cmcm (63)	oS28 / Na_2CrO_4	[4, 24]
	$Na_2CrO_4(S_2)$	Hexagonal	$P6_3/mmc$ (194)	*	
$Na_2Cr_2O_7$	$Na_2Cr_2O_7(S_1)$	Triclinic	$P\bar{1}$ (2)	aP44 / $Na_2Cr_2O_7$	[17, 25, 26]
	$Na_2Cr_2O_7(S_2)$	Triclinic	$A\bar{1}$ (2)	aP22 / $Cd_2P_2O_7$	
K_2CrO_4	$K_2CrO_4(S_1)$	Orthorhombic	Pnma (62)	oP28 / K_2SO_4	[4, 27]
	$K_2CrO_4(S_2)$	Hexagonal	$P6_3/mmc$ (194)	*	
$K_2Cr_2O_7$	$K_2Cr_2O_7(S_1)$	Triclinic	$P\bar{1}$ (2)	aP44 / $K_2Cr_2O_7$	[17, 22, 28]
	$K_2Cr_2O_7(S_2)$	Monoclinic	$P2_1/c$ (14)	-	
Na_2MoO_4	$Na_2MoO_4(S_1)$	Cubic	$Fd\bar{3}m$ (227)	cF56 / $MgAl_2O_4$	[4, 22, 29]
	$Na_2MoO_4(S_2)$	Orthorhombic	$Pbn2_1$ (33)	-	
	$Na_2MoO_4(S_3)$	Orthorhombic	Fddd (70)	**	
	$Na_2MoO_4(S_4)$	Hexagonal	$P6_3/mmc$ (194)	*	
$Na_2Mo_2O_7$	$Na_2Mo_2O_{7(S1)}$	Orthorhombic	Cmca D_{2h}^{18} (64)	oS88 / $Na_2W_2O_7$	[17, 30]
	$Na_2Mo_2O_{7(S2)}$	Monoclinic	-	-	
K_2MoO_4	$K_2MoO_{4(S1)}$	Monoclinic	C2/m (12)	mS28 / K_2MoO_4	[4, 22, 31]
	$K_2MoO_{4(S2)}$	Orthorhombic	Cmcm (63)	***	

	$K_2MoO_{4(S3)}$	Trigonal	$P\bar{3}m1$ (164)	-	
$K_2Mo_2O_7$	$K_2Mo_2O_{7(S1)}$	Triclinic	$P\bar{1}$ (2)	aP22 / $K_2Mo_2O_7$	[17, 22, 32]
	$K_2Mo_2O_{7(S2)}$	Monoclinic (assumption)	$P2_1/c$ or $C_{2h}^5 - P2_1/n$ (assumption) (14)	-	

[*] The corresponding Pearson symbols / prototypes for $Na_2CrO_4(S_2)$, $K_2CrO_4(S_2)$ and $Na_2MoO_4(S_4)$ are not available to our knowledge. Thus, since these three compounds have the same crystal structure and space group as $Na_2CO_3(S_3)$, $Na_2SO_4(S_2)$, $K_2CO_3(S_2)$, and $K_2SO_4(S_2)$, they were assumed to have the same Pearson symbol / prototype phase (that is, hP22 / K_2SO_4).

[**] The corresponding Pearson symbol / prototype for $Na_2MoO_4(S_3)$ is not available to our knowledge. Thus, since this compound has the same crystal structure and space group as $Na_2SO_4(S_3)$, it was assumed to have the same Pearson symbol / prototype phase (that is, oF56 / Na_2SO_4).

[***] The corresponding Pearson symbol / prototype for $K_2MoO_4(S_2)$ is not available to our knowledge. Thus, since this compound has the same crystal structure and space group as $Na_2CrO_4(S_1)$ and $Na_2SO_4(S_1)$, it was assumed to have the same Pearson symbol / prototype phase (that is, oS28 / Na_2CrO_4).

Table 2 : Thermodynamic properties of solid compounds optimized in the present study

Compound	***T* Range (K)**	$\Delta H^{\circ}_{298.15\,K}$ **(J/mol)** [a]	$S^{\circ}_{298.15\,K}$ **(J/mol.K)** [b]	C_P **(J/mol.K)**
Na_3ClMoO_4	298.15 to 950	-1,872,914.8	248.5426	171.284592 + 0.09489312 *T*/K
$K_3Na(MoO_4)_2$ (below 513K)	298.15 to 564	-2,976,566.0	389.6457	232.914912 + 0.184602264 *T*/K + 1,094,534.4 $(T/K)^{-2}$

[a] Enthalpy relative to the enthalpy of the elements in their stable standard states at 298.15 K.

[b] Absolute (third law) entropy.

3. Thermodynamic model for the liquid phase

The liquid phase of the (NaCl + Na_2CO_3 + Na_2SO_4 + $Na_2S_2O_7$ + Na_2CrO_4 + $Na_2Cr_2O_7$ + Na_2MoO_4 + $Na_2Mo_2O_7$ + Na_2O + KCl + K_2CO_3 + K_2SO_4 + $K_2S_2O_7$ + K_2CrO_4 + $K_2Cr_2O_7$ + K_2MoO_4 + $K_2Mo_2O_7$ + K_2O) system (diluted in free oxides) was modeled using the

Modified Quasichemical Model in the Quadruplet Approximation (MQMQA). [33] The cations (Na^+ and K^+ in this work) and the anions (Cl^-, CO_3^{2-}, SO_4^{2-}, $S_2O_7^{2-}$, CrO_4^{2-}, $Cr_2O_7^{2-}$, MoO_4^{2-}, $Mo_2O_7^{2-}$ and O^{2-} in this work) are distributed over a cationic and anionic sublattice, respectively. The MQMQA takes into account coupled 1st- and 2nd-nearest-neighbour short-range order (*i.e.* between sublattices and within a sublattice respectively). A quadruplet such as $Na_2(MoO_4)_2$, $NaK(MoO_4)_2$, $Na_2(CO_3)(MoO_4)$ or $NaK(CO_3)(MoO_4)$ consists of two 2nd-nearest-neighbour cations and two 2nd-nearest-neighbour anions, which are mutual 1st-nearest-neighbours. Quadruplets all have a Gibbs energy and are assumed to mix randomly, constrained by an elemental mass balance. The equilibrium quadruplet composition (configuration) is obtained by minimizing the Gibbs energy of the liquid solution at a given temperature, pressure and composition, and the equilibrium configuration reflects 1st- and 2nd-nearest-neighbour short-range order among ions.

The model is described in detail in reference [33] and its main features were given in our previous work. [16] A brief summary is provided below.

Second-nearest-neighbour (cation-cation) short-range ordering is described in terms of the following equilibrium :

$$[\text{A-X-A}]_{\text{pair}} + [\text{B-X-B}]_{\text{pair}} = 2\,[\text{A-X-B}]_{\text{pair}}; \quad \Delta g_{AB/X_2} \quad (1)$$

where A and B are two different cations (Na^+ and K^+ in this work), and X is an anion. The Gibbs energy change $\Delta g_{AB/X_2}$ is a model parameter that can be expressed as a function of composition by an empirical polynomial expression (see equation [11] in reference [33]). As $\Delta g_{AB/X_2}$ becomes progressively more negative, reaction (1) is shifted to the right, [A-X-B] pairs predominate and 2nd-nearest-neighbour (cation-cation) short-range ordering results. Random mixing occurs when $\Delta g_{AB/X_2}$ is zero. To a lesser extent, 2nd-nearest-neighbour anion-anion ordering can play a role. Hence, the following pair exchange reactions are also taken into account :

$$[\text{X-A-X}]_{\text{pair}} + [\text{Y-A-Y}]_{\text{pair}} = 2\,[\text{X-A-Y}]_{\text{pair}}; \quad \Delta g_{A_2/XY} \quad (2)$$

where A is a cation (Na^+ or K^+ in this work), and X and Y are two different anions.

In the case of reciprocal salt solutions (that is, solutions with two or more cations, and two or more anions), first-nearest-neighbour (cation-anion) short-range ordering can occur. Its

extent is related to the Gibbs energy change for the following exchange reaction :

$$[\text{A-X}]_{\text{pair}} + [\text{B-Y}]_{\text{pair}} = [\text{A-Y}]_{\text{pair}} + [\text{B-X}]_{\text{pair}}; \quad \Delta g^{\text{exchange}}_{\text{AB/XY}} \qquad (3)$$

where A and B are two different cations (Na^+ and K^+ in this work), and X and Y are two different anions. $\Delta g^{\text{exchange}}_{\text{AB/XY}}$ only depends on the Gibbs energies of the four pure liquid salts. If it is negative, then [A-Y] and [B-X] 1st-nearest-neighbour pairs predominate. For instance, $\Delta g^{\text{exchange}}_{\text{NaK/Cl(MoO}_4\text{)}}$ for the exchange reaction NaCl(l) + 0.5 K_2MoO_4(l) ↔ KCl(l) + 0.5 Na_2MoO_4(l) is calculated to be about -4.3 kJ/mol at 1250K (i.e. above the highest melting temperature of the four pure salts).

To obtain quantitative fits, small empirical "ternary reciprocal parameters" may have to be included in the liquid model. These parameters represent the Gibbs energies of formation of the ABXY quadruplets from the binary quadruplets [33] :

$$\frac{1}{2}(\text{ABX}_2 + \text{ABY}_2 + \text{A}_2\text{XY} + \text{B}_2\text{XY}) = 2(\text{ABXY}); \quad \Delta g_{\text{AB/XY}} \quad (4)$$

The model parameter $\Delta g_{\text{AB/XY}}$ is expanded as an empirical polynomial in the mole fractions $x_{\text{A}_2/\text{X}_2}$, $x_{\text{A}_2/\text{Y}_2}$, $x_{\text{B}_2/\text{X}_2}$ and $x_{\text{B}_2/\text{Y}_2}$ of the A_2X_2, A_2Y_2, B_2X_2 and B_2Y_2 unary quadruplets as follows:

$$\Delta g_{\text{AB/XY}} = \Delta g^{\text{o}}_{\text{AB/XY}} + \sum_{i\geq 1}\left[g^{i}_{\text{AB/XY(AX)}} x^{i}_{\text{A}_2/\text{X}_2} + g^{i}_{\text{AB/XY(BX)}} x^{i}_{\text{B}_2/\text{X}_2} + g^{i}_{\text{AB/XY(AY)}} x^{i}_{\text{A}_2/\text{Y}_2} + g^{i}_{\text{AB/XY(BY)}} x^{i}_{\text{B}_2/\text{Y}_2}\right] \quad (5)$$

The empirical parameters $\Delta g^{\text{o}}_{\text{AB/XY}}$ and $g^{i}_{\text{AB/XY(AX)}}$, etc. may be temperature-dependent and can be obtained by optimizing thermodynamic and phase diagram data in the ternary reciprocal system A, B // X, Y. They are all expected to be relatively small.

The 2nd-nearest-neighbour "coordination numbers" are model parameters, and are permitted to change with composition in the liquid solution. [33] Such a flexibility permits to select the compositions of maximum short-range ordering in the A, B // X and A // X, Y common-ion binary systems through the ratios $\left(Z^{\text{B}}_{\text{AB/X}_2}/Z^{\text{A}}_{\text{AB/X}_2}\right)$ and $\left(Z^{\text{Y}}_{\text{A}_2/\text{XY}}/Z^{\text{X}}_{\text{A}_2/\text{XY}}\right)$, where $Z^{i}_{\text{AB/X}_2}$ and $Z^{i}_{\text{A}_2/\text{XY}}$ are the 2nd-nearest-neighbour "coordination numbers" of the ion *i* when all *i* exist in ABX_2 and A_2XY quadruplets, respectively. "Default values" of the 2nd-nearest-neighbour (cation-cation or anion-anion) "coordination numbers" for the ABXY

quadruplets were proposed previously (equation [23] of reference [33]). These "default values" were used for the (Na_2SO_4 + K_2SO_4 + Na_2CrO_4 + K_2CrO_4), (NaCl + KCl + Na_2CrO_4 + K_2CrO_4) and (Na_2CO_3 + K_2CO_3 + Na_2CrO_4 + K_2CrO_4) ternary reciprocal systems modeled in our previous work, [16] and for the (NaCl + KCl + Na_2MoO_4 + K_2MoO_4) ternary reciprocal system modeled in the present study.

It is required to designate all ternary common-cation sub-systems of the (NaCl + Na_2CO_3 + Na_2SO_4 + $Na_2S_2O_7$ + Na_2CrO_4 + $Na_2Cr_2O_7$ + Na_2MoO_4 + $Na_2Mo_2O_7$ + KCl + K_2CO_3 + K_2SO_4 + $K_2S_2O_7$ + K_2CrO_4 + $K_2Cr_2O_7$ + K_2MoO_4 + $K_2Mo_2O_7$) main system as either "symmetric" or "asymmetric". [34] The liquid model consists of the Na^+ and K^+ cations, and of the main anions Cl^-, CO_3^{2-}, SO_4^{2-}, $S_2O_7^{2-}$, CrO_4^{2-}, $Cr_2O_7^{2-}$, MoO_4^{2-}, $Mo_2O_7^{2-}$. All anions are divided into two different chemical groups, based on their valence: group 1 = Cl^-; and group 2 = CO_3^{2-}, SO_4^{2-}, $S_2O_7^{2-}$, CrO_4^{2-}, $Cr_2O_7^{2-}$, MoO_4^{2-}, $Mo_2O_7^{2-}$.

For all ternary common-cation sub-systems containing NaCl or KCl, two anions belong to the same group and Cl^- belongs to another group; a Kohler-Toop-like (asymmetric) interpolation method is then used with Cl^- as the asymmetric component. For all ternary common-cation sub-systems without NaCl or KCl (such as (Na_2SO_4 + Na_2CrO_4 + Na_2MoO_4) modeled in the present work), all three anions belong to the same group; a Kohler-like (symmetric) interpolation method is then used.

Using the available experimental data (such as phase diagram data) for the A, B // X and A // X, Y common-ion binary systems, the model parameters $\Delta g_{AB/X_2}$ (reaction (1)) and $\Delta g_{A_2/XY}$ (reaction (2)) can be optimized through expansion as empirical polynomials in the composition variables χ_{ij} and χ_{ji}. After selecting an interpolation method for each ternary common-ion sub-system, χ_{ij} and χ_{ji} are defined unambiguously. [34] For any ternary common-cation sub-system (AX + AY + AZ) (where A is Na^+ or K^+, and X, Y, Z are three different anions), terms may be included that give the effect of the third component, AZ, on the quadruplet-formation energy $\Delta g_{A_2/XY}$ of the binary A_2XY quadruplet. This is done by introducing the empirical ternary parameter $g^{ijk}_{A/XY(Z)}$, which can be obtained by optimizing thermodynamic and phase diagram data in the common-cation ternary system (AX + AY + AZ). [34]

The Gibbs energy of the solution can be expressed as follows:

$$G = \sum n_{ij/kl}\, g_{ij/kl} - T\,\Delta S^{config} \quad (6)$$

where $n_{ij/kl}$ refers to the number of moles of unary, binary, and reciprocal quadruplets; $g_{ij/kl}$ is the Gibbs energy of the quadruplets, and ΔS^{config} represents the configurational entropy of mixing. A random distribution of all quadruplets over "quadruplet positions" is assumed. However, no exact mathematical expression of ΔS^{config} is available for this distribution, and an approximate expression was thus proposed (equation [39] in reference [33]).

As explained in reference [35], the MQMQA has been improved to address the limitation of the previous model when the Gibbs energy change $\Delta g^{exchange}_{AB/XY}$ of reaction (3) becomes very negative. The expression of the configurational entropy has been refined; slight modifications have been made in the interpolation expression of the Gibbs energy excess parameters in reciprocal systems; and the parameter ζ, related to the ratio between the 2nd-nearest-neighbour and 1st-nearest-neighbour "coordination numbers" for a species *i* (equation [17] in reference [33]), is no longer constant. In the improved version of the MQMQA, the notation $\zeta_{A/X}$ is used, and this parameter is defined as follows:

$$\zeta_{A/X} = 2Z^{A}_{A_2/X_2} Z^{X}_{A_2/X_2} / \left(Z^{A}_{A_2/X_2} + Z^{X}_{A_2/X_2}\right) \quad (7)$$

where $Z^{i}_{A_2/X_2}$ is the 2nd-nearest-neighbour "coordination number" of the ion *i* (*i* = A, X) when all *i* exist in A_2X_2 quadruplets.

Tables 3 and 4 list, respectively, the values of the 2nd-nearest-neighbour "coordination numbers" and of the newly optimized model parameters for the liquid phase of the Na^+, K^+ // Cl^-, CO_3^{2-}, SO_4^{2-}, $S_2O_7^{2-}$, CrO_4^{2-}, $Cr_2O_7^{2-}$, MoO_4^{2-}, $Mo_2O_7^{2-}$, O^{2-} reciprocal system (diluted in free oxides).

For the Na^+, K^+ // Cl^-, CO_3^{2-}, SO_4^{2-}, $S_2O_7^{2-}$, CrO_4^{2-}, $Cr_2O_7^{2-}$, MoO_4^{2-}, $Mo_2O_7^{2-}$, O^{2-} reciprocal system, the values of $\zeta_{A/X}$ (equation (7)) are:

$$\zeta_{A/X} = 4; \quad \zeta_{A/Cl} = 6 \quad (8)$$

where A = Na^+, K^+; and X = CO_3^{2-}, SO_4^{2-}, $S_2O_7^{2-}$, CrO_4^{2-}, $Cr_2O_7^{2-}$, MoO_4^{2-}, $Mo_2O_7^{2}$, O^{2-}.

Table 3: 2nd-nearest-neighbour ''coordination numbers'' for the quadruplets ABXY of the newly optimized systems of the Na^+, K^+ // Cl^-, CO_3^{2-}, SO_4^{2-}, $S_2O_7^{2-}$, CrO_4^{2-}, $Cr_2O_7^{2-}$, MoO_4^{2-}, $Mo_2O_7^{2-}$, O^{2-} liquid phase

A	B	X	Y	$Z^{A}_{AB/XY}$	$Z^{B}_{AB/XY}$	$Z^{X}_{AB/XY}$	$Z^{Y}_{AB/XY}$
Na	Na	Cl	Cl	6	6	6	6
K	K	Cl	Cl	6	6	6	6
Na	Na	CO_3	CO_3	3	3	6	6
K	K	CO_3	CO_3	3	3	6	6
Na	Na	SO_4	SO_4	3	3	6	6
K	K	SO_4	SO_4	3	3	6	6
Na	Na	S_2O_7	S_2O_7	3	3	6	6
K	K	S_2O_7	S_2O_7	3	3	6	6
Na	Na	CrO_4	CrO_4	3	3	6	6
K	K	CrO_4	CrO_4	3	3	6	6
Na	Na	Cr_2O_7	Cr_2O_7	3	3	6	6
K	K	Cr_2O_7	Cr_2O_7	3	3	6	6
Na	Na	MoO_4	MoO_4	3	3	6	6
K	K	MoO_4	MoO_4	3	3	6	6
Na	Na	Mo_2O_7	Mo_2O_7	3	3	6	6
K	K	Mo_2O_7	Mo_2O_7	3	3	6	6
Na	Na	O	O	3	3	6	6
K	K	O	O	3	3	6	6
Na	Na	Cl	MoO_4	4	4	4	8
K	K	Cl	MoO_4	4	4	4	8
Na	Na	CO_3	MoO_4	3	3	6	6
Na	Na	SO_4	MoO_4	3	3	6	6
Na	Na	CrO_4	MoO_4	3	3	6	6
K	K	CO_3	MoO_4	3	3	6	6
K	K	SO_4	MoO_4	3	3	6	6
K	K	CrO_4	MoO_4	3	3	6	6
Na	K	MoO_4	MoO_4	3	3	6	6
K	K	Cr_2O_7	Mo_2O_7	3	3	6	6
Na	Na	MoO_4	Mo_2O_7	3	3	6	6
K	K	MoO_4	Mo_2O_7	3	3	6	6

The 2nd-nearest-neighbour "coordination numbers" for the ABXY quadruplets of the Na^+, K^+ // Cl^-, CO_3^{2-}, SO_4^{2-}, $S_2O_7^{2-}$, CrO_4^{2-}, $Cr_2O_7^{2-}$, O^{2-} liquid phase were given previously by Lindberg et al. [14, 15] and in our previous work, [16] and they were directly used in the present work.

Table 4: Model parameters optimized in the present work for the Na^+, K^+ // Cl^-, CO_3^{2-}, SO_4^{2-}, $S_2O_7^{2-}$, CrO_4^{2-}, $Cr_2O_7^{2-}$, MoO_4^{2-}, $Mo_2O_7^{2-}$, O^{2-} liquid phase (diluted in free oxides)

System	Model parameter (J/mol)
($NaCl + Na_2MoO_4$)	$\Delta g_{Na_2/(Cl)(MoO_4)} = 300.0\chi_{(Cl)(MoO_4)}$
($KCl + K_2MoO_4$)	$\Delta g_{K_2/(Cl)(MoO_4)} = -1{,}100.0 + 500.0\chi_{(Cl)(MoO_4)} - 750.0\chi_{(MoO_4)(Cl)}$
($Na_2CO_3 + Na_2MoO_4$)	$\Delta g_{Na_2/(CO_3)(MoO_4)} = 700.0$
($K_2CO_3 + K_2MoO_4$)	$\Delta g_{K_2/(CO_3)(MoO_4)} = 1{,}050.0 + 650.0\chi_{(MoO_4)(CO_3)}$
($Na_2SO_4 + Na_2MoO_4$)	$\Delta g_{Na_2/(SO_4)(MoO_4)} = -5{,}700.0 + 3{,}000.0\chi_{(MoO_4)(SO_4)}$
($K_2SO_4 + K_2MoO_4$)	$\Delta g_{K_2/(SO_4)(MoO_4)} = 500.0 + 800.0\chi_{(SO_4)(MoO_4)}$
($Na_2CrO_4 + Na_2MoO_4$)	$\Delta g_{Na_2/(CrO_4)(MoO_4)} = 1{,}000.0 - 1{,}200.0\chi_{(CrO_4)(MoO_4)} + 1{,}000.0\chi_{(MoO_4)(CrO_4)}$
($K_2CrO_4 + K_2MoO_4$)	$\Delta g_{K_2/(CrO_4)(MoO_4)} = 2{,}000.0 + 1{,}500.0\chi_{(CrO_4)(MoO_4)}$
($Na_2MoO_4 + K_2MoO_4$)	$\Delta g_{NaK/(MoO_4)_2} = -500.0 + 750.0\chi_{NaK}$
($Na_2MoO_4 + Na_2Mo_2O_7$)	$\Delta g_{Na_2/(MoO_4)(Mo_2O_7)} = -450.0\chi_{(MoO_4)(Mo_2O_7)} + 3{,}500.0\chi_{(Mo_2O_7)(MoO_4)}$
($NaCl + Na_2MoO_4 + KCl + K_2MoO_4$)	$\Delta g_{NaK/(Cl)(MoO_4)} = 7{,}000.0x_{K_2/(MoO_4)_2}$

4. Thermodynamic model for the solid solutions

Several solid solutions were modeled in the Na^+, K^+ // Cl^-, CO_3^{2-}, SO_4^{2-}, $S_2O_7^{2-}$, CrO_4^{2-}, $Cr_2O_7^{2-}$, MoO_4^{2-}, $Mo_2O_7^{2-}$main system. Table 5 describes in detail all solid solutions considered in the present work, and lists all optimized model parameters. A large part of the information displayed in this table was given previously, [16] and is repeated here for the sake of clarity. The new work performed in this study refers to the addition in the relevant existing solid solutions of Na_2MoO_4, K_2MoO_4, $Na_2Mo_2O_7$, and / or $K_2Mo_2O_7$,

and to the introduction of new solid solutions ($K_2MoO_4(s_3)$-ht-ss, cF56, and $Na_2MoO_4(s_2)$-ss rich).

The Na^+, K^+ // CO_3^{2-}, SO_4^{2-}, CrO_4^{2-}, MoO_4^{2-} sub-system displays a hexagonal solid solution (hP22) at high temperatures with limited solubility of K_2MoO_4, and complete mutual miscibility over the entire composition range for the remaining salts. The MQMQA [33] was used to model this reciprocal solid solution, with two sublattices (a cationic one and an anionic one). As explained previously, [16] the MQM is more suited than the Compound Energy Formalism (CEF) [36-38] to model complex solid solutions such as (Na_2SO_4 + K_2SO_4) dissolving divalent cation sulfates like $CaSO_4$, $ZnSO_4$ and $PbSO_4$. In particular, in a recent work, [39] the MQM was used to add $ZnSO_4$ and $PbSO_4$ as solutes in the high-temperature (Na_2SO_4 + K_2SO_4) hexagonal solid solution. For the sake of consistency, the MQMQA was retained in the present work to model the hP22 solid solution (with Na^+ and K^+ as the cations, and CO_3^{2-}, SO_4^{2-}, CrO_4^{2-}, and MoO_4^{2-} as the anions). All other solid solutions exhibited limited solubility, and were modeled with the CEF. [36-38] In most cases, two sublattices were required. However, three sublattices were used for the molybdenum-glaserite phase $K_3Na(MoO_4)_2$, which exhibits significant non-stoichiometry at temperatures above 240°C. [40]

As an example, let us consider the aP44 solid solution which consists of the triclinic low-temperature allotropes $Na_2Cr_2O_{7(S1)}$, $K_2Cr_2O_{7(S1)}$, and $K_2Mo_2O_{7(S1)}$ (mutually soluble) dissolving $Na_2Mo_2O_7$. The sublattice structure $(Na^+, K^+)_2(Cr_2O_7^{2-}, Mo_2O_7^{2-})$ was used, where Na^+ and K^+ reside on the cationic sublattice C while $Cr_2O_7^{2-}$ and $Mo_2O_7^{2-}$ reside on the anionic sublattice A. The molar Gibbs energy of the solution is given by the following expression :

$$\begin{aligned} G_m = {} & y^C_{Na^+} y^A_{Cr_2O_7^{2-}} G^\circ_{Na^+:Cr_2O_7^{2-}} + y^C_{K^+} y^A_{Cr_2O_7^{2-}} G^\circ_{K^+:Cr_2O_7^{2-}} + y^C_{Na^+} y^A_{Mo_2O_7^{2-}} G^\circ_{Na^+:Mo_2O_7^{2-}} \\ & + y^C_{K^+} y^A_{Mo_2O_7^{2-}} G^\circ_{K^+:Mo_2O_7^{2-}} + 2RT\left(y^C_{Na^+} \ln y^C_{Na^+} + y^C_{K^+} \ln y^C_{K^+}\right) + \\ & RT\left(y^A_{Cr_2O_7^{2-}} \ln y^A_{Cr_2O_7^{2-}} + y^A_{Mo_2O_7^{2-}} \ln y^A_{Mo_2O_7^{2-}}\right) + G^E \quad (9) \end{aligned}$$

The first four terms give the reference Gibbs energy of the solution, where $y^C_{Na^+}$ and $y^C_{K^+}$ are the site fractions of Na^+ and K^+ on the cationic sublattice C, and $y^A_{Cr_2O_7^{2-}}$ and $y^A_{Mo_2O_7^{2-}}$ are the site fractions of $Cr_2O_7^{2-}$ and $Mo_2O_7^{2-}$ on the anionic sublattice A. The standard molar

Gibbs energies of the end-member components $Na_2Cr_2O_7$, $K_2Cr_2O_7$, $Na_2Mo_2O_7$ and $K_2Mo_2O_7$ are represented by $G^{\circ}_{Na^+:Cr_2O_7^{2-}}$, $G^{\circ}_{K^+:Cr_2O_7^{2-}}$, $G^{\circ}_{Na^+:Mo_2O_7^{2-}}$ and $G^{\circ}_{K^+:Mo_2O_7^{2-}}$, respectively.

Since the cations and anions are assumed to be randomly distributed on their respective sublattice, as in the Temkin-type, [41] the fifth and sixth terms in equation (9) correspond to the ideal entropy of mixing. The final term represents the molar excess Gibbs energy and is given by:

$$G^E = y^C_{Na^+} y^C_{K^+} y^A_{Cr_2O_7^{2-}} L_{Na^+,K^+:Cr_2O_7^{2-}} + y^C_{Na^+} y^C_{K^+} y^A_{Mo_2O_7^{2-}} L_{Na^+,K^+:Mo_2O_7^{2-}}$$
$$+ y^C_{Na^+} y^A_{Cr_2O_7^{2-}} y^A_{Mo_2O_7^{2-}} L_{Na^+:Cr_2O_7^{2-},Mo_2O_7^{2-}} + y^C_{K^+} y^A_{Cr_2O_7^{2-}} y^A_{Mo_2O_7^{2-}} L_{K^+:Cr_2O_7^{2-},Mo_2O_7^{2-}}$$
$$+ y^C_{Na^+} y^C_{K^+} y^A_{Cr_2O_7^{2-}} y^A_{Mo_2O_7^{2-}} L_{Na^+,K^+:Cr_2O_7^{2-},Mo_2O_7^{2-}} \quad (10)$$

In equation (10), the first four terms are interaction parameters in the four common-ion binary sub-systems, and the last term is a reciprocal interaction parameter. The L factors can be made temperature-dependent and also composition-dependent, where Redlich-Kister terms $L^i_{i\geq 0}(y_A - y_B)^i$ as a function of site fractions are generally employed.

Table 5: Description and list of optimized model parameters for the various solid solutions in the Na^+, K^+ // Cl^-, CO_3^{2-}, SO_4^{2-}, $S_2O_7^{2-}$, CrO_4^{2-}, $Cr_2O_7^{2-}$, MoO_4^{2-}, $Mo_2O_7^{2-}$ main system modeled in the present work

Hexagonal solid solution hP22 High-temperature allotropes $Na_2CO_{3(S3)}$, $K_2CO_{3(S2)}$, $Na_2SO_{4(S2)}$, $K_2SO_{4(S2)}$, $Na_2CrO_{4(S2)}$, $K_2CrO_{4(S2)}$, and $Na_2MoO_{4(S4)}$ mutually soluble, and dissolving K_2MoO_4 $P6_3/mmc$ space group Sublattice structure: $(Na^+, K^+)_2(CO_3^{2-}, SO_4^{2-}, CrO_4^{2-}, MoO_4^{2-})$ Use of the MQMQA The Gibbs energies of the "end-members" are: $g^{\circ}_{Na_2CO_3} = g^{\circ}_{Na_2CO_{3(S3)}}$ $g^{\circ}_{K_2CO_3} = g^{\circ}_{K_2CO_{3(S2)}}$ $g^{\circ}_{Na_2SO_4} = g^{\circ}_{Na_2SO_{4(S2)}}$ $g^{\circ}_{K_2SO_4} = g^{\circ}_{K_2SO_{4(S2)}}$

$\overset{\circ}{g}_{Na_2CrO_4} = \overset{\circ}{g}_{Na_2CrO_{4(S2)}}$

$\overset{\circ}{g}_{K_2CrO_4} = \overset{\circ}{g}_{K_2CrO_{4(S2)}}$

$\overset{\circ}{g}_{Na_2MoO_4} = \overset{\circ}{g}_{Na_2MoO_{4(S4)}}$

$\overset{\circ}{g}_{K_2MoO_4} = \overset{\circ}{g}_{K_2MoO_{4(S3)}} + 10$ (J/mol)

The 2nd-nearest-neighbour coordination number of each cationic species is 3.0, and that of each anionic species is 6.0. Thus, all $\zeta_{A/X}$ are equal to 4.0 (with A = Na^+, K^+ and X = CO_3^{2-}, SO_4^{2-}, CrO_4^{2-} and MoO_4^{2-}).

The following interaction parameters for (Na_2CO_3 + Na_2SO_4), (K_2CO_3 + K_2SO_4), (Na_2CO_3 + K_2CO_3), (Na_2SO_4 + K_2SO_4) and Na, K // CO_3, SO_4 were obtained previously:

$\Delta g_{Na_2/(CO_3)(SO_4)} = 1{,}106.7 + 1{,}060.0\, Y_{CO_3}$ (J/mol) [20] (This is a Bragg-Williams type term and Y_{CO_3} is the equivalent site fraction of CO_3)

$\Delta g_{K_2/(CO_3)(SO_4)} = 1{,}571.7 + 105.0\, Y_{CO_3}$ (J/mol) [20]

$\Delta g_{NaK/(CO_3)_2} = 4{,}935.0 - 2{,}928.2 Y_K$ (J/mol) [20]

$\Delta g_{NaK/(SO_4)_2} = 3{,}040.4 + (2{,}370.9 - 3.1241 \times T)\, Y_K$ (J/mol) [14, 20]

$\Delta g_{NaK/(CO_3)(SO_4)} = 1{,}401.3$ (J/mol) [20]

The following interaction parameters for (Na_2CO_3 + Na_2CrO_4), (K_2CO_3 + K_2CrO_4), (Na_2SO_4 + Na_2CrO_4), (K_2SO_4 + K_2CrO_4) and (Na_2CrO_4 + K_2CrO_4) were obtained in our previous work [16]:

$\Delta g_{Na_2/(CO_3)(CrO_4)} = 8{,}000.0 - 1{,}800.0\, Y_{CrO_4}$ (J/mol)

$\Delta g_{K_2/(CO_3)(CrO_4)} = 5{,}600.0 - 800.0\, Y_{CrO_4}$ (J/mol)

$\Delta g_{Na_2/(SO_4)(CrO_4)} = 800.0$ (J/mol)

$\Delta g_{K_2/(SO_4)(CrO_4)} = 1{,}000.0 - 500.0\, Y_{SO_4}$ (J/mol)

$\Delta g_{NaK/(CrO_4)_2} = 2{,}700.0 + (2{,}000.0 - 2.4500 \times T) Y_K$ (J/mol)

The following MoO_4-based interaction parameters were obtained in the present work:

$\Delta g_{Na_2/(CO_3)(MoO_4)} = 100{,}000.0$ (J/mol)

$\Delta g_{K_2/(CO_3)(MoO_4)} = 100{,}000.0$ (J/mol)

$\Delta g_{Na_2/(SO_4)(MoO_4)} = 500.0 - 5{,}000.0\ Y_{SO_4} - 1{,}600.0\ Y_{MoO_4}$ (J/mol)

$\Delta g_{Na_2/(CrO_4)(MoO_4)} = 500.0\ Y_{CrO_4} + 2{,}500.0\ Y_{MoO_4}$ (J/mol)

$\Delta g_{K_2/(SO_4)(MoO_4)} = 2{,}000.0 + 2{,}000.0\ Y_{SO_4}$ (J/mol)

$\Delta g_{K_2/(CrO_4)(MoO_4)} = 600.0 + 3{,}550.0\ Y_{CrO_4} + 2{,}070.0\ Y_{MoO_4}$ (J/mol)

$\Delta g_{NaK/(MoO_4)_2} = 3{,}500.0$ (J/mol)

Solid solution $K_2MoO_{4(S3)}$-ht-ss

Trigonal high-temperature allotrope $K_2MoO_{4(S3)}$ dissolving K_2SO_4, K_2CrO_4, Na_2MoO_4, Na_2SO_4 and Na_2CrO_4

$P\bar{3}m1$ space group

Sublattice structure: $(K^+, Na^+)_2(MoO_4^{2-}, SO_4^{2-}, CrO_4^{2-})$

The Gibbs energies of the "end-members" are:

$g^{\circ}_{K_2MoO_4} = g^{\circ}_{K_2MoO_4(s3)}$

$g^{\circ}_{K_2SO_4} = g^{\circ}_{K_2SO_4(s2)} + 6{,}129.6$ (J/mol)

$g^{\circ}_{K_2CrO_4} = g^{\circ}_{K_2CrO_4(s2)} + 7{,}363.8$ (J/mol)

$g^{\circ}_{Na_2MoO_4} = g^{\circ}_{Na_2MoO_4(s4)} + 10{,}250.8$ (J/mol)

$g^{\circ}_{Na_2SO_4}{}^{(1)} = g^{\circ}_{Na_2SO_4(s2)} + 6{,}129.6$ (J/mol)

$g^{\circ}_{Na_2CrO_4}{}^{(2)} = g^{\circ}_{Na_2CrO_4(s2)} + 7{,}322.0$ (J/mol)

Solid solution oS28

Orthorhombic low-temperature allotropes $Na_2CrO_{4(S1)}$, $Na_2SO_{4(S1)}$ and $K_2MoO_{4(S2)}$ mutually soluble, and dissolving K_2CrO_4, Na_2CO_3, K_2SO_4, K_2CO_3 and Na_2MoO_4

Cmcm space group

Sublattice structure: $(Na^+, K^+)_2(SO_4^{2-}, CrO_4^{2-}, MoO_4^{2-}, CO_3^{2-})$

The Gibbs energies of the "end-members" are:

$g^{\circ}_{Na_2CrO_4} = g^{\circ}_{Na_2CrO_{4(S1)}}$

$g^{\circ}_{Na_2SO_4} = g^{\circ}_{Na_2SO_{4(S1)}}$

$g^{\circ}_{Na_2MoO_4} = g^{\circ}_{Na_2MoO_{4(S3)}} + 6{,}276.0$ (J/mol)

$g^{\circ}_{Na_2CO_3} = g^{\circ}_{Na_2CO_{3(S2)}} + 7{,}112.8$ (J/mol) [20]

$g^{\circ}_{K_2CrO_4} = g^{\circ}_{K_2CrO_{4(S1)}} + (33{,}472.0 - 7.7404 \times T)$ (J/mol) [16]

$g^{\circ}_{K_2SO_4} = g^{\circ}_{K_2SO_{4(S1)}} + 33{,}472.0$ (J/mol) [20]

$g^{\circ}_{K_2MoO_4} = g^{\circ}_{K_2MoO_4(s2)}$

$g^{\circ}_{K_2CO_3} = g^{\circ}_{K_2CO_{3(S1)}} + 4{,}184.0$ (J/mol) [20]

The following Redlich-Kister interaction parameter for (Na_2CO_3 + Na_2SO_4) was obtained previously:

$L^0_{Na/(CO_3)(SO_4)} = 3{,}347.2$ (J/mol) [20]

The following Redlich-Kister interaction parameters for (Na_2CO_3 + Na_2CrO_4) and (Na_2SO_4 + Na_2CrO_4) were obtained in our previous work [16]:

$L^0_{Na/(CrO_4)(CO_3)} = 100{,}000.0$ (J/mol)

$L^0_{Na/(CrO_4)(SO_4)} = 3{,}000.0$ (J/mol)

The following MoO_4-based Redlich-Kister interaction parameters were obtained in the present work:

$L^0_{K/(CO_3)(MoO_4)} = 100{,}000.0$ (J/mol)

$L^0_{Na/(SO_4)(MoO_4)} = 100{,}000.0$ (J/mol)

$L^0_{Na/(CrO_4)(MoO_4)} = 500.0$ (J/mol)

$L^0_{K/(SO_4)(MoO_4)} = -26{,}000.0$ (J/mol)

$L^0_{K/(CrO_4)(MoO_4)} = -19{,}500.0$ (J/mol)

$L^0_{NaK/(MoO_4)} = 6{,}200.0$ (J/mol)

Solid solution oP28

Orthorhombic low-temperature allotropes $K_2CrO_{4(S1)}$ and $K_2SO_{4(S1)}$ mutually soluble, and dissolving Na_2CrO_4, K_2CO_3, Na_2SO_4, Na_2CO_3, K_2MoO_4 and Na_2MoO_4

Pnma space group

Sublattice structure: $(K^+, Na^+)_2(SO_4^{2-}, CrO_4^{2-}, MoO_4^{2-}, CO_3^{2-})$

The Gibbs energies of the "end-members" are:

$g^\circ_{K_2CrO_4} = g^\circ_{K_2CrO_{4(S1)}}$

$g^\circ_{K_2SO_4} = g^\circ_{K_2SO_{4(S1)}}$

$g^\circ_{K_2CO_3} = g^\circ_{K_2CO_{3(S1)}} + 209.2$ (J/mol) [20]

$g^\circ_{K_2MoO_4} = g^\circ_{K_2MoO_{4(S3)}} + 13{,}388.8$ (J/mol)

$g^\circ_{Na_2CrO_4} = g^\circ_{Na_2CrO_{4(S1)}} + (13{,}388.8 + 2.7196 \times T)$ (J/mol) [16]

$g^\circ_{Na_2SO_4} = g^\circ_{Na_2SO_{4(S1)}} + (29{,}288.0 - 20.9200 \times T)$ (J/mol) [20]

$g^\circ_{Na_2CO_3} = g^\circ_{Na_2CO_{3(S1)}} + 20{,}920.0$ (J/mol) [20]

$g^{\circ\ (3)}_{Na_2MoO_4} = g^\circ_{Na_2MoO_{4(S1)}} + 20{,}920.0$ (J/mol)

The following Redlich-Kister interaction parameters for (K_2CO_3 + K_2SO_4) were obtained

previously:

$L^0_{K/(CO_3)(SO_4)} = 3{,}765.6$ (J/mol) [20]

$L^1_{K/(CO_3)(SO_4)} = -2{,}008.3$ (J/mol) [20]

The following Redlich-Kister interaction parameters for (K_2CO_3 + K_2CrO_4) and (K_2SO_4 + K_2CrO_4) were obtained in our previous work [16]:

$L^0_{K/(CO_3)(CrO_4)} = 17{,}500.0$ (J/mol)

$L^1_{K/(CO_3)(CrO_4)} = 3{,}000.0$ (J/mol)

$L^0_{K/(CrO_4)(SO_4)} = 1{,}800.0$ (J/mol)

Glaserite solid solution hP14

Solid $K_3Na(SO_4)_2$, $K_3Na(CrO_4)_2$ and $K_3Na(MoO_4)_2$ mutually soluble, and dissolving Na^+

$P\bar{3}m1$ space group

Sublattice structure: $(K^+, Na^+)_3\ (Na^+)\ (SO_4^{2-}, CrO_4^{2-}, MoO_4^{2-})_2$

The Gibbs energies of the "end-members" are:

$g^\circ_{K_3Na(SO_4)_2} = 1.5 \times g^\circ_{K_2SO_{4(S1)}} + 0.5 \times g^\circ_{Na_2SO_{4(S2)}} - 10{,}878.4 + 9.7906 \times T$ (J/mol) [14]

$g^\circ_{Na_3Na(SO_4)_2} = 2 \times g^\circ_{Na_2SO_{4(S2)}} + 16{,}736.0 - 10.7110 \times T$ (J/mol) [14]

$g^\circ_{K_3Na(CrO_4)_2} = 1.5 \times g^\circ_{K_2CrO_{4(S1)}} + 0.5 \times g^\circ_{Na_2CrO_{4(S1)}} - 17{,}154.4 + 9.4140 \times T$ (J/mol) [16]

$g^\circ_{Na_3Na(CrO_4)_2} = 2 \times g^\circ_{Na_2CrO_{4(S1)}} + 12{,}970.4 - 8.1588 \times T$ (J/mol) [16]

$g^\circ_{K_3Na(MoO_4)_2} = 1.5 \times g^\circ_{K_2MoO_{4(S3)}} + 0.5 \times g^\circ_{Na_2MoO_{4(S4)}} - 10{,}460.0$ (J/mol)

$g^\circ_{Na_3Na(MoO_4)_2} = 2 \times g^\circ_{Na_2MoO_{4(S4)}} + 23{,}012.0$ (J/mol)

Solid solution oF56

Orthorhombic low-temperature allotropes $Na_2SO_{4(S3)}$ and $Na_2MoO_{4(S3)}$ mutually soluble, and dissolving Na_2CrO_4, K_2SO_4, K_2CrO_4 and K_2MoO_4

Fddd space group

Sublattice structure: $(Na^+, K^+)_2(SO_4^{2-}, CrO_4^{2-}, MoO_4^{2-})$

The Gibbs energies of the "end-members" are:

$g^\circ_{Na_2SO_4} = g^\circ_{Na_2SO_{4(S3)}}$

$g^{\circ}_{K_2SO_4} = g^{\circ}_{K_2SO_{4(S1)}}$ + 66,944.0 (J/mol) [16]
$g^{\circ}_{Na_2CrO_4} = g^{\circ}_{Na_2CrO_{4(S1)}} + 4{,}100.3$ (J/mol) [16]
$g^{\circ}_{K_2CrO_4} = g^{\circ}_{K_2CrO_{4(S1)}} + 66{,}944.0$ (J/mol) [16]
$g^{\circ}_{Na_2MoO_4} = g^{\circ}_{Na_2MoO_{4(S3)}}$
$g^{\circ}_{K_2MoO_4} = g^{\circ}_{K_2MoO_{4(S3)}} + (-7{,}531.2 + 37.0284 \times T)$ (J/mol)

The following MoO_4-based Redlich-Kister interaction parameters were obtained in the present work:
$L^0_{NaK/MoO_4} = -18{,}000.0$ (J/mol)

$L^1_{NaK/MoO_4} = 15{,}000.0$ (J/mol)

$L^0_{Na/(SO_4)(MoO_4)} = 100{,}000.0$ (J/mol)

$L^0_{Na/(CrO_4)(MoO_4)} = 100{,}000.0$ (J/mol)

Solid solution cF56
Cubic low-temperature allotrope $Na_2MoO_{4(S1)}$ dissolving Na_2SO_4 and Na_2CrO_4

$Fd\bar{3}m$ space group
Sublattice structure: $(Na^+)_2(MoO_4^{2-}, SO_4^{2-}, CrO_4^{2-})$

The Gibbs energies of the "end-members" are:
$g^{\circ}_{Na_2MoO_4} = g^{\circ}_{Na_2MoO_{4(S1)}}$
$g^{\circ}_{Na_2SO_4} = g^{\circ}_{Na_2SO_{4(S1)}} + (8{,}368.0 + 16.7360 \times T)$ (J/mol)
$g^{\circ}_{Na_2CrO_4} = g^{\circ}_{Na_2CrO_{4(S1)}} + (8{,}368.0 + 16.7360 \times T)$ (J/mol)

Solid solution $Na_2MoO_{4(S2)}$-ss-rich
Orthorhombic intermediate-temperature allotrope $Na_2MoO_{4(S2)}$ dissolving Na_2SO_4 and Na_2CrO_4

$Pbn2_1$ space group
Sublattice structure: $(Na^+)_2(MoO_4^{2-}, SO_4^{2-}, CrO_4^{2-})$

The Gibbs energies of the "end-members" are:
$g^{\circ}_{Na_2MoO_4} = g^{\circ}_{Na_2MoO_{4(S2)}}$
$g^{\circ}_{Na_2SO_4} = g^{\circ}_{Na_2SO_{4(S2)}} + (1{,}046.0 + 16.7360 \times T)$ (J/mol)
$g^{\circ}_{Na_2CrO_4} = g^{\circ}_{Na_2CrO_{4(S2)}} + (1{,}046.0 + 16.7360 \times T)$ (J/mol)

Solid solution aP22
Triclinic allotropes $Na_2S_2O_7$ and $Na_2Cr_2O_{7(S2)}$ mutually soluble, and dissolving $K_2S_2O_7$ and $K_2Cr_2O_7$

$A\bar{1}$ space group

Sublattice structure: $(Na^+, K^+)_2(S_2O_7^{2-}, Cr_2O_7^{2-})$

The Gibbs energies of the "end-members" are:
$g^{\circ}_{Na_2S_2O_7} = g^{\circ}_{Na_2S_2O_{7(S)}}$
$g^{\circ}_{K_2S_2O_7} = g^{\circ}_{K_2S_2O_{7(S2)}} + 29{,}288.0$ (J/mol) [14]
$g^{\circ}_{Na_2Cr_2O_7} = g^{\circ}_{Na_2Cr_2O_{7(S2)}}$
$g^{\circ}_{K_2Cr_2O_7} = g^{\circ}_{K_2Cr_2O_{7(S2)}} + 7{,}531.2 + 5.6484 \times T$ (J/mol) [16]

Solid solution aP44
Triclinic low-temperature allotropes $Na_2Cr_2O_{7(S1)}$, $K_2Cr_2O_{7(S1)}$ and $K_2Mo_2O_{7(S1)}$ mutually soluble, and dissolving $Na_2Mo_2O_7$

$P\bar{1}$ space group

Sublattice structure: $(K^+, Na^+)_2(Cr_2O_7^{2-}, Mo_2O_7^{2-})$

The Gibbs energies of the "end-members" are:
$g^{\circ}_{Na_2Cr_2O_7} = g^{\circ}_{Na_2Cr_2O_{7(S1)}}$
$g^{\circ}_{K_2Cr_2O_7} = g^{\circ}_{K_2Cr_2O_{7(S1)}}$
$g^{\circ}_{K_2Mo_2O_7} = g^{\circ}_{K_2Mo_2O_{7(S1)}}$
$g^{\circ}_{Na_2Mo_2O_7}{}^{(4)} = g^{\circ}_{Na_2Mo_2O_{7(S1)}} + 11{,}296.8 + 3.8911 \times T$ (J/mol)

The following Redlich-Kister interaction parameter for ($Na_2Cr_2O_7$ + $K_2Cr_2O_7$) was obtained in our previous study [16] :
$L^0_{NaK/Cr_2O_7} = 20{,}000.0$ (J/mol)

The following Mo_2O_7-based Redlich-Kister interaction parameter was obtained in the present work:
$L^0_{K/(Cr_2O_7)(Mo_2O_7)} = 2{,}000.0$ (J/mol)

Solid solution $K_2Cr_2O_7$(s.s)
Monoclinic high-temperature allotropes $K_2Cr_2O_{7(S2)}$ and $K_2Mo_2O_{7(S2)}$ mutually soluble, and dissolving $Na_2Cr_2O_7$ and $Na_2Mo_2O_7$

$P2_1/c$ space group

Sublattice structure: $(K^+, Na^+)_2(Cr_2O_7^{2-}, Mo_2O_7^{2-})$

The Gibbs energies of the "end-members" are:

$g^{\circ}_{K_2Cr_2O_7} = g^{\circ}_{K_2Cr_2O_{7(S2)}}$

$g^{\circ}_{Na_2Cr_2O_7} = g^{\circ}_{Na_2Cr_2O_{7(S2)}} + 11{,}296.8 + 3.8911 \times T$ (J/mol) [16]

$g^{\circ}_{K_2Mo_2O_7} = g^{\circ}_{K_2Mo_2O_{7(S2)}}$

$g^{\circ}_{Na_2Mo_2O_7}$ [(5)] $= g^{\circ}_{Na_2Mo_2O_{7(S2)}} + 11{,}296.8 + 3.8911 \times T$ (J/mol)

The following Mo_2O_7-based Redlich-Kister interaction parameter was obtained in the present work:

$L^0_{K/(Cr_2O_7)(Mo_2O_7)} = 2{,}000.0$ (J/mol)

Rocksalt solid solution cF8

Cubic NaCl and KCl mutually soluble

$Fm\bar{3}m$ space group

The Gibbs energies of the "end-members" are:

$g^{\circ}_{NaCl} = g^{\circ}_{NaCl(S)}$

$g^{\circ}_{KCl} = g^{\circ}_{KCl(S)}$

The following Redlich-Kister interaction parameters for (NaCl + KCl) were obtained previously:

$L^0_{NaK/Cl} = 15{,}972.0 + 32.7960 \times T - 5.593 \times T \times ln(T)$ (J/mol) [42]

$L^1_{NaK/Cl} = 1{,}639.0$ (J/mol) [42]

[(1),(2)] The "end-members" Na_2SO_4 and Na_2CrO_4 were added to the $K_2MoO_{4(S3)}$-ht-ss solid solution. The corresponding Gibbs energies are those of $Na_2SO_{4(S2)}$ and $Na_2CrO_{4(S2)}$ augmented by a positive Gibbs energy, respectively. The latter were assumed to be identical to those for the "end-members" K_2SO_4 (i.e. 6,129.6 J/mol) and K_2CrO_4 (i.e. 7,322.0 J/mol), respectively. The "end-members" Na_2SO_4 and Na_2CrO_4 are only required for calculations in the K, Na // MoO_4, SO_4 and K, Na // MoO_4, CrO_4 reciprocal systems, respectively, and higher-order systems.

[(3)] The "end-member" Na_2MoO_4 was added to the oP28 solid solution. The corresponding Gibbs energy is that of $Na_2MoO_{4(S1)}$ augmented by a positive Gibbs energy. As a first approximation, the latter was assumed to be identical to that for the "end-member" Na_2CO_3 (i.e. 20,920.0 J/mol). The "end-member" Na_2MoO_4 is only required for calculations in the K, Na // SO_4, MoO_4 and K, Na // CrO_4, MoO_4 reciprocal systems, and higher-order systems.

[4],[5] The "end-member" $Na_2Mo_2O_7$ was added to both of the solid solutions aP44 and $K_2Cr_2O_7$(s.s). The corresponding Gibbs energies are those of $Na_2Mo_2O_{7(S1)}$ and $Na_2Mo_2O_{7(S2)}$ augmented by a positive Gibbs energy, respectively. As a first approximation, the latter were assumed to be identical to that for the "end-member" $Na_2Cr_2O_7$ in the $K_2Cr_2O_7$(s.s) solid solution (that is, $11{,}296.8 + 3.8911 \times T$ J/mol), which was obtained in our previous work. The "end-member" $Na_2Mo_2O_7$ is only required for calculations in the K, Na // Cr_2O_7, Mo_2O_7 ternary reciprocal system and higher-order systems.

5. Experimental procedure

5.1 DSC-TGA

Materials and measurements

The present work was carried out using high purity gases (99.999% pure Ar, 99.999% pure N_2, and 99.999% pure CO_2) from Oy Linde Gas AB (Finland). For all initial solid reagents (Na_2CO_3, Na_2SO_4, K_2SO_4, $Na_2CrO_4.4H_2O$, K_2CrO_4, Na_2MoO_4, and K_2MoO_4), the supplier's name, CAS number and purity are reported in Table 6.

Table 6 : **Purity and origin of the solid reagents used in our experiments**

Chemical formula	Supplier	CAS number	Purity (%)
Na_2CO_3	Sigma-Aldrich	497-19-8	≥ 99.95
Na_2SO_4	Sigma-Aldrich	7757-82-6	≥ 99.0
K_2SO_4	Sigma-Aldrich	7778-80-5	≥ 99.0
$Na_2CrO_4.4H_2O$	Sigma-Aldrich	10034-82-9	99.0
K_2CrO_4	Alfa-Aesar	7789-00-6	99.9
Na_2MoO_4	Sigma-Aldrich	7631-95-0	99.9
K_2MoO_4	Sigma-Aldrich	13446-49-6	98

The binary common-ion sub-systems (Na_2CO_3 + Na_2MoO_4), (K_2SO_4 + K_2MoO_4), (Na_2CrO_4 + Na_2MoO_4), (K_2CrO_4 + K_2MoO_4) and (Na_2MoO_4 + K_2MoO_4) were investigated by DSC-TGA using a NETZSCH STA 449 F1 Jupiter® instrument at compositions where experimental phase diagram data were lacking in the literature. Additional DSC-TGA

measurements were carried out using the SDT Q600 TA Instrument (New Castle, DE, U.S.A.). Such measurements were made in the binary common-ion sub-systems (Na_2SO_4 + Na_2MoO_4) and (K_2SO_4 + K_2MoO_4). The SDT Q600 TA Instrument can perform baseline-free runs. Thus, the baseline is not horizontal as shown, for instance, in the thermogram displayed in Figure 6.

A detailed description of the calibration of the NETZSCH STA 449 F1 Jupiter® instrument was given in our previous work. [4] The experimental error for the temperatures was estimated as ±1°C. The SDT Q600 TA Instrument was calibrated by measuring the temperatures of fusion of high purity zinc, aluminum and gold. The experimental error for the temperatures was estimated as ±2°C. The mass change and heat flux upon heating and cooling were measured simultaneously.

All pure compounds used in the present study were dehydrated prior to the DSC-TGA measurements. Further information can be found in reference [4]. Pt/Rh (80/20) and Al_2O_3 (corundum) crucibles were employed for the DSC-TGA measurements, using the NETZSCH STA 449 F1 Jupiter® instrument and the SDT Q600 TA Instrument, respectively.

All DSC-TGA measurements performed in the present work are reported in the Supporting Information (see Tables S1 to S9).

Flow rates of 90 ml/min CO_2 and 10 ml/min Ar were used as the shielding gas for all runs related to the three (Na_2CO_3 + Na_2MoO_4) binary mixtures investigated. A saturated CO_2 atmosphere was maintained to prevent dissociation of Na_2CO_3 at high temperatures into $Na_2O_{(S)}$ and $CO_{2(g)}$ and/or partial volatilization. Five other compositions were studied under CO_2-free conditions, including the composition of (78.0 mol% Na_2CO_3 + 22.0 mol% Na_2MoO_4) previously measured in the presence of CO_2(g).

A flow rate of 70 ml/min Ar was used as the shielding gas for all runs performed in the (K_2SO_4 + K_2MoO_4), (Na_2CrO_4 + Na_2MoO_4), (K_2CrO_4 + K_2MoO_4) and (Na_2MoO_4 + K_2MoO_4) binary sub-systems. Finally, the (Na_2SO_4 + Na_2MoO_4) and (K_2SO_4 + K_2MoO_4) binary sub-systems were investigated using a flow rate of 70 ml/min N_2.

For all DSC-TGA experiments conducted in the present work, an approach similar to that used in our previous study was adopted. [4] That is, the sample and reference were initially

heated from room temperature to 40°C, and then kept at constant temperature for 10 minutes to ensure thermal stability. Then, three consecutive heating-cooling cycles were conducted for each sample, with a heating/cooling rate of 10°C/min.

Mass loss was measured continuously throughout the experiments, with a maximum mass loss target of 3%.

Usually, only heating runs were taken into account. Each solid-solid transition was defined as the temperature at the onset of the peak while each liquidus temperature and eutectic temperature was defined as the temperature at the maximum of the peak. [43]

To avoid including non-reproducible data resulting from the thermal history of the sample, the first heating/cooling cycle was usually excluded from our analysis. However, for the two equilibrated molybdenum-glaserite compositions investigated in this work (see Table S9 in the Supporting Information), the first heating/cooling cycle was also considered since the corresponding samples had been equilibrated for four weeks at 400°C prior to the DSC-TGA measurements.

To perform the equilibration process of the molybdenum-glaserite phase, pre-treated pure powders of Na_2MoO_4 and K_2MoO_4 were mechanically mixed at the stoichiometric composition of (35 mol% Na_2MoO_4 + 65 mol% K_2MoO_4). This mixture was sealed in a fused silica tube, heated from room temperature to 800°C for 50 minutes at a heating rate of 15°C/min, and then cooled to 400°C at a cooling rate of 15°C/min for 27 minutes in a muffle furnace. After annealing at 400°C for four weeks under a flow rate of approximately 1 ml/min Ar, the equilibrated sample was quenched in air, mechanically ground, and analyzed subsequently by scanning electron microscopy (SEM)-energy dispersive X-ray spectroscopy (EDS) and DSC-TGA.

5.2 Scanning Electron Microscopy (SEM) and Energy Dispersive X-ray Spectroscopy (EDS)

The equilibrated molybdenum-glaserite (solid solution of 35 mol% Na_2MoO_4 + 65 mol% K_2MoO_4) after quenching was analyzed at room temperature with a LEO 1450 scanning electron microscope (SEM) (Carl Zeiss Microscopy GmbH, Jena, Germany) coupled with

an Oxford Instruments X-Max 50 mm² energy dispersive spectrometer (EDS) (Oxford Instruments plc, Abingdon, Oxfordshire, UK).

To confirm the formation of the molybdenum-glaserite phase, EDS analyses were conducted on six different crystals. The analytical results for those selected crystals are presented in Table 7, with a corresponding experimental error of ±5%. For three crystals, the estimated compositions of the equilibrated sample were in good agreement with the composition of the original mechanical mixture, whereas there were some discrepancies for the other three crystals. Overall, our results confirmed the global homogeneity of the equilibrated molybdenum-glaserite phase. The estimated composition of this phase is $K_{1.29}Na_{0.70}Mo_{0.98}O_{3.92}$ while the original mechanical mixture had the composition $K_{1.3}Na_{0.7}MoO_4$.
SEM image spots for which the EDS analyses were conducted are presented in Figure S1 of the Supporting Information.

Table 7: EDS analysis results of selected spectra for the quenched molybdenum-glaserite sample with an estimated experimental error of ±5%

Element	Spectrum 3	Spectrum 5	Spectrum 7	Average
O	4.275	3.644	3.841	**3.920**
Na	0.700	0.700	0.700	**0.700**
K	1.272	1.234	1.364	**1.291**
Mo	0.954	0.945	1.032	**0.977**
K / (Na + K)	0.645	0.638	0.661	**0.648**
(Na + K) / Mo	2.066	2.050	1.999	**2.037**

6. Molybdate-based common-ion binary sub-systems

This section describes all MoO_4-based and Mo_2O_7-based common-ion binary sub-systems

for which thermodynamic data (mainly phase equilibria) were available. Calculation of the phase diagrams was made in air ($p(O_2) = 0.21$ atm). The gas phase was assumed to be ideal, and all gaseous species were taken from the FactPS database in FactSage [18]. These were C, C_2, C_3, C_4, C_5, O, O_2, O_3, CO, C_2O, CO_2, C_3O_2, Na, Na_2, NaO, S, S_2, S_3, S_4, S_5, S_6, S_7, S_8, CS, CS_2, SO, SO_2, SO_3, SSO, COS, Na_2SO_4, Cl, Cl_2, CCl, C_2Cl, CCl_2, C_2Cl_2, CCl_3, C_2Cl_3, CCl_4, C_2Cl_4, C_2Cl_5, C_2Cl_6, C_6Cl_6, ClO, ClO_2, ClO_3, Cl_2O, ClOOCl, ClOClO, ClClOO, COCl, $COCl_2$, NaCl, $(NaCl)_2$, SCl, S_2Cl, SCl_2, ClSSCl, $SOCl_2$, SO_2Cl_2, K, K_2, KO, K_2SO_4, KCl, $(KCl)_2$, Cr, CrO, CrO_2, CrO_3, CrS, CrCl, $CrCl_2$, $CrCl_3$, $CrCl_4$, $CrCl_5$, $CrCl_6$, CrOCl, CrO_2Cl, $CrOCl_2$, CrO_2Cl_2, $CrOCl_3$, $CrOCl_4$, Mo, Mo_2, MoO, MoO_2, MoO_3, Mo_2O_6, Mo_3O_9, Mo_4O_{12}, Mo_5O_{15}, $Mo(CO)_6$, $MoCl_4$, $MoCl_5$, $MoCl_6$, and MoO_2Cl_2.

The possible reactions $2\ A_2MO_4 = A_2M_2O_7 + A_2O$ (where A = Na, K and M = Mo, Cr) were taken into account in the calculated phase diagrams for all MO_4-based binary sub-systems. However, those reactions were shown to be very limited up to temperatures above the liquidus. [17]

6.1 The ($NaCl + Na_2MoO_4$) system

The phase diagram has been measured by Bukhalova and Mateiko [44] using the visual-polythermal method. These authors reported the existence of the intermediate compound $NaCl.Na_2MoO_4$ melting congruently at around 644°C, with the presence of a flat maximum. Bukhalova and Mateiko [44] reported two eutectics at 40.8 mol% Na_2MoO_4 and 628°C, and at 68.1 mol% Na_2MoO_4 and 606°C. The calculated characteristics of these eutectics are 42.6 mol% Na_2MoO_4 and 642°C, and 77.6 mol% Na_2MoO_4 and 612°C, respectively. The experimental characteristics of the two eutectics have limited accuracy owing to the experimental technique that was used.

The compound Na_3ClMoO_4 was considered in the present work. Its Gibbs energy was estimated by starting with a Gibbs energy of formation from the pure end members [$NaCl_{(S)} + Na_2MoO_{4(S1)} = Na_3ClMoO_{4(S)}$] equal to zero. Then, $\Delta H^{\circ}_{298.15\,K}$ and $S^{\circ}_{298.15\,K}$ were adjusted to best reproduce the measured eutectic temperatures and temperature of fusion, [44] while ensuring that the compound was calculated to remain stable at room temperature. The optimized thermodynamic properties ($\Delta H^{\circ}_{298.15\,K}$, $S^{\circ}_{298.15\,K}$, and C_P) of solid

Na_3ClMoO_4 are given in Table 2; they correspond to an enthalpy of formation of 4,075.1 J/mol and an entropy of formation of 17.0000 J/mol-K. The calculated ($NaCl + Na_2MoO_4$) phase diagram in air ($p(O_2) = 0.21$ atm) is shown along with the measurements in Figure 1.

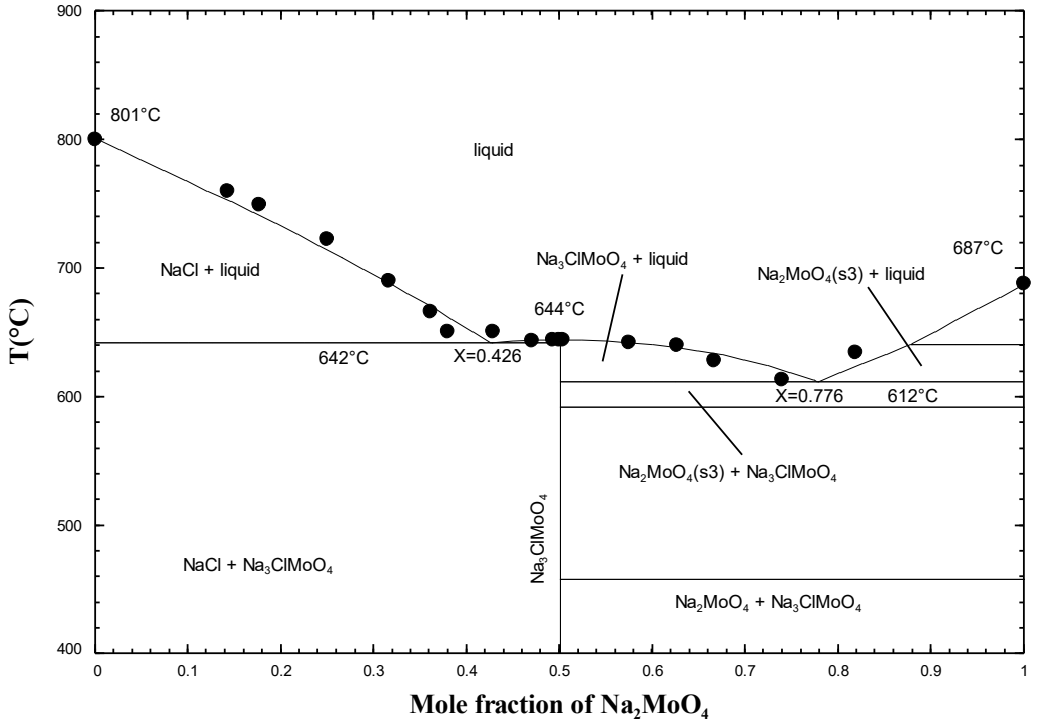

Figure 1: Calculated ($NaCl + Na_2MoO_4$) phase diagram in air ($p(O_2) = 0.21$ atm). Experimental data from Bukhalova and Mateiko [44] (●)

6.2 The ($KCl + K_2MoO_4$) system

The phase diagram has been measured using the visual-polythermal method. [44] According to Bukhalova and Mateiko, [44] ($KCl + K_2MoO_4$) is a simple eutectic system with no reported solid solutions or intermediate compounds. These authors reported a eutectic at 36.9 mol% K_2MoO_4 and 622°C. The calculated characteristics of the eutectic are 36.0 mol% K_2MoO_4 and 624°C.

The calculated ($KCl + K_2MoO_4$) phase diagram in air ($p(O_2) = 0.21$ atm) is compared to the measurements in Figure 2.

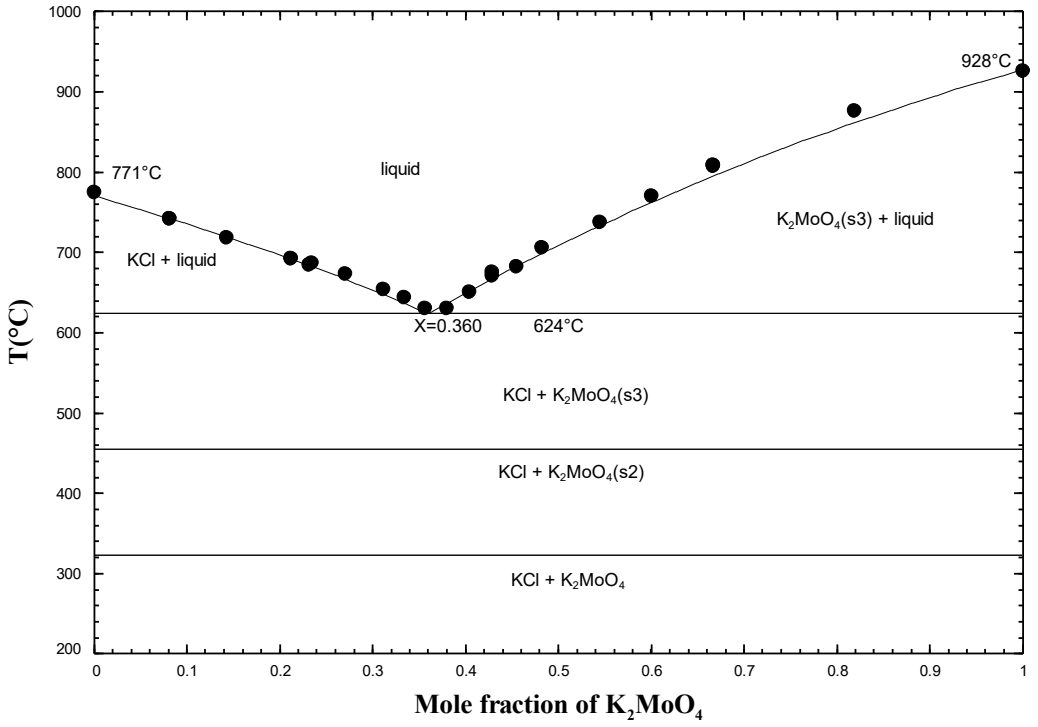

Figure 2: Calculated (KCl + K_2MoO_4) phase diagram in air ($p(O_2)$ = 0.21 atm). Experimental data from Bukhalova and Mateiko [44] (●)

6.3 The (Na_2CO_3 + Na_2MoO_4) system

The phase diagram has been measured by Shurdumov et al. [45] using thermal analysis. A eutectic was reported by these authors at 67.0 mol% Na_2MoO_4 and 588°C. The calculated characteristics of the eutectic are 66.8 mol% Na_2MoO_4 and 586°C. No solid solutions or intermediate compounds were reported. The measured limiting slopes of the Na_2CO_3 and Na_2MoO_4 liquidus curves at $x(Na_2CO_3)$ = 1 and $x(Na_2MoO_4)$ = 1 respect the limiting liquidus slope equation (11), which assumes no solid solubility :

$$\left(\frac{\mathrm{d}T}{\mathrm{dx}_{\mathrm{m}}^{\mathrm{liquidus}}}\right) = \frac{\mathrm{R}T_{\mathrm{fusion(m)}}^{2}}{\Delta h_{\mathrm{fusion(m)}}^{\circ}} \text{ at } [x_m = 1] \qquad (11)$$

where $\Delta h_{\mathrm{fusion(m)}}^{\circ}$ and $T_{\mathrm{fusion\ (m)}}$ are, respectively, the enthalpy and temperature of fusion of the pure salt m. The high-temperature allotropes $Na_2CO_{3(S3)}$ and $Na_2MoO_{4(S4)}$ have the same hexagonal crystal structure and space group $P6_3/mmc$ (see Table 1). A constant interaction parameter of +100,000.0 J/mol was introduced in the hP22 solid solution in

order to calculate negligible mutual solid solubility.

In the present work, DSC-TGA measurements were performed for several binary mixtures with various contents of Na_2MoO_4, in the absence or presence of $CO_2(g)$: 2.5, 12.7, 22, 90 and 95 mol% (from 300 to 860°C, and in the absence of $CO_2(g)$); 22 mol% (from 300 to 830°C, and in the presence of $CO_2(g)$); and 50 and 85 mol% (from 300 to 700°C, and in the presence of $CO_2(g)$). As an example, the DSC thermogram for the binary composition (78 mol% Na_2CO_3 + 22 mol% Na_2MoO_4) in the presence of $CO_2(g)$ is displayed in Figure 3.

The calculated (Na_2CO_3 + Na_2MoO_4) phase diagram in air ($p(O_2)$ = 0.21 atm) is shown along with the experimental data in Figure 4. As seen in this figure, our experimental thermal arrests agree satisfactorily with the solid-solid transitions $Na_2MoO_{4(S1)}$ = $Na_2MoO_{4(S2)}$ [4], $Na_2CO_{3(S2)}$ = $Na_2CO_{3(S3)}$, [20] and $Na_2MoO_{4(S3)}$ = $Na_2MoO_{4(S4)}$. [4] Our measured liquidus temperatures in the presence of $CO_2(g)$ at 22, 50 and 85 mol% Na_2MoO_4 are in excellent agreement with the data of Shurdumov et al. [45]. At 22 mol% Na_2MoO_4, our measured liquidus temperatures were about 787°C and 768°C, respectively, in the presence and absence of $CO_2(g)$. This temperature shift of about 19°C is believed to be mainly attributed to the partial dissociation of $Na_2CO_{3(S3)}$ to form liquid Na_2O (dissolved in the molten salt phase) and $CO_2(g)$. The calculated isobar at 1 atm is displayed in Figure 4, and shows that such a dissociation occurs. However, it is calculated to be extremely limited (mole fraction of Na_2O of the order of 10^{-8}). The calculated liquidus temperature of the (78 mol% Na_2CO_3 + 22 mol% Na_2MoO_4) binary mixture is 779°C, and becomes about 775°C if 1 mol% of Na_2CO_3 decomposes into Na_2O (dissolved in the liquid) and $CO_2(g)$. This calculated decrease in temperature is consistent with the trend observed experimentally. When a $CO_2(g)$ saturated atmosphere was used in our DSC-TGA experiments, such a decomposition was avoided.

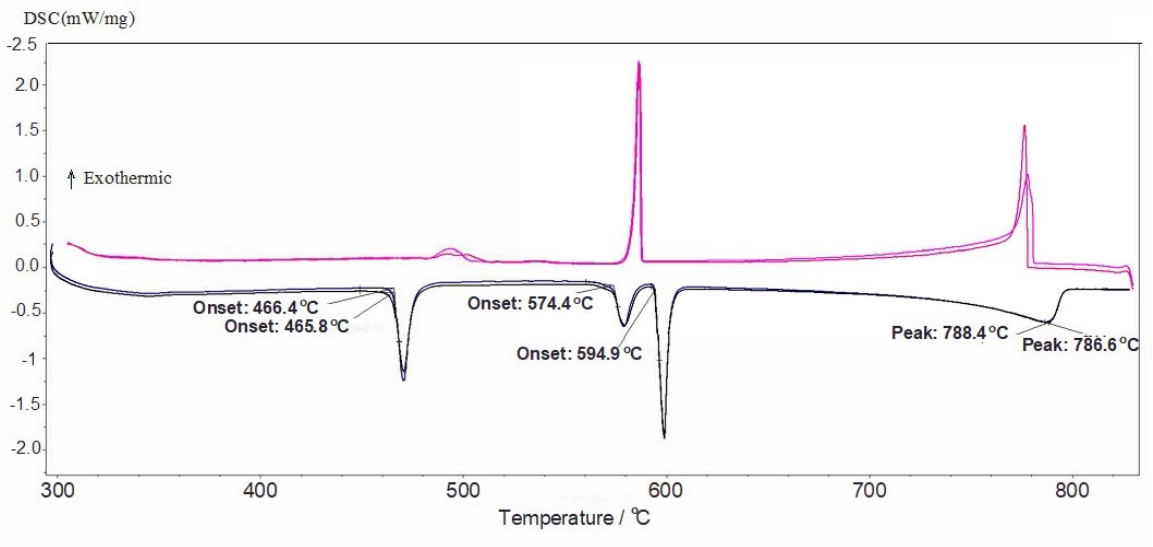

Figure 3 : DSC thermogram for the mixture (78 mol% Na_2CO_3 + 22 mol% Na_2MoO_4) in the presence of CO_2(g) (2nd and 3rd heating/cooling cycles only)

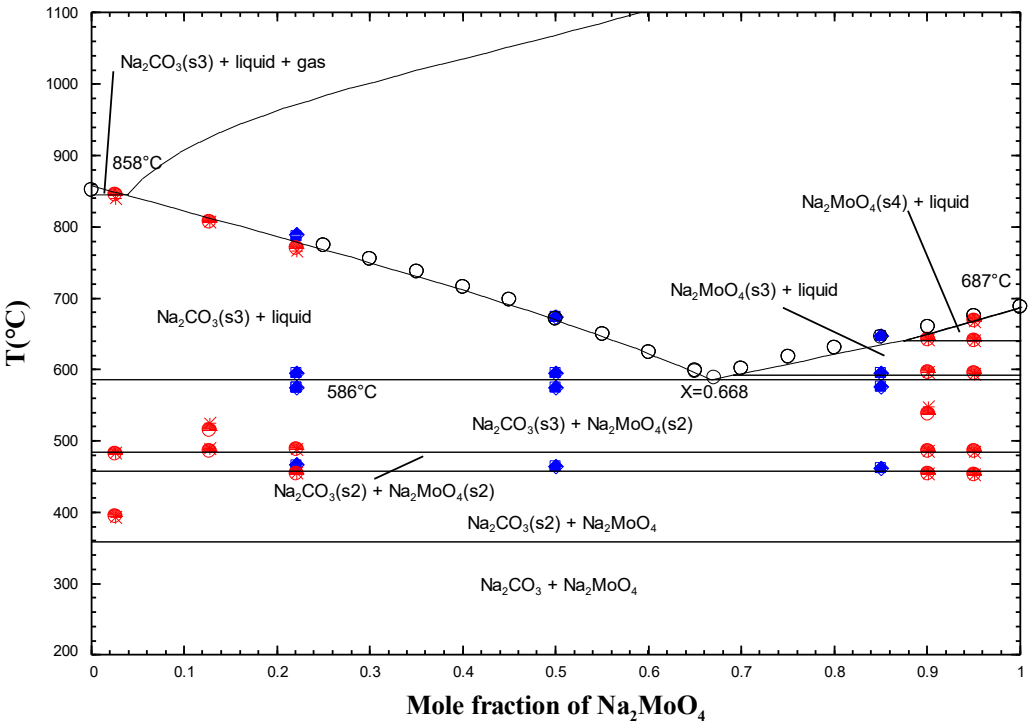

Figure 4 : Calculated (Na_2CO_3 + Na_2MoO_4) phase diagram in air ($p(O_2)$ = 0.21 atm). Experimental data from Shurdumov et al. [45] (○) and this work (red and blue symbols) (DSC, red ◓ : 2nd heating without CO_2(g), blue ⬓ : 2nd heating with CO_2(g), red ✳ : 3rd heating without CO_2(g), blue ⬘ : 3rd heating with CO_2(g))

6.4 The (K_2CO_3 + K_2MoO_4) system

The phase diagram has been investigated by Shurdumov et al. [45] using thermal analysis. A eutectic was reported by these authors at 41.0 mol% K_2MoO_4 and 728°C. The calculated characteristics of the eutectic are 40.7 mol% K_2MoO_4 and 729°C. No solid solutions or intermediate compounds were reported. The measured limiting slope of the K_2MoO_4 liquidus curve agrees with equation (11), which shows that there is negligible solid solubility of K_2CO_3 in the high-temperature allotrope $K_2MoO_{4(S3)}$. Since no phase diagram measurements are available for K_2CO_3-rich binary mixtures, it is not known if K_2MoO_4 is partly soluble in the high-temperature allotrope $K_2CO_{3(S2)}$, which is present as an "end-member" in the hexagonal hP22 solid solution. By analogy with the (Na_2CO_3 + Na_2MoO_4) binary system, this solid solubility was assumed to be negligible, and a constant interaction parameter of +100,000.0 J/mol was thus introduced in the model for hP22 (see Table 5). Note that K_2MoO_4 was introduced as an "end-member" in the latter model in order to reproduce its experimental solubilities in $K_2SO_{4(S2)}$, $K_2CrO_{4(S2)}$ and $Na_2MoO_{4(S4)}$ (which are all hexagonal with the $P6_3/mmc$ space group), as will be discussed later in the sections devoted to the (K_2SO_4 + K_2MoO_4), (K_2CrO_4 + K_2MoO_4) and (Na_2MoO_4 + K_2MoO_4) binary common-ion sub-systems.

A regular parameter of +100,000.0 J/mol was introduced in the oS28 solid solution in order to calculate a negligible solid solubility of K_2CO_3 in $K_2MoO_{4(S2)}$ (see Table 5).

The calculated (K_2CO_3 + K_2MoO_4) phase diagram in air ($p(O_2)$ = 0.21 atm) is compared to the measurements in Figure 5. According to the calculated isobar at 1 atm shown in this figure, $K_2CO_{3(S2)}$ partly decomposes into liquid K_2O (dissolved in the liquid solution) and CO_2(g). Nevertheless, this decomposition is calculated to be extremely limited (mole fraction of K_2O of the order of 10^{-10}).

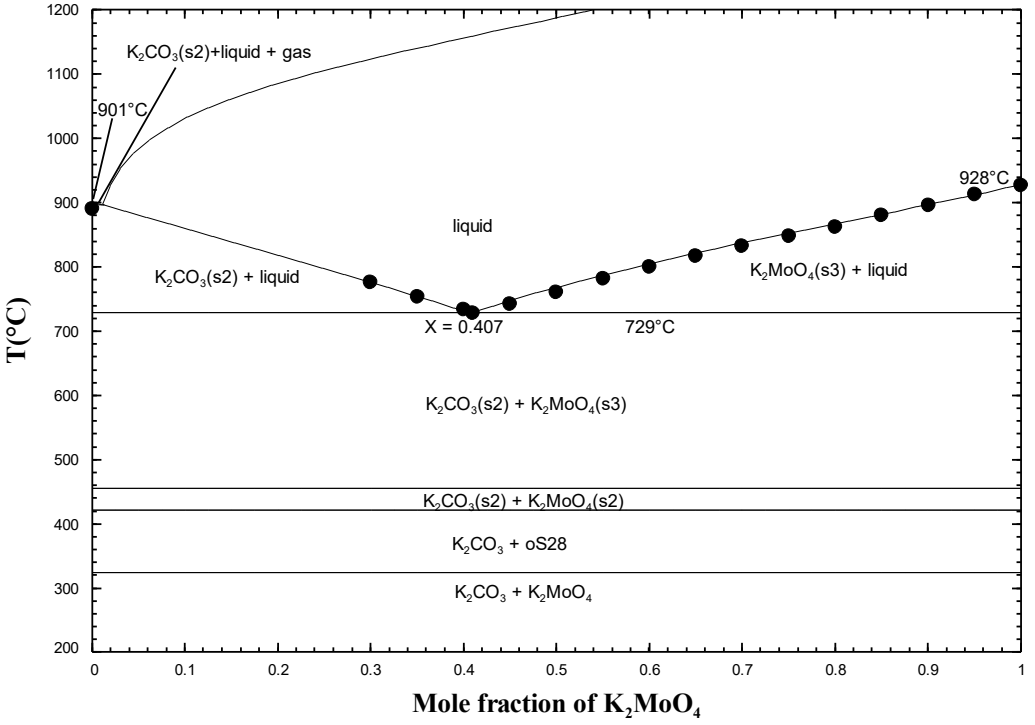

Figure 5 : Calculated (K_2CO_3 + K_2MoO_4) phase diagram in air ($p(O_2)$ = 0.21 atm). Experimental data from Shurdumov et al. [45] (●)

6.5 The (Na_2SO_4 + Na_2MoO_4) system

The phase diagram has been measured by the method of cooling curves with visual readings and optical observations, [46] and by the visual-polythermal method. [47, 48]

A complete solid solution at high temperatures exhibiting a minimum at about 70 mol% Na_2MoO_4 was reported by Boeke. [46] Belyaev and Doroshenko, [47] and Mateiko and Bukhalova [48] also observed the existence of a complete solid solution with a minimum at 75 mol% Na_2MoO_4 and 673ºC, and at 70 mol% Na_2MoO_4 and 672ºC, respectively.

The data of Boeke [46] suggest in particular a small solubility of Na_2SO_4 in the low-temperature allotrope $Na_2MoO_{4(S1)}$ (see Figure 7). In this work, DSC-TGA measurements were conducted for several binary mixtures with very high concentrations of Na_2MoO_4: 90, 92, 95, 98, and 99 mol% (from 120 to 730°C). As an example, the DSC thermogram for the binary composition (5 mol% Na_2SO_4 + 95 mol% Na_2MoO_4) is shown in Figure 6.

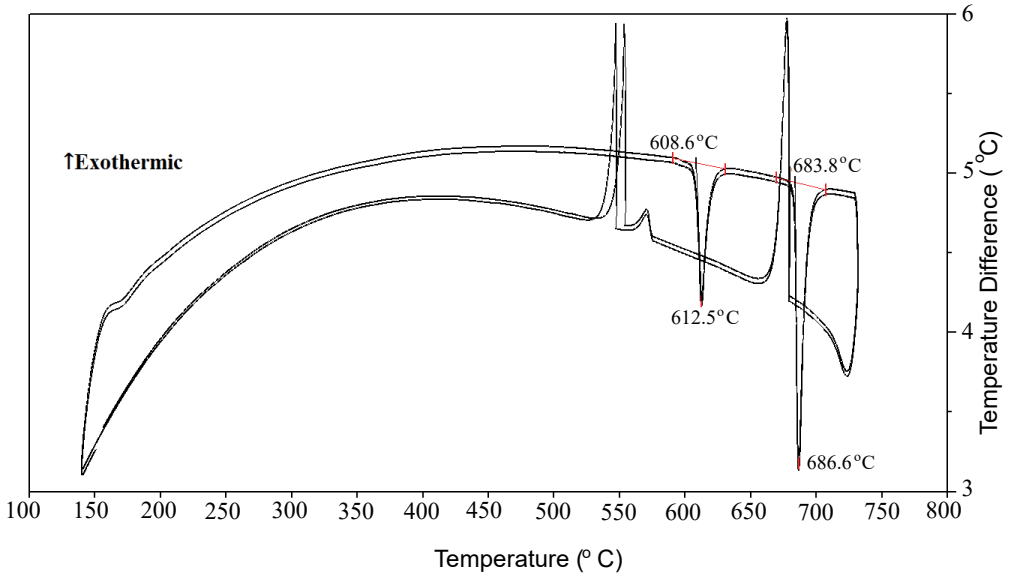

Figure 6 : DSC thermogram for the mixture (5 mol% Na_2SO_4 + 95 mol% Na_2MoO_4) (2nd and 3rd heating/cooling cycles only)

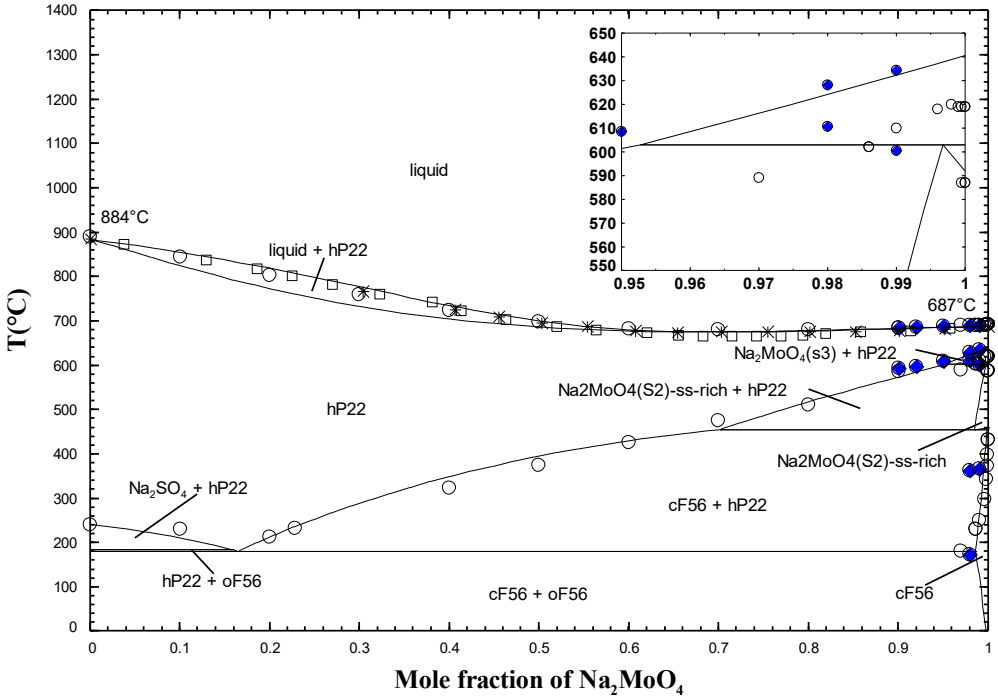

Figure 7 : Calculated (Na_2SO_4 + Na_2MoO_4) phase diagram in air ($p(O_2)$ = 0.21 atm). Experimental data from Boeke [46] (○), Belyaev and Doroshenko [47] (□), Mateiko and Bukhalova [48] (✳) and this work (blue symbols) (DSC, ◆ : average of temperatures from 2nd and 3rd heating runs). Insert: close-up of the calculated phase diagram near pure Na_2MoO_4

The calculated (Na_2SO_4 + Na_2MoO_4) phase diagram in air ($p(O_2)$ = 0.21 atm) is shown along with the measurements in Figure 7.

The high-temperature allotropes $Na_2SO_{4(S2)}$ and $Na_2MoO_{4(S4)}$ have the same hexagonal crystal structure and space group $P6_3/mmc$ (see Table 1), and therefore a high-temperature solid solution (hP22) was modeled over the entire composition range. Three interaction parameters (see Table 5) were introduced to best reproduce the experimental data of Boeke [46] at intermediate temperatures.

Then, the liquid solution was modeled in order to reproduce our experimental high-temperature data and those of [46-48]. No experimental data (such as enthalpy of mixing or activity data) were available to calibrate the liquid phase. As seen in Table 4, the two model parameters required for the liquid have a significant amplitude. The enthalpy of mixing of the liquid calculated at 900°C (that is, above the melting temperatures of the pure salts Na_2SO_4 and Na_2MoO_4) has a minimum of about -4.45 kJ/mol. Thus, the common-cation liquid displays negative deviations from ideality. It was expected to be close to ideal owing to the close similarity of the anionic radii (2.31 Å for SO_4^{2-} and 2.33 Å for MoO_4^{2-} [49]). The SO_4^{2-} and MoO_4^{2-} anions have a significant mass difference, which may lead to a substantial vibrational entropy at high temperatures. This may explain the negative deviations from ideality of the binary liquid.

In order to best reproduce our DSC-TGA measurements and the data of Boeke [46] at low temperatures, some solid solubility of Na_2SO_4 was introduced in $Na_2MoO_{4(S1)}$ (see the cF56 solid solution in Table 5). By analogy with the (Na_2CrO_4 + Na_2MoO_4) binary system (discussed later) for which Na_2CrO_4 is partly soluble in $Na_2MoO_{4(S2)}$, some solid solubility of Na_2SO_4 was also introduced in $Na_2MoO_{4(S2)}$ (see the $Na_2MoO_{4(S2)}$-ss-rich solid solution in Table 5). $Na_2SO_{4(S2)}$ and $Na_2CrO_{4(S2)}$ have the same crystal structure and space group (see Table 1). Therefore, the Gibbs energy of the "end-member" Na_2SO_4 in the $Na_2MoO_{4(S2)}$-ss-rich solid solution was that of $Na_2SO_{4(S2)}$ augmented by a positive Gibbs energy identical to that for the "end-member" Na_2CrO_4. The latter model parameter was obtained from reproduction of the available phase diagram data in (Na_2CrO_4 + Na_2MoO_4). Finally, a regular parameter of +100,000.0 J/mol was introduced in the oS28 solid solution to calculate a negligible solid solubility of Na_2MoO_4 in $Na_2SO_{4(S1)}$, and also in the oF56 solid solution to calculate negligible mutual solubility between $Na_2MoO_{4(S3)}$ and

$Na_2SO_{4(S3)}$ (see Table 5).

6.6 The (K_2SO_4 + K_2MoO_4) system

The phase diagram has been measured by the method of cooling curves with visual readings [50], and by the visual-polythermal method. [51, 52] Amadori [50] reported a complete solid solution at high temperatures with a very flat minimum at about 6°C below the melting temperature of K_2MoO_4 (that is, at about 920°C). Similarly, Bergman et al. [51], and Mateiko and Bukhalova [52] observed the formation of a complete solid solution with no marked minimum.

According to Amadori, [50] it was difficult to measure the thermal arrests at around 450°C, and between 50 and 90 mol% K_2MoO_4. This author suggested that K_2SO_4 and K_2MoO_4 are mutually soluble at intermediate temperatures, with the formation of a continuous solid solution.

In this work, DSC-TGA measurements were performed using the NETZSCH STA 449 F1 Jupiter® instrument for several binary mixtures with various contents of K_2MoO_4 : 60, 80, and 95 mol% (from 150 to 930°C). DSC-TGA measurements were conducted using the SDT Q600 TA Instrument over the same temperature range at 70 and 80 mol% K_2MoO_4. No systematic difference was observed between the two apparatuses, which were both used to investigate the (20 mol% K_2SO_4 + 80 mol% K_2MoO_4) mixture. As an example, the DSC thermogram for the binary composition (30 mol% K_2SO_4 + 70 mol% K_2MoO_4) is displayed in Figure 8.

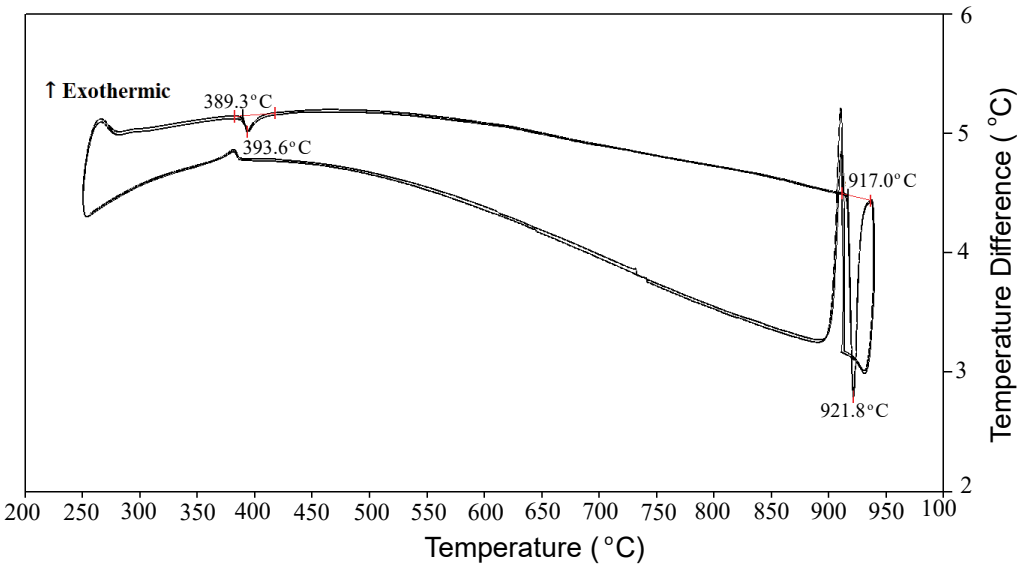

Figure 8 : DSC thermogram for the mixture (30 mol% K_2SO_4 + 70 mol% K_2MoO_4) (2nd and 3rd heating/cooling cycles only)

The calculated (K_2SO_4 + K_2MoO_4) phase diagram in air ($p(O_2)$ = 0.21 atm) is compared to the measurements in Figure 9. This phase diagram displays four different solid solutions : a high-temperature hexagonal solid solution (hP22) rich in $K_2SO_{4(S2)}$ and existing over a large composition range, a high-temperature trigonal solid solution ($K_2MoO_{4(S3)}$-ht-ss) rich in $K_2MoO_{4(S3)}$ and diluted in K_2SO_4, an orthorhombic low-temperature solid solution (oP28) rich in $K_2SO_{4(S1)}$ and diluted in K_2MoO_4, and an orthorhombic low-temperature solid solution (oS28) rich in $K_2MoO_{4(S2)}$ and diluted in K_2SO_4.

The high-temperature allotropes $K_2SO_{4(S2)}$ (hexagonal, $P6_3/mmc$) and $K_2MoO_{4(S3)}$ (trigonal, $P\bar{3}m1$) do not have the same crystal structure (see Table 1). Therefore, two terminal solid solutions (hP22 and $K_2MoO_{4(S3)}$-ht-ss) were introduced at high temperatures. The hP22 solid solution was first modeled to best reproduce the low-temperature data of Amadori; [50] two interaction parameters were required (see Table 5).

Simultaneously, some solubility of K_2MoO_4 in $K_2SO_{4(S1)}$ (oP28 solid solution) was introduced in order to improve the agreement between our calculations and the corresponding measurements [50] for K_2SO_4-rich mixtures. Note that $K_2SO_{4(S1)}$ and $K_2CrO_{4(S1)}$ are mutually soluble in oP28. The Gibbs energy of the "end-member" K_2MoO_4 in oP28 was selected in this work to best reproduce simultaneously the (K_2SO_4 + K_2MoO_4)

and (K_2CrO_4 + K_2MoO_4) experimental phase diagrams. (The latter system will be discussed later). Once the hP22 solid solution was optimized, the (K_2SO_4 + K_2MoO_4) liquid was modeled in order to best reproduce the high-temperature measurements. The $K_2MoO_{4(S3)}$-ht-ss solid solution was then modeled; the maximum solubility of K_2SO_4 in $K_2MoO_{4(S3)}$ was arbitrarily set to about 6 mol%.

Finally, some solubility of K_2SO_4 in $K_2MoO_{4(S2)}$ (oS28 solid solution) was introduced to best reproduce the low-temperature thermal arrest of Amadori [50] at 93.3 mol% K_2MoO_4 along with our low-temperature DSC thermal arrest at 95 mol% K_2MoO_4.

The Gibbs energy of the "end-member" K_2SO_4 in the oS28 solid solution was previously obtained by Lindberg et al. [14] upon optimization of the (K_2SO_4 + Na_2SO_4) binary system. A very negative (-26,000.0 J/mol) constant Redlich-Kister interaction parameter had to be introduced by us between K_2SO_4 and K_2MoO_4 in the oS28 solid solution (see Table 5).

No experimental data (such as enthalpy of mixing or activity data) were available to calibrate the (K_2SO_4 + K_2MoO_4) liquid phase. As seen in Table 4, this common-cation binary liquid exhibits small positive deviations from ideality. It was expected to be close to ideal owing to the very close similarity of the radii of the SO_4^{2-} and MoO_4^{2-} anions. [49]

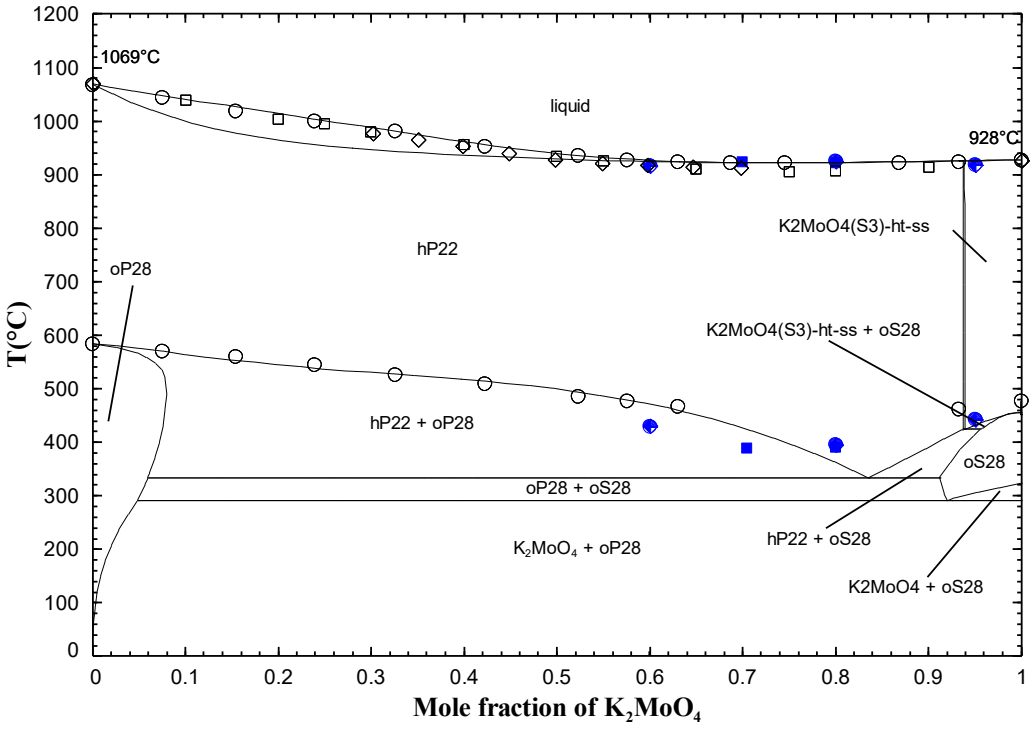

Figure 9 : Calculated (K_2SO_4 + K_2MoO_4) phase diagram in air ($p(O_2)$ = 0.21 atm). Experimental data from Amadori [50] (○) , Bergman et al. [51] (□), Mateiko and Bukhalova [52] (◇), and this work (blue symbols) (DSC using the NETZSCH STA 449 F1 Jupiter® instrument // ◓ : 2nd heating, ◆ : 3rd heating; DSC using the SDT Q600 TA Instrument // ■ : average of temperatures from 2nd and 3rd heating runs)

6.7 The (Na_2CrO_4 + Na_2MoO_4) system

The phase diagram has been measured by visual observation with a Pt/Pt-Rh thermocouple and a sensitive millivoltmeter. [48] Mateiko and Bukhalova [48] reported a complete solid solution at high temperatures with no minimum.

In this work, DSC-TGA measurements were conducted for several binary mixtures with various contents of Na_2MoO_4 : 10 mol% (from 200 to 790°C), 30 and 50 mol% (from 200 to 765°C), and 70 and 90 mol% (from 200 to 725°C).

As an example, the DSC thermogram for the binary composition (10 mol% Na_2CrO_4 + 90 mol% Na_2MoO_4) is shown in Figure 10.

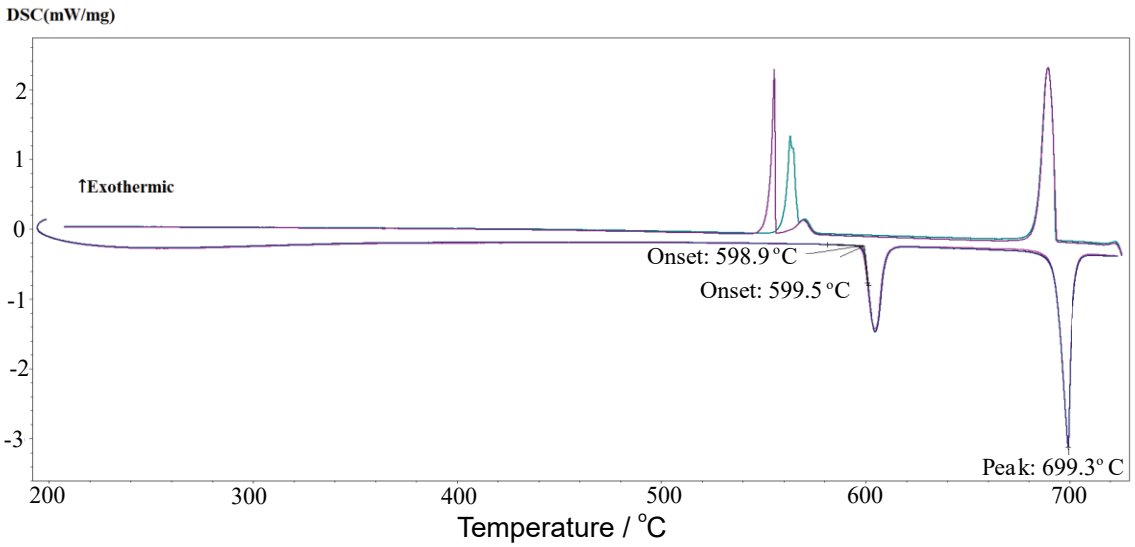

Figure 10 : DSC thermogram for the mixture (10 mol% Na_2CrO_4 + 90 mol%

Na_2MoO_4) (2nd and 3rd heating/cooling cycles only)

The calculated (Na_2CrO_4 + Na_2MoO_4) phase diagram in air ($p(O_2)$ = 0.21 atm) is shown along with the measurements in Figure 11. This phase diagram exhibits four different solid solutions : a high-temperature hexagonal solid solution (hP22) existing over the entire composition range (owing to the fact that $Na_2CrO_{4(S2)}$ and $Na_2MoO_{4(S4)}$ are both hexagonal with the space group $P6_3/mmc$ as seen in Table 1), an orthorhombic low-temperature solid solution (oS28) rich in $Na_2CrO_{4(S1)}$ and diluted in Na_2MoO_4, an intermediate-temperature orthorhombic solid solution ($Na_2MoO_{4(S2)}$-ss-rich) rich in $Na_2MoO_{4(S2)}$ and diluted in Na_2CrO_4, and a cubic low-temperature solid solution (cF56) rich in $Na_2MoO_{4(S1)}$ and diluted in Na_2CrO_4.

Those four solid solutions were modeled simultaneously to best reproduce our low-temperature DSC thermal arrests. Two positive interaction parameters were required for hP22. The Gibbs energy of the "end-member" Na_2CrO_4 in the $Na_2MoO_{4(S2)}$-ss-rich solid solution was selected to best reproduce our DSC data at 50, 70 and 90 mol% Na_2MoO_4. Then, by analogy with the (Na_2SO_4 + Na_2MoO_4) binary system (previously discussed) for which Na_2SO_4 is partly soluble in $Na_2MoO_{4(S1)}$, some solid solubility of Na_2CrO_4 was introduced in $Na_2MoO_{4(S1)}$ (see the cF56 solid solution in Table 5). $Na_2SO_{4(S1)}$ and $Na_2CrO_{4(S1)}$ have the same crystal structure and space group (see Table 1). Therefore, the Gibbs energy of the "end-member" Na_2CrO_4 in the cF56 solid solution was that of $Na_2CrO_{4(S1)}$ augmented by a positive Gibbs energy identical to that for the "end-member" Na_2SO_4, which was obtained from the low-temperature data of Boeke [46] in (Na_2SO_4 + Na_2MoO_4). The oS28 solid solution was then modeled to best reproduce our low-temperature DSC measurements at 10 and 30 mol% Na_2MoO_4. For the first composition, an intense peak was observed at about 406ºC while a low intensity peak was measured at about 446ºC. As seen in Figure 11, the former temperature is satisfactorily reproduced by our model.

The (Na_2CrO_4 + Na_2MoO_4) liquid phase was modeled to best reproduce the high-temperature phase equilibria. Again, no enthalpy of mixing or activity data were available to calibrate the liquid. As seen in Table 4, the three optimized model parameters are not large. The enthalpy of mixing of the liquid calculated at 800ºC (that is, above the melting

temperatures of the pure salts Na_2CrO_4 and Na_2MoO_4) is always positive, with a maximum value of about 0.84 kJ/mol. The common-cation liquid thus displays small positive deviations from ideality. It was expected to be close to ideal due to the very close similarity of the anionic radii (2.32 Å for CrO_4^{2-}, and 2.33 Å for MoO_4^{2-} [49]).

A regular parameter of +100,000.0 J/mol was introduced in the oF56 solid solution in order to calculate a negligible solid solubility of Na_2CrO_4 in $Na_2MoO_{4(S3)}$ (see Table 5).

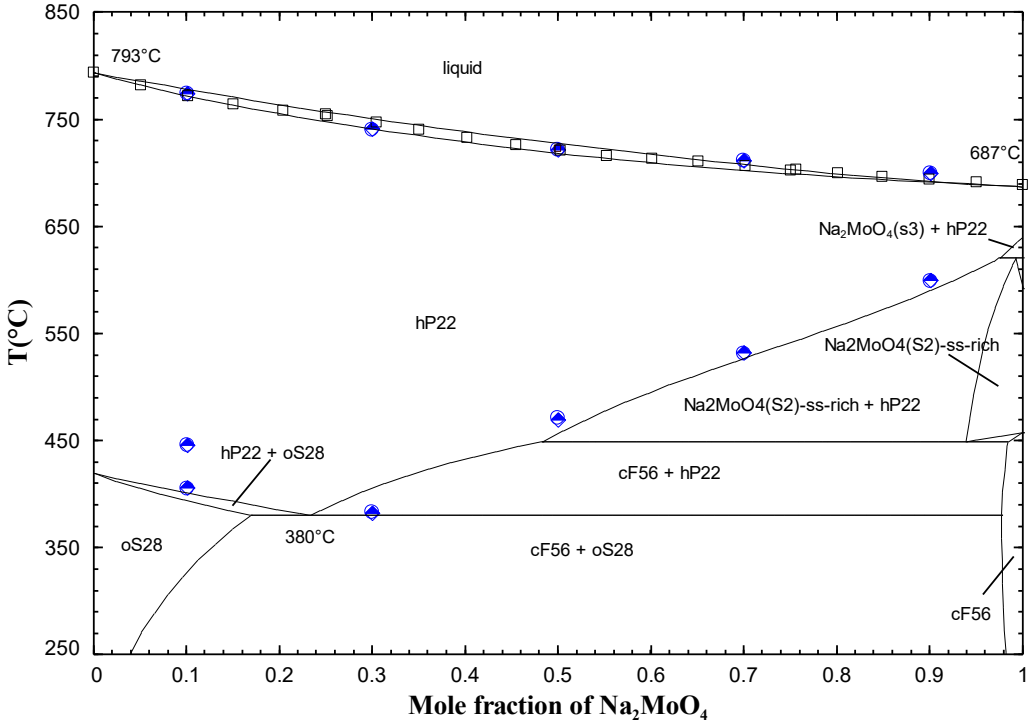

Figure 11 : Calculated (Na_2CrO_4 + Na_2MoO_4) phase diagram in air ($p(O_2)$ = 0.21 atm). Experimental data from Mateiko and Bukhalova [48] (□) and this work (blue symbols) (DSC, blue ○ : 2nd heating, blue ◆ : 3rd heating)

6.8 The (K_2CrO_4 + K_2MoO_4) system

The phase diagram has been measured by the method of cooling curves with visual readings, [50] and the visual-polythermal method. [52] A complete solid solution was reported at high temperatures, without any marked minimum. [52]

According to Amadori, [50] owing to the large mutual solubility existing between K_2CrO_4

and K_2MoO_4 at 25°C, a complete solid solution is likely to exist between $K_2CrO_{4(S1)}$ and $K_2MoO_{4(S2)}$ at 450°C, with the presence of a minimum in the range of 65 to 100 mol% K_2MoO_4.

In the present work, DSC-TGA measurements were performed for several binary mixtures with various contents of K_2MoO_4 : 75, 85, and 95 mol% (from 200 to 965°C). As an example, the DSC thermogram for the binary composition (15 mol% K_2CrO_4 + 85 mol% K_2MoO_4) is displayed in Figure 12.

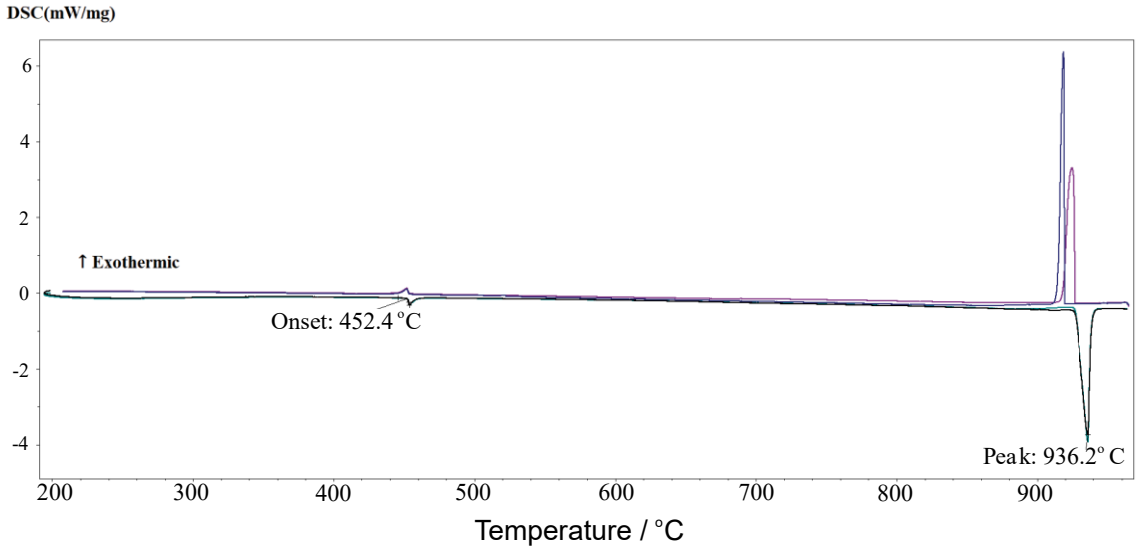

Figure 12 : DSC thermogram for the mixture (15 mol% K_2CrO_4 + 85 mol% K_2MoO_4) (2nd and 3rd heating/cooling cycles only)

The calculated (K_2CrO_4 + K_2MoO_4) phase diagram in air ($p(O_2)$ = 0.21 atm) is compared to the measurements in Figure 13. Its morphology is very similar to that of the (K_2SO_4 + K_2MoO_4) phase diagram discussed previously. There are four different solid solutions: a high-temperature hexagonal solid solution (hP22) rich in $K_2CrO_{4(S2)}$ and existing over a large composition range, a high-temperature trigonal solid solution ($K_2MoO_{4(S3)}$-ht-ss) rich in $K_2MoO_{4(S3)}$ and diluted in K_2CrO_4, an orthorhombic low-temperature solid solution (oP28) rich in $K_2CrO_{4(S1)}$ and diluted in K_2MoO_4, and an orthorhombic low-temperature solid solution (oS28) rich in $K_2MoO_{4(S2)}$ and diluted in K_2CrO_4. Since the high-temperature allotropes $K_2CrO_{4(S2)}$ (hexagonal, $P6_3/mmc$) and $K_2MoO_{4(S3)}$ (trigonal, $P\bar{3}m1$) do not have the same crystal structure (see Table 1), two terminal solid solutions (hP22 and

$K_2MoO_{4(S3)}$-ht-ss) were considered at high temperatures.

The hP22 solid solution was first modeled to best reproduce the low-temperature data of Amadori [50] and our low-temperature DSC thermal arrest at 75 mol% K_2MoO_4; three positive interaction parameters were necessary (see Table 5). Some solubility of K_2MoO_4 in $K_2CrO_{4(S1)}$ (oP28 solid solution) was introduced to improve the agreement between our calculations and the data of Amadori [50] for K_2CrO_4-rich mixtures. As explained previously, the Gibbs energy of the "end-member" K_2MoO_4 in oP28 was obtained by optimizing simultaneously the (K_2CrO_4 + K_2MoO_4) and (K_2SO_4 + K_2MoO_4) phase diagrams. The $K_2MoO_{4(S3)}$-ht-ss solid solution was then modeled to best reproduce our low-temperature DSC thermal arrest at 85 mol% K_2MoO_4.

Once the hP22 solid solution was optimized, the (K_2CrO_4 + K_2MoO_4) liquid was modeled in order to best reproduce the available high-temperature phase equilibria. No enthalpy of mixing or activity data were available to calibrate the liquid. As seen in Table 4, it exhibits positive deviations from ideality. The enthalpy of mixing of the liquid calculated at 1000°C (that is, above the temperatures of fusion of K_2CrO_4 and K_2MoO_4) has a maximum value of about 1.75 kJ/mol. The common-cation liquid was expected to be somewhat closer to ideal owing to the very close similarity of the radii of the CrO_4^{2-} and MoO_4^{2-} anions. [49]

Finally, some solubility of K_2CrO_4 in $K_2MoO_{4(S2)}$ (oS28 solid solution) was introduced to best reproduce the low-temperature measurement of Amadori [50] and our low-temperature DSC thermal arrest at 95 mol% K_2MoO_4. The Gibbs energy of the "end-member" K_2CrO_4 in the oS28 solid solution was previously selected by us [16] upon optimization of the (K_2CrO_4 + Na_2CrO_4) binary system ($K_2MoO_{4(S2)}$ and $Na_2CrO_{4(S1)}$ are mutually soluble). In this work, a very negative (-19,500.0 J/mol) constant Redlich-Kister interaction parameter had to be introduced between K_2CrO_4 and K_2MoO_4 in the oS28 solid solution (see Table 5).

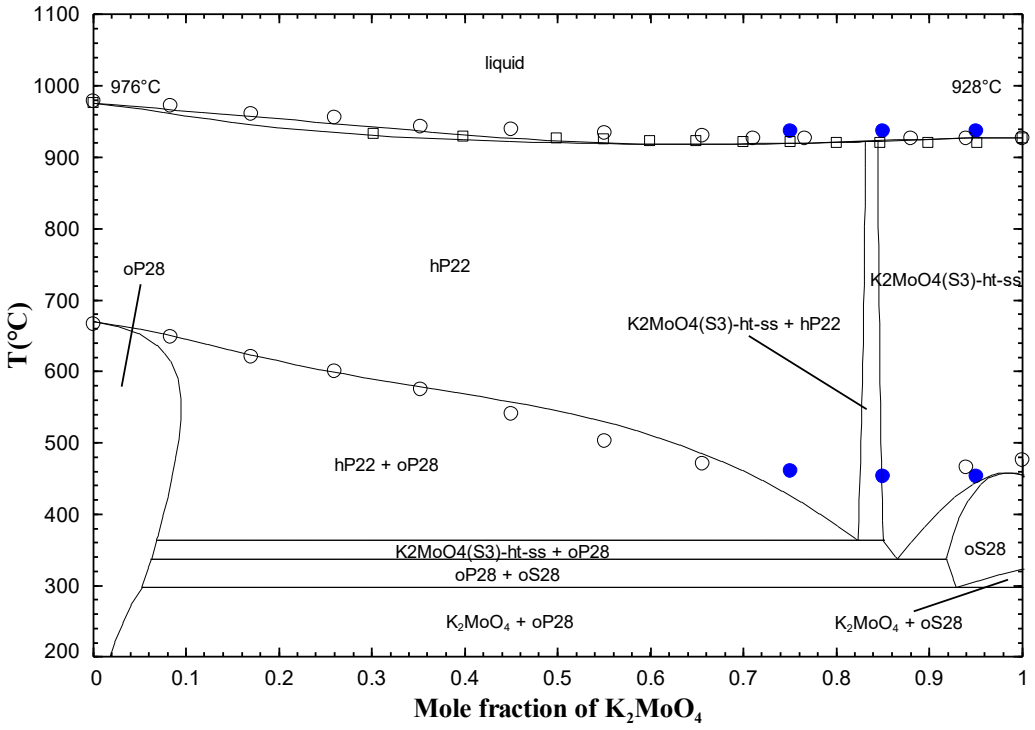

Figure 13: Calculated (K_2CrO_4 + K_2MoO_4) phase diagram in air ($p(O_2)$ = 0.21 atm). Experimental data from Amadori [50] (○), Mateiko and Bukhalova [52] (□) and this work (blue symbols) (DSC, blue ● : average of temperatures from 2nd and 3rd heating runs)

6.9 The (Na_2MoO_4 + K_2MoO_4) system

Several studies have been performed on the (Na_2MoO_4 + K_2MoO_4) binary phase diagram. [44, 53-55] Amadori [54] used the method of cooling curves with visual readings, while Belyaev and Sholokhovich [53] used the visual-polythermal method. The latter authors reported the formation of a complete solid solution at high temperatures, with the presence of a minimum at around 21 mol% K_2MoO_4 and 656°C. According to Amadori, [54] two terminal solid solutions (based on the high-temperature allotropes of Na_2MoO_4 and K_2MoO_4) were formed at high temperatures, and the intermediate compound $Na_2MoO_4.K_2MoO_4$ was formed upon cooling.

Using the visual-polythermal method, Bukhalova and Mateiko [44] observed a eutectic at 19 mol% K_2MoO_4 and 667°C, and also two transition points at 37 mol% K_2MoO_4 and 686°C,

and at 54 mol% K_2MoO_4 and 737°C, respectively. They suggested the formation of two intermediate compounds ($Na_2MoO_4.K_2MoO_4$ and $Na_2MoO_4.2K_2MoO_4$) melting incongruently.

Ding et al. [55] conducted DTA and XRD measurements at both low and high temperatures. In particular, they investigated by XRD two (Na_2MoO_4 + K_2MoO_4) binary mixtures at 50 and 66.7 mol% K_2MoO_4, and the high-temperature allotropes of Na_2MoO_4 and K_2MoO_4. They ruled out the eutectic and the two intermediate compounds reported by Bukhalova and Mateiko. [44] According to Ding et al. [55], the visual-polythermal method used by Bukhalova and Mateiko to identify incongruently melting compounds cannot provide reliable results.

The calculated (Na_2MoO_4 + K_2MoO_4) phase diagram in air ($p(O_2)$ = 0.21 atm) is shown along with the measurements in Figure 14. This phase diagram displays five different solid solutions : a high-temperature hexagonal solid solution (hP22) rich in $Na_2MoO_{4(S4)}$ and existing over a large composition range, a high-temperature trigonal solid solution ($K_2MoO_{4(S3)}$-ht-ss) rich in $K_2MoO_{4(S3)}$ and diluted in Na_2MoO_4, an intermediate-temperature orthorhombic solid solution (oF56) rich in $Na_2MoO_{4(S3)}$ and diluted in K_2MoO_4, a low-temperature orthorhombic solid solution (oS28) rich in $K_2MoO_{4(S2)}$ and diluted in Na_2MoO_4, and the non-stoichiometric phase $K_3Na(MoO_4)_2$ (molybdenum-glaserite, hP14). These various solid solutions and the optimized model parameters are described in detail in Table 5.

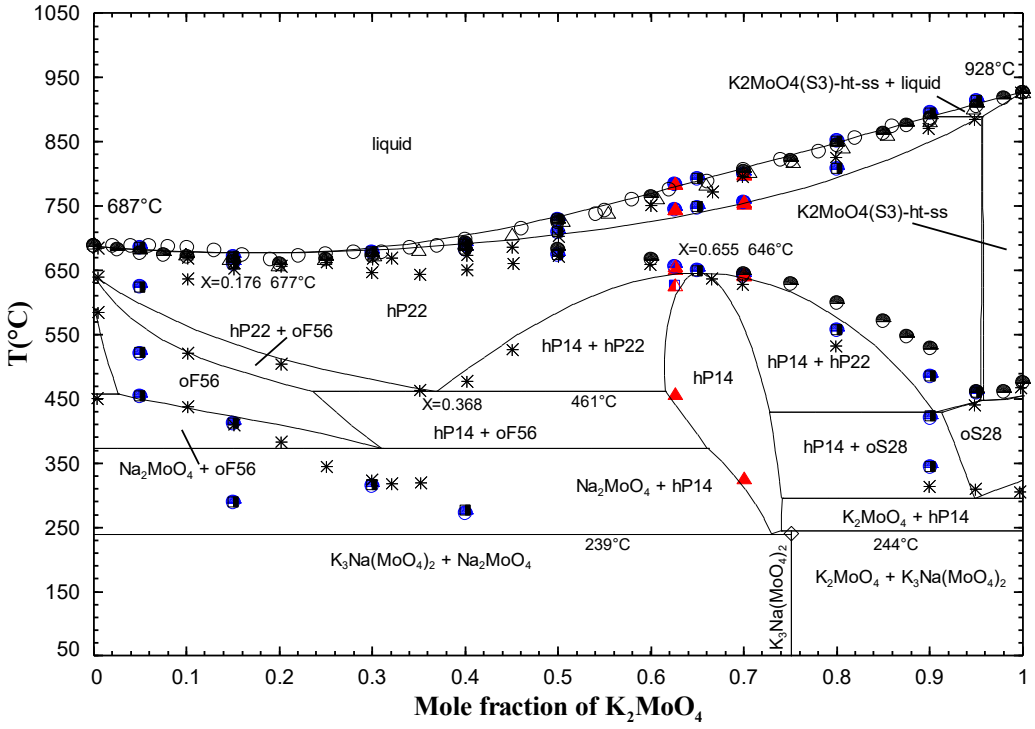

Figure 14: Calculated (Na_2MoO_4 + K_2MoO_4) phase diagram in air ($p(O_2)$ = 0.21 atm). Experimental data from Amadori [54] (◓), Belyaev and Sholokhovich [53] (△), Bukhalova and Mateiko [44] (○) , Ding et al. [55] (✳), Fabry et al. [40] (◇) and this work (red and blue symbols) (DSC , red ▲ : 1st heating for molybdenum-glaserite equilibrated at 400°C for 4 weeks, red ◭ : 2nd heating for molybdenum-glaserite equilibrated at 400°C for 4 weeks, red ◭ : 3rd heating for molybdenum-glaserite equilibrated at 400°C for 4 weeks, blue ◓ : 2nd heating for mechanical mixtures of pre-treated reagents, blue ◧ : 3rd heating for mechanical mixtures of pre-treated reagents)

Ding et al. [55] claimed that the high temperature allotropes of Na_2MoO_4 and K_2MoO_4 are isomorphic (i.e. same crystal structure and space group). However, based on our previous work, [4] $Na_2MoO_{4(S4)}$ (hexagonal, $P6_3/mmc$) and $K_2MoO_{4(S3)}$ (trigonal, $P\bar{3}m1$) do not have the same crystal structure (see Table 1). Therefore, two terminal solid solutions (hP22 and $K_2MoO_{4(S3)}$-ht-ss) were modeled at high temperatures in the present work.

For the molybdenum-glaserite phase $K_3Na(MoO_4)_2$, a solid-solid transition occurs at 513K [40] between a stoichiometric compound (monoclinic, space group C2/c), which is stable at

room temperature, and a non-stoichiometric phase (trigonal, $P\bar{3}m1$). [40, 56] There is some similarity with cryolite (Na_3AlF_6), for which a solid-solid transition occurs at about 834K between a stoichiometric compound (monoclinic, space group $P2_1/n$) and a non-stoichiometric phase (cubic, space group Fm3m). [57]

As shown in Table 5, the high-temperature non-stoichiometric glaserite phase (hP14) was modeled with the following sublattice structure : $(K^+, Na^+)_3(Na^+)(SO_4^{2-}, CrO_4^{2-}, MoO_4^{2-})_2$. The sulfur-glaserite [14] and chrome-glaserite [16] phases were modeled previously, and the corresponding model parameters were used directly in this work. To model the molybdenum-glaserite phase, the two new "end-members" $K_3Na(MoO_4)_2$ and $Na_3Na(MoO_4)_2$ were added in the existing hP14 solid solution. Their Gibbs energies were the only model parameters. That is, no interaction parameters were required in this work. To our knowledge, the enthalpy change for the solid-solid transition between the two forms of molybdenum-glaserite has not been measured. As a first approximation, the corresponding entropy change was estimated as half that for the transition $Na_2MoO_{4(S1)} = Na_2MoO_{4(S2)}$ plus 1.5 times that for the transition $K_2MoO_{4(S1)} = K_2MoO_{4(S2)}$. Note that the temperatures and enthalpy changes for these two solid-solid transitions were directly taken from our previous study. [4]

The enthalpy change for the solid-solid transition of $K_3Na(MoO_4)_2$ was estimated as 21,733.4 J/mol at 513K. The low-temperature stoichiometric compound $K_3Na(MoO_4)_2$ was introduced in this work. Its Gibbs energy was estimated by starting with a Gibbs energy of formation from the pure end-members [$0.5\ Na_2MoO_{4(S1)} + 1.5\ K_2MoO_{4(S1)} = K_3Na(MoO_4)_{2(S)}$] equal to zero. Then, $\Delta H^{\circ}_{298.15\,K}$ and $S^{\circ}_{298.15\,K}$ were adjusted to best reproduce the experimental temperature [40] and assessed enthalpy change for the solid-solid transition of molybdenum-glaserite. The reactions $0.055\ Na_2MoO_{4(S1)} + 0.945\ K_3Na(MoO_4)_{2(S)} = 0.973$ hP14 and $K_3Na(MoO_4)_{2(S)} = 0.961$ hP14 $+ 0.079\ K_2MoO_{4(S1)}$ were calculated at 239°C (enthalpy change of 21,746 J/mol) and 244°C (enthalpy change of 20,346 J/mol), respectively.

The optimized thermodynamic properties ($\Delta H^{\circ}_{298.15\,K}$, $S^{\circ}_{298.15\,K}$, and C_P) of the stoichiometric compound $K_3Na(MoO_4)_2$ are given in Table 2. The Open Quantum Materials Database (OQMD) [58, 59] reported an enthalpy of formation at 0 K of -3,139,247 J/mol derived from Density Functional Theory (DFT) calculations. The corresponding

value given in Materials Project [60] is -2,955,539 J/mol.

In this work, DSC-TGA measurements were conducted for mechanical mixtures of the pre-treated reagents Na_2MoO_4 and K_2MoO_4. Nine different binary mixtures with various contents of K_2MoO_4 were investigated : 5, 15, 30, 40 and 50 mol% (from 45 to 750°C), 65 mol% (from 45 to 860°C), 80 mol% (from 45 to 890°C), and 90 and 95 mol% (from 45 to 950°C). In addition, DSC-TGA measurements were performed for the molybdenum-glaserite composition of (35 mol% Na_2MoO_4 + 65 mol% K_2MoO_4) equilibrated at 400ºC for four weeks, to which an excess of Na_2MoO_4 or K_2MoO_4 was added subsequently. Two binary mixtures at 62.5 and 70 mol% K_2MoO_4 were studied under those conditions, from 180 to 840°C. All measured thermal arrests are listed in the Supporting Information (see Tables S8 and S9). As an example, the DSC thermogram for the mechanical mixture (70 mol% Na_2MoO_4 + 30 mol% K_2MoO_4) is displayed in Figure 15.

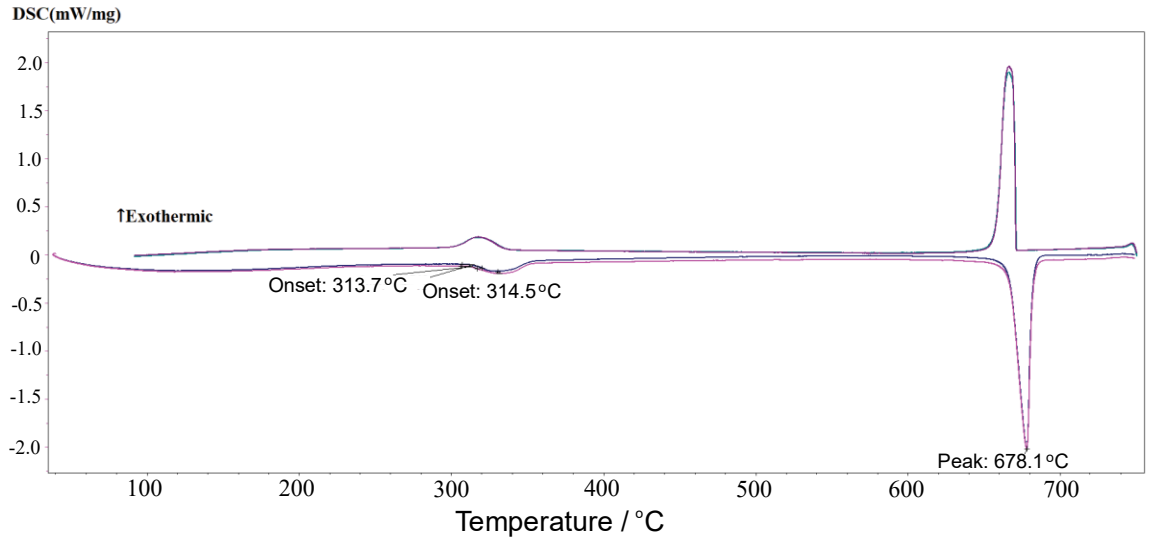

Figure 15 : DSC thermogram for the mixture (70 mol% Na_2MoO_4 + 30 mol% K_2MoO_4) (2nd and 3rd heating/cooling cycles only)

No experimental data (such as enthalpy of mixing or activity data) were available to calibrate the (Na_2MoO_4 + K_2MoO_4) liquid phase. First, a constant parameter of -1,419.6 J/mol was used by analogy with the (Na_2SO_4 + K_2SO_4) [14] and (Na_2CrO_4 + K_2CrO_4) [16] liquid

phases, which were modeled previously. However, it was not possible to obtain a set of parameters for the five solid solutions permitting the calculation of a satisfactory phase diagram. Finally, two model parameters (including one composition-dependent parameter) were used for the (Na_2MoO_4 + K_2MoO_4) liquid (see Table 4). The enthalpy of mixing of the liquid calculated at 950ºC (that is, above the temperatures of fusion of Na_2MoO_4 and K_2MoO_4) has a minimum value of about -0.28 kJ/mol, which is reasonable. The common-anion liquid was expected to be close to ideal owing to the similarity of the radii of the Na^+ and K^+ cations. [61]

Then, the hexagonal solid solution (hP22) was modeled in order to best reproduce the high-temperature measurements (i.e. phase equilibria with the liquid solution) and the maximum extension of the molybdenum-glaserite phase (hP14) at about 646ºC and 65.5 mol% K_2MoO_4. Only one positive model parameter was required for hP22, and the Gibbs energies of the two "end-members" $K_3Na(MoO_4)_2$ and $Na_3Na(MoO_4)_2$ in hP14 were optimized simultaneously. To model the oF56 solid solution, the data of Ding et al. [55] were favoured, and four model parameters were used : two parameters (including one temperature-dependent parameter) for the Gibbs energy of the "end-member" K_2MoO_4, and two Redlich-Kister interaction parameters. As seen in Figure 14, the calculated extent of oF56 is reasonable, and the eutectoid reaction hP22 = oF56 + hP14 is calculated at about 36.8 mol% K_2MoO_4 and 461ºC. Finally, the $K_2MoO_{4(S3)}$-ht-ss and oS28 solid solutions were modeled to best reproduce, respectively, the high-temperature and low-temperature measurements of Amadori [54] and Ding et al. [55] The maximum solubility of Na_2MoO_4 in $K_2MoO_{4(S3)}$ was arbitrarily set to about 4.3 mol%.

6.10 The ($K_2Cr_2O_7$ + $K_2Mo_2O_7$) system

The phase diagram has been measured by Amadori [62] using the method of cooling curves with visual readings, and a complete solid solution was reported at high temperatures.

The calculated ($K_2Cr_2O_7$ + $K_2Mo_2O_7$) phase diagram in air ($p(O_2)$ = 0.21 atm) is compared to the measurements in Figure 16.

To our knowledge, there are no enthalpy of mixing or activity data to calibrate the liquid

solution. The latter was assumed to be ideal (that is, $\Delta g_{K_2/(Cr_2O_7)(Mo_2O_7)} = 0$) owing to the expected similarity of the radii of the anions $Cr_2O_7^{2-}$ and $Mo_2O_7^{2-}$. As seen in Table 1, the high-temperature allotropes $K_2Cr_2O_{7(S2)}$ and $K_2Mo_2O_{7(S2)}$ are both monoclinic with the space group $P2_1/c$. Therefore, a high-temperature solid solution ($K_2Cr_2O_7$(s.s)) was introduced over the entire composition range. One positive regular parameter was used to reproduce the experimental solidus of Amadori [62] from 0 to about 90 mol% $K_2Mo_2O_7$. Amadori reported for $K_2Mo_2O_7$ a melting temperature about 14°C lower than our selected value, which was based on the available data from the literature [17]. Hence, it was not possible to reproduce the experimental solidus of Amadori [62] above 90 mol% $K_2Mo_2O_7$.

The low-temperature allotropes $K_2Cr_2O_{7(S1)}$ and $K_2Mo_2O_{7(S1)}$ are both triclinic with the space group $P\bar{1}$ (see Table 1). Thus, a low-temperature solid solution (aP44) was modeled over the entire composition range. Owing to the lack of relevant phase diagram data, as a first approximation, a regular parameter identical to that in the $K_2Cr_2O_7$(s.s) solid solution was used.

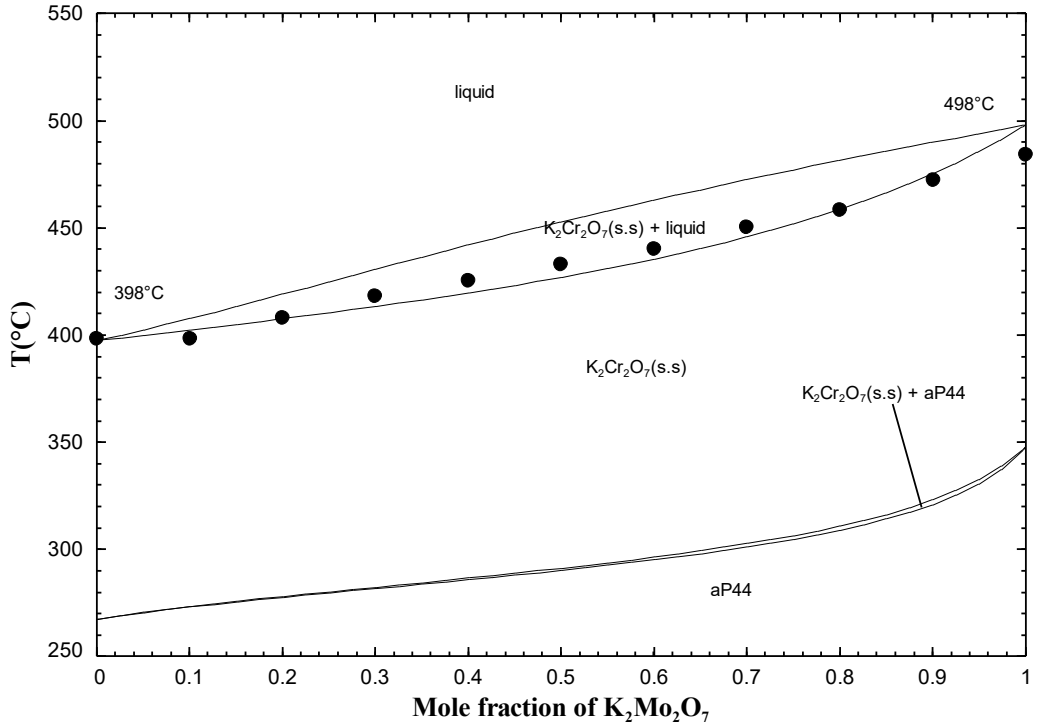

Figure 16 : Calculated ($K_2Cr_2O_7$ + $K_2Mo_2O_7$) phase diagram in air ($p(O_2)$ = 0.21 atm). Experimental data from Amadori [62] (●)

6.11 The (Na_2MoO_4 + $Na_2Mo_2O_7$) system

The (Na_2MoO_4 + MoO_3) phase diagram has been measured by thermal analysis [63, 64] and DTA. [65] The relevant compositions were expressed in terms of the (Na_2MoO_4 + $Na_2Mo_2O_7$) binary sub-system. These various authors reported a eutectic at 37.0 mol% $Na_2Mo_2O_7$ and 551ºC, 35.1 mol% $Na_2Mo_2O_7$ and 556ºC, and 25.0 mol% $Na_2Mo_2O_7$ and 559ºC, respectively. The calculated characteristics of the eutectic are 35.4 mol% $Na_2Mo_2O_7$ and 555ºC. Using thermal analysis, Mokhosoev and Fedorov [66] measured the ($Na_2Mo_2O_7$ + Na_2CO_3) phase diagram, and claimed that "this system can be represented as two binary systems : ($Na_2Mo_2O_7$ + Na_2MoO_4) and (Na_2MoO_4 + Na_2CO_3)". Measurements were provided graphically for the ($Na_2Mo_2O_7$ + Na_2MoO_4) phase diagram, and a eutectic was reported at 40.0 mol% $Na_2Mo_2O_7$ and 538ºC.

The calculated (Na_2MoO_4 + $Na_2Mo_2O_7$) phase diagram in air ($p(O_2)$ = 0.21 atm) is shown along with the measurements in Figure 17. The data of Mokhosoev and Fedorov [66] were discarded since it is not clear how they were obtained. Also, the corresponding experimental liquidus of $Na_2Mo_2O_7$ substantially disagrees with those of the other studies. [63-65] The measurements of Groschuff [63] were favoured in this work since, at the same time, this author obtained satisfactory data for the (K_2CrO_4 + $K_2Cr_2O_7$) phase diagram. [16] As seen in Table 4, one of the two model parameters required for the (Na_2MoO_4 + $Na_2Mo_2O_7$) liquid has a significant amplitude. The enthalpy of mixing of the liquid calculated at 700ºC (that is, above the melting temperatures of the pure salts Na_2MoO_4 and $Na_2Mo_2O_7$) has a maximum of about 1.07 kJ/mol. Thus, the common-cation liquid exhibits positive deviations from ideality. It was expected to be relatively close to ideal owing to the similarity of the two anions.

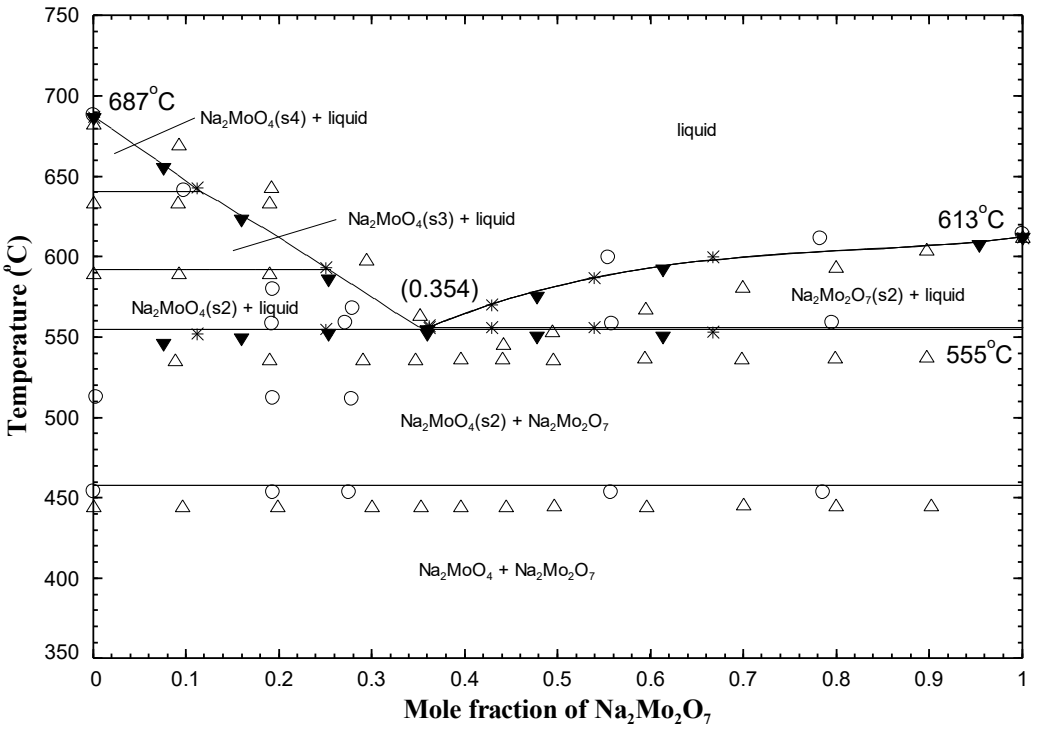

Figure 17 : Calculated (Na_2MoO_4 + $Na_2Mo_2O_7$) phase diagram in air ($p(O_2)$ = 0.21 atm). Experimental data from Groschuff [63] (▼), Hoermann [64] (✳), Caillet [65] (○), and Mokhosoev and Fedorov [66] (△)

6.12 The (K_2MoO_4 + $K_2Mo_2O_7$) system

The (K_2MoO_4 + MoO_3) phase diagram has been measured by thermal analysis [64, 67] and DTA. [65] The relevant compositions were expressed in terms of the (K_2MoO_4 + $K_2Mo_2O_7$) binary sub-system. Amadori [67] and Caillet [65] reported a eutectic at 475-480ºC, and 61.3 mol% $K_2Mo_2O_7$ and 480ºC, respectively. The calculated (K_2MoO_4 + $K_2Mo_2O_7$) phase diagram in air ($p(O_2)$ = 0.21 atm) is compared to the measurements in Figure 18. The (K_2MoO_4 + $K_2Mo_2O_7$) binary liquid was assumed to be ideal (that is, $\Delta g_{K_2/(MoO_4)(Mo_2O_7)} = 0$). Under those conditions, the experimental liquiduses of K_2MoO_4 from Amadori [67] and Hoermann [64] are satisfactorily reproduced by the model up to about 80 mol% $K_2Mo_2O_7$. The calculated characteristics of the eutectic are 88.3 mol% $K_2Mo_2O_7$ and 484ºC. The latter is close to the measured eutectic temperatures of Amadori [67] and Caillet. [65]

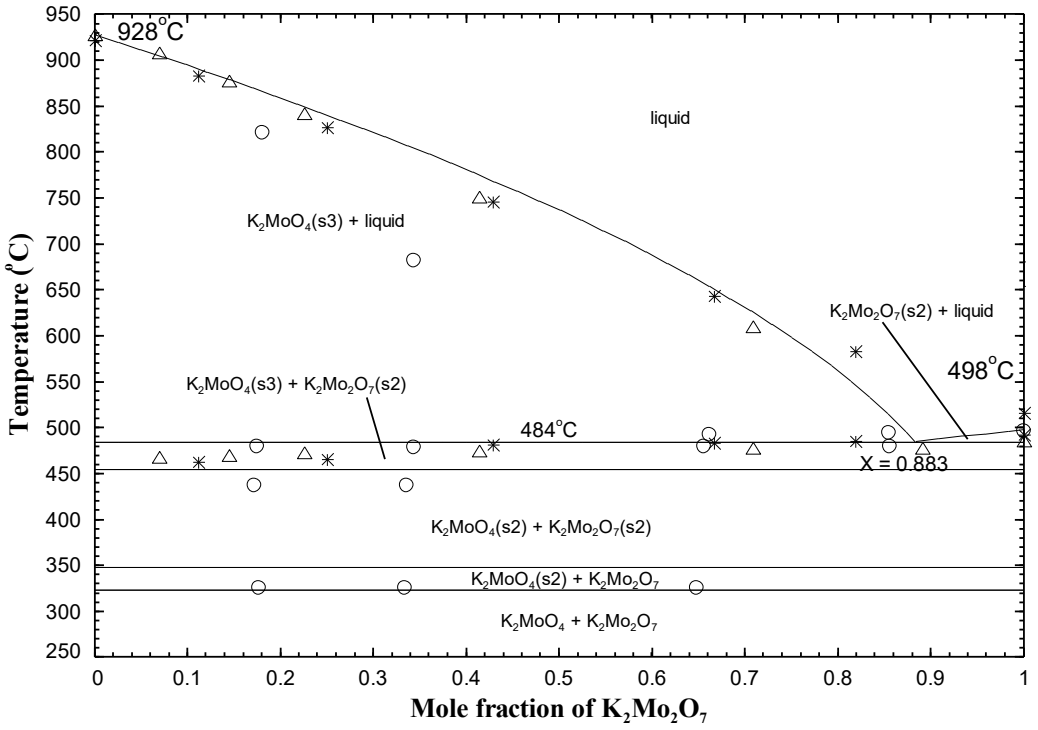

Figure 18: Calculated (K_2MoO_4 + $K_2Mo_2O_7$) phase diagram in air ($p(O_2)$ = 0.21 atm). Experimental data from Amadori [67] (△), Hoermann [64] (✳), and Caillet [65] (○)

7. Molybdate-based common-cation ternary sub-systems : (Na_2SO_4 + Na_2CrO_4 + Na_2MoO_4)

To our knowledge, experimental data are available only for the (Na_2SO_4 + Na_2CrO_4 + Na_2MoO_4) sub-system. The liquidus surface of this system was investigated by Mateiko and Bukhalova [48] using visual observations. Six isoplethal sections were measured. The calculated liquidus projection is shown in Figure 19; the hexagonal solid solution hP22 precipitates from the liquid phase over the entire composition range. As an example, three calculated isoplethal sections are compared to the available data in Figures 20 to 22. The remaining three isoplethal sections are given in the Supplementary Information (see Figures S2 to S4). No ternary excess parameter was included for the liquid phase. That is, calculations were made using solely the optimized model parameters for the three

common-cation binary sub-systems. The (Na_2SO_4 + Na_2CrO_4) binary sub-system was modeled previously, [16] and the corresponding model parameters were used directly in this work. Measurements in Figures 20, 22, S2 and S4 agree better with the calculated liquidus whereas data in Figure 21 agree better with the calculated solidus. Overall, agreement between the calculations and the measurements of Mateiko and Bukhalova [48] is satisfactory.

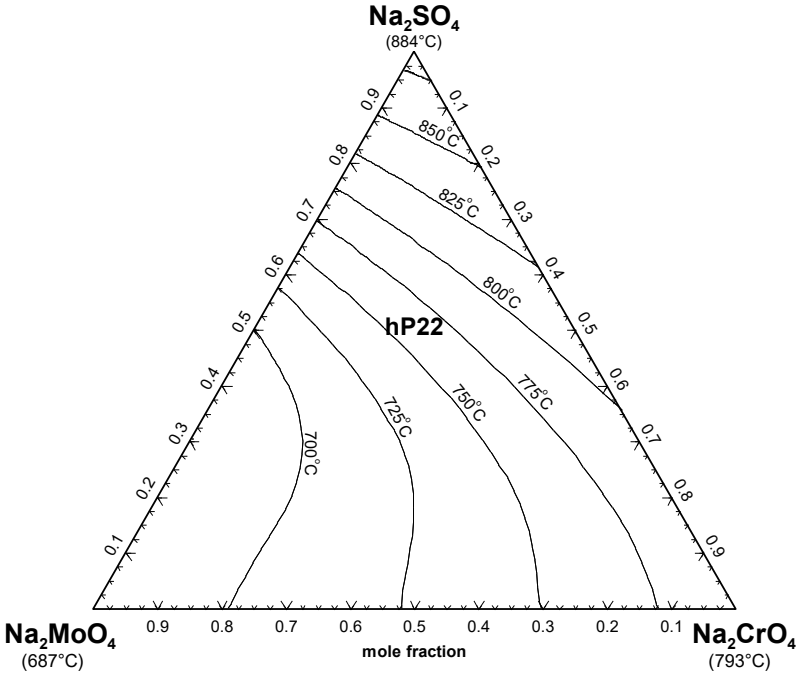

Figure 19 : Calculated liquidus projection of the (Na_2SO_4 + Na_2CrO_4 + Na_2MoO_4) system

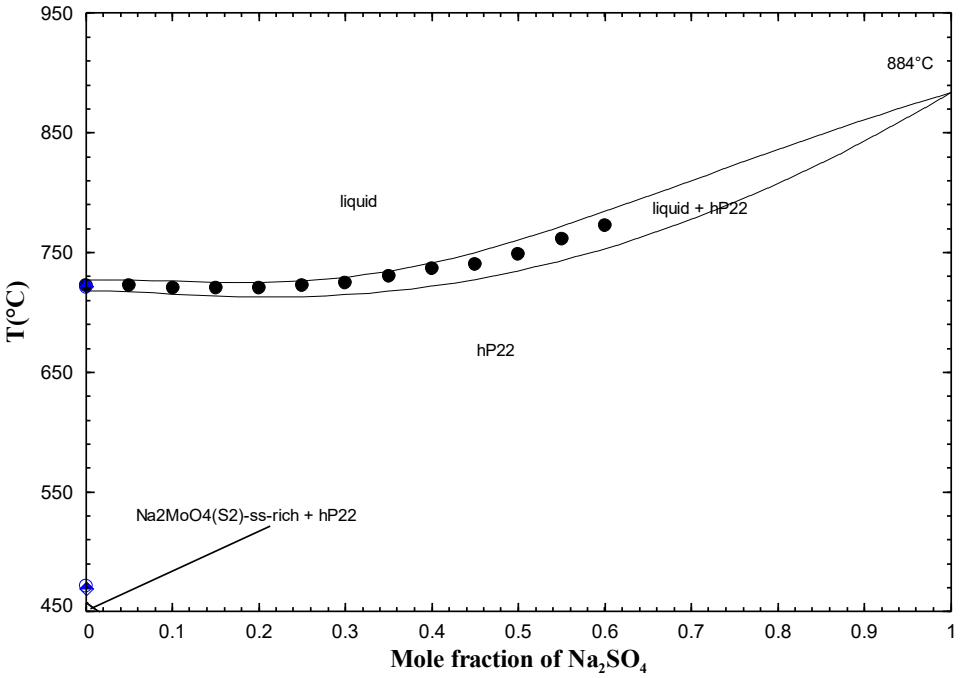

Figure 20 : Calculated isoplethal section in the (Na_2SO_4 + Na_2CrO_4 + Na_2MoO_4) system ((Na_2CrO_4)$_{0.5}$(Na_2MoO_4)$_{0.5}$-Na_2SO_4). Experimental data from Mateiko and Bukhalova [48] (●) and this work (blue symbols) (DSC, blue ○ : 2nd heating, blue ◆ : 3rd heating)

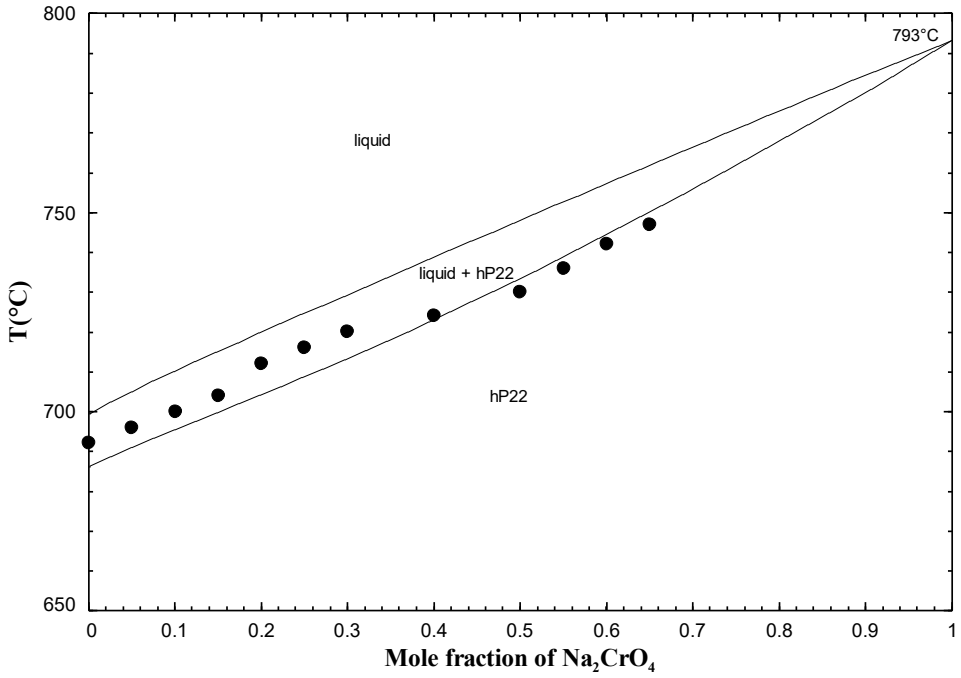

Figure 21 : Calculated isoplethal section in the (Na_2SO_4 + Na_2CrO_4 + Na_2MoO_4)

system ($(Na_2SO_4)_{0.5}(Na_2MoO_4)_{0.5}$-$Na_2CrO_4$). Experimental data from Mateiko and Bukhalova [48] (●)

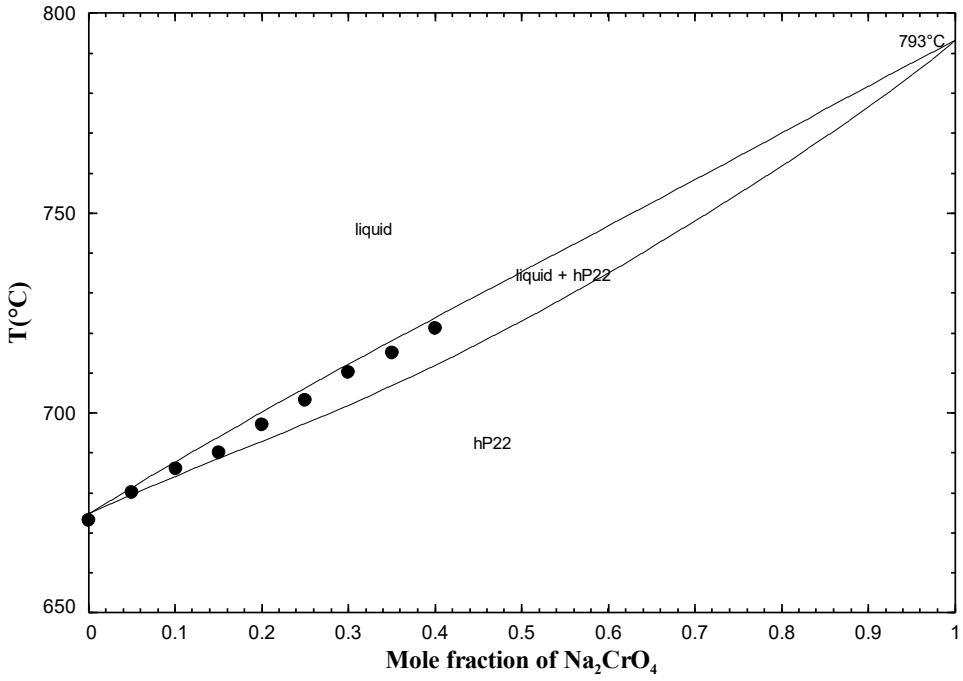

Figure 22 : Calculated isoplethal section in the (Na_2SO_4 + Na_2CrO_4 + Na_2MoO_4) system ($(Na_2SO_4)_{0.3}(Na_2MoO_4)_{0.7}$-$Na_2CrO_4$). Experimental data from Mateiko and Bukhalova [48] (●)

8. Molybdate-based ternary reciprocal sub-systems : (NaCl + KCl + Na_2MoO_4 + K_2MoO_4)

To our knowledge, experimental data are available only for the (NaCl + KCl + Na_2MoO_4 + K_2MoO_4) sub-system. Seventeen isoplethal sections (including the (K_2MoO_4 + Na_2Cl_2) and (Na_2MoO_4 + K_2Cl_2) diagonal sections) were measured by Bukhalova and Mateiko [44] using the visual-polythermal method. In each case, a pure salt was added to a common-cation or common-anion binary mixture. The calculated liquidus projection of this system is displayed in Figure 23. In the reciprocal square in this figure, the four apices correspond to the pure salts: NaCl, KCl, Na_2MoO_4, and K_2MoO_4. The compositions are expressed in

terms of cationic and anionic equivalent fractions to ensure that tie-lines are straight lines. The *X*-axis corresponds to the cationic molar ratio $n_K/(n_{Na}+n_K)$ while the *Y*-axis corresponds to the anionic molar ratio $n_{Cl}/(n_{Cl}+2n_{MoO_4})$. A small ternary reciprocal parameter was introduced for the liquid phase (see Table 4). The (NaCl + KCl) common-anion binary sub-system was modeled previously, [19] and the corresponding model parameters were used directly in this work.

As an example, five calculated isoplethal sections are compared to the available measurements in Figures 24 to 28. The remaining twelve isoplethal sections are given in the Supplementary Information (see Figures S5 to S16). In these various figures, the filled circles refer to the original data while the empty circles refer to interpolated liquidus temperatures that were determined from the intersections with other sections. In most cases, these two series of symbols agreed well, and thus no major inconsistency was detected in the reported data of Bukhalova and Mateiko. [44] Overall, agreement between the calculations and the available measurements is satisfactory.

In Figures 24, 26, S5, S6, S9, S10, S15 and S16, a solid-solid miscibility gap, which can be attributed to the (NaCl + KCl) solid solution (cF8), is calculated at low temperatures (below 500°C).

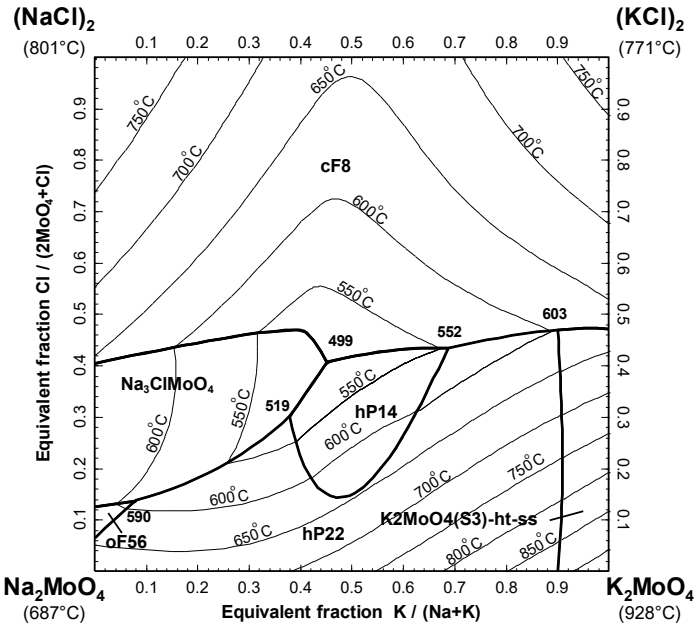

Figure 23 : Calculated liquidus projection of the (NaCl + KCl + Na_2MoO_4 +

K_2MoO_4) system

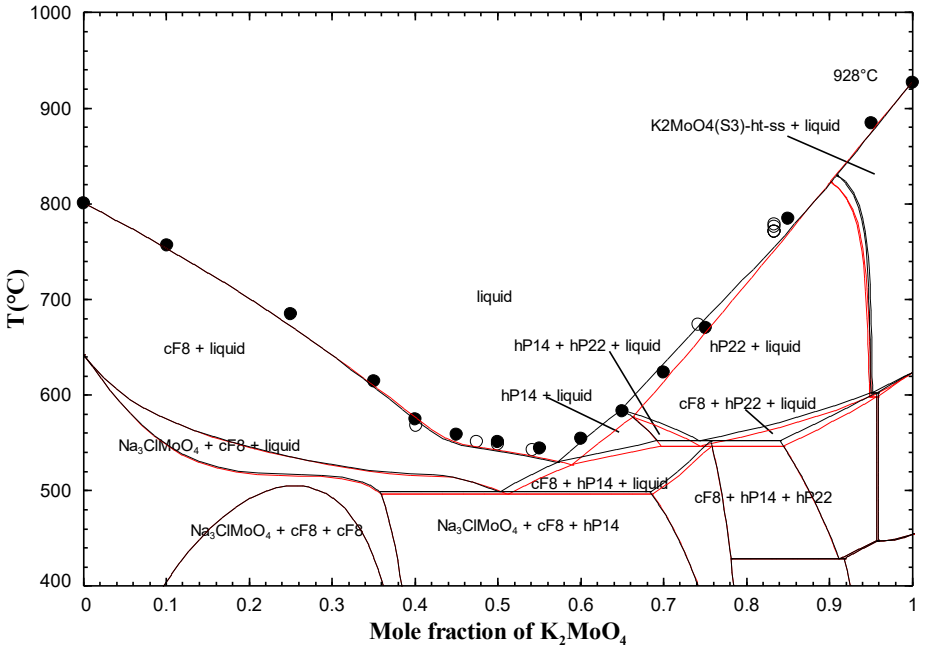

Figure 24: Calculated isoplethal section in the (NaCl + KCl + Na_2MoO_4 + K_2MoO_4) system (Na_2Cl_2-K_2MoO_4). Black lines: final calculations (with one ternary reciprocal parameter); red lines: predictions (without any ternary reciprocal parameter). Experimental data from Bukhalova and Mateiko [44] (●, ○)

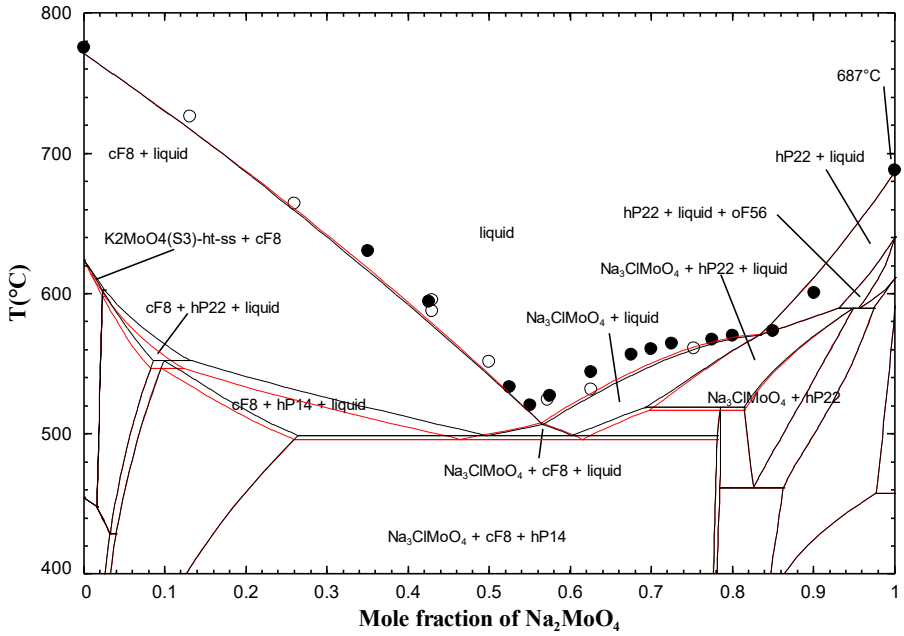

Figure 25 : Calculated isoplethal section in the (NaCl + KCl + Na_2MoO_4 + K_2MoO_4)

system (K_2Cl_2-Na_2MoO_4). Black lines: final calculations (with one ternary reciprocal parameter); red lines: predictions (without any ternary reciprocal parameter). Experimental data from Bukhalova and Mateiko [44] (●, ○)

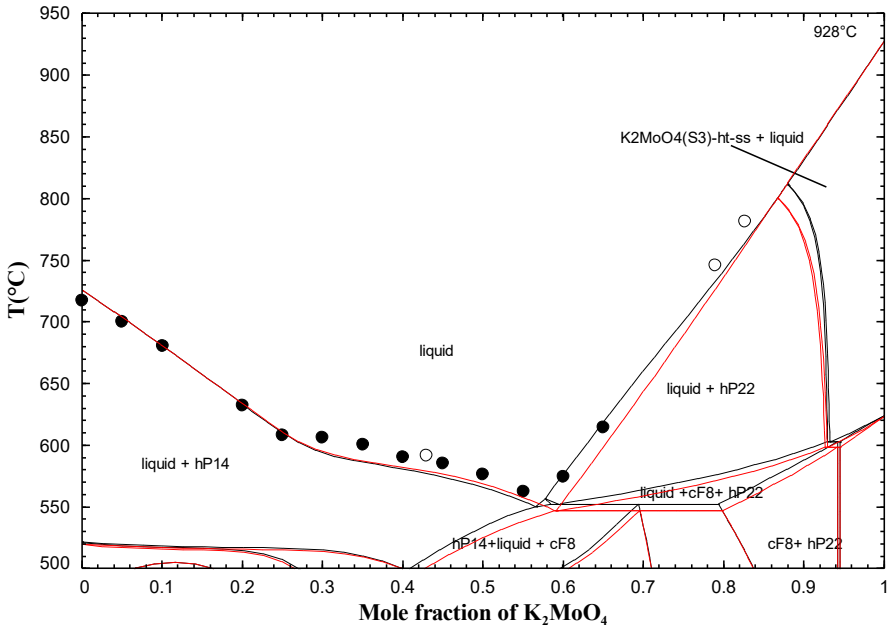

Figure 26 : Calculated isoplethal section in the (NaCl + KCl + Na_2MoO_4 + K_2MoO_4) system ($(Na_2Cl_2)_{0.75}(K_2Cl_2)_{0.25}$-$K_2MoO_4$). Black lines: final calculations (with one ternary reciprocal parameter); red lines: predictions (without any ternary reciprocal parameter). Experimental data from Bukhalova and Mateiko [44] (●, ○)

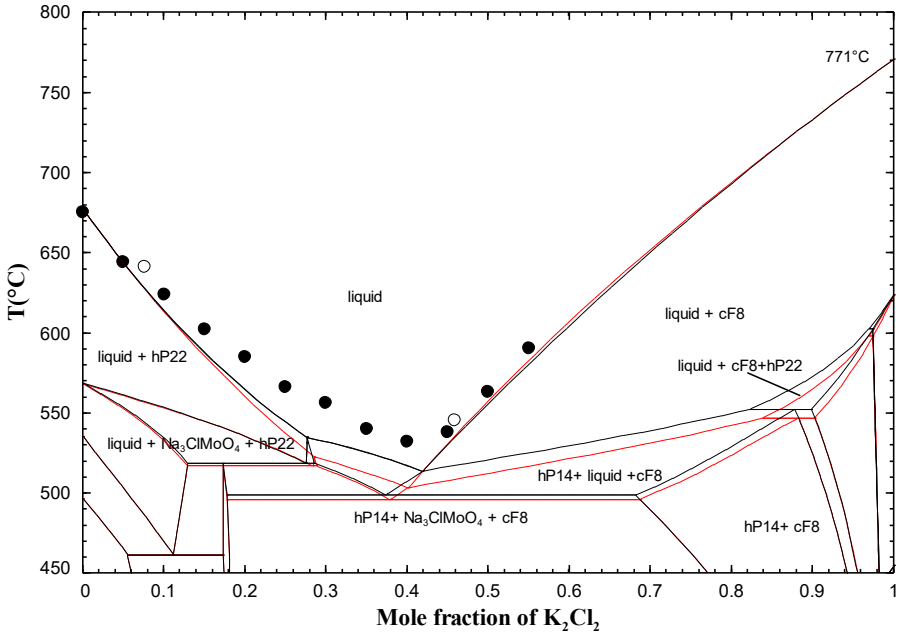

Figure 27: Calculated isoplethal section in the (NaCl + KCl + Na_2MoO_4 + K_2MoO_4) system ($(Na_2MoO_4)_{0.85}(K_2MoO_4)_{0.15}$-$K_2Cl_2$). Black lines: final calculations (with one ternary reciprocal parameter); red lines: predictions (without any ternary reciprocal parameter). Experimental data from Bukhalova and Mateiko [44] (●, ○)

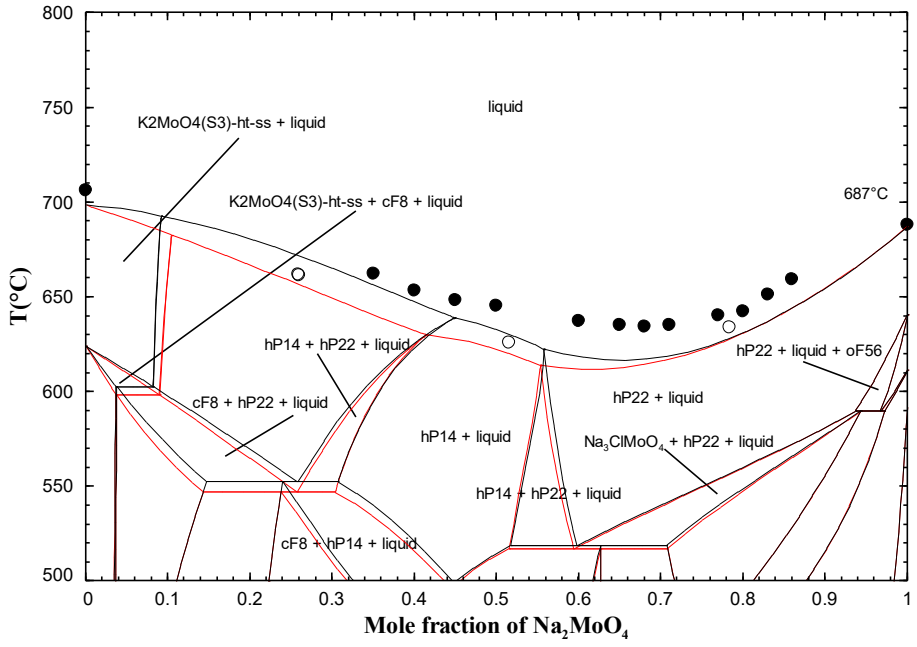

Figure 28 : Calculated isoplethal section in the (NaCl + KCl + Na_2MoO_4 + K_2MoO_4) system ($(K_2Cl_2)_{0.35}(K_2MoO_4)_{0.65}$-$Na_2MoO_4$). Black lines: final calculations (with one

ternary reciprocal parameter); red lines: predictions (without any ternary reciprocal parameter). Experimental data from Bukhalova and Mateiko [44] (●, ○)

9. Multicomponent system ($NaCl + Na_2CO_3 + Na_2SO_4 + Na_2S_2O_7 + Na_2CrO_4 + Na_2Cr_2O_7 + Na_2MoO_4 + Na_2Mo_2O_7 + Na_2O + KCl + K_2CO_3 + K_2SO_4 + K_2S_2O_7 + K_2CrO_4 + K_2Cr_2O_7 + K_2MoO_4 + K_2Mo_2O_7 + K_2O$) (diluted in free oxides)

The MQMQA described in section 3 was used for the liquid phase of the 18-component system (diluted in free oxides). Phase diagram data were very limited for Na_2MoO_4- and K_2MoO_4-containing ternary common-cation sub-systems, ternary reciprocal sub-systems (i.e. systems with Na, K, and two anions) and higher-order sub-systems. Satisfactory predictions were obtained in the ($Na_2SO_4 + Na_2CrO_4 + Na_2MoO_4$) system, whereas one small ternary reciprocal parameter was required for the ($NaCl + KCl + Na_2MoO_4 + K_2MoO_4$) system. In our previous work, [16] satisfactory predictions were obtained in the ($KCl + K_2CO_3 + K_2CrO_4$), ($Na_2CO_3 + Na_2SO_4 + Na_2CrO_4$), ($Na_2SO_4 + K_2SO_4 + Na_2CrO_4 + K_2CrO_4$), and ($NaCl + KCl + Na_2CrO_4 + K_2CrO_4$) systems, while one small ternary excess parameter and three small ternary reciprocal parameters were necessary for the ($K_2CO_3 + K_2SO_4 + K_2CrO_4$) and ($Na_2CO_3 + K_2CO_3 + Na_2CrO_4 + K_2CrO_4$) systems, respectively. For all ternary and ternary reciprocal sub-systems evaluated in the present work and previously, [14-16, 20] no, or only small, ternary or ternary reciprocal excess parameters were necessary to reproduce the available experimental data. Therefore, assuming that ternary or ternary reciprocal excess parameters can be neglected for all ternary and ternary reciprocal sub-systems for which data are lacking is expected to lead to accurate predictions of the 18-component liquid phase (diluted in free oxides).

Various multicomponent solid solutions (hP22, oS28, oP28, hP14, oF56, cF56, $K_2MoO_{4(S3)}$-ht-ss, $Na_2MoO_{4(S2)}$-ss-rich, $K_2Cr_2O_{7(S.S)}$, aP44 and aP22) were modeled in this study and previously [14-16, 20] using the MQMQA for hP22 and the CEF described in section 4 for all other solid solutions. In the present work, experimental phase equilibria involving hP22, hP14 and $K_2MoO_{4(S3)}$-ht-ss were satisfactorily reproduced in the ($Na_2SO_4 + Na_2CrO_4$

+ Na_2MoO_4) and (NaCl + KCl + Na_2MoO_4 + K_2MoO_4) systems without introducing any additional parameters in the models for those solid solutions. Similarly, in our previous work, [16] measured phase equilibria involving hP22, hP14 and oP28 were satisfactorily reproduced in the (Na_2SO_4 + K_2SO_4 + Na_2CrO_4 + K_2CrO_4) and (NaCl + KCl + Na_2CrO_4 + K_2CrO_4) systems without any additional parameters. Therefore, the developed thermodynamic model is expected to predict accurately phase equilibria in the multicomponent system.

10. Conclusions

A thorough critical evaluation of all available phase diagram and thermodynamic data for all condensed phases of the (NaCl + Na_2CO_3 + Na_2SO_4 + $Na_2S_2O_7$ + Na_2CrO_4 + $Na_2Cr_2O_7$ + Na_2MoO_4 + $Na_2Mo_2O_7$ + Na_2O + KCl + K_2CO_3 + K_2SO_4 + $K_2S_2O_7$ + K_2CrO_4 + $K_2Cr_2O_7$ + K_2MoO_4 + $K_2Mo_2O_7$ + K_2O) system was conducted in the present study and previously [14-16], and optimized model parameters were obtained. Since the reactions 2 A_2MO_4 = $A_2M_2O_7$ + A_2O (where A = Na, K and M = Cr, Mo) are very limited up to above the liquidus temperatures, [17] the free oxides were present in the liquid phase in dilute amounts. The present paper describes all molybdate-based and dimolybdate-based sub-systems for which experimental data (mainly phase equilibria) were available. Due to the lack of data, DSC-TGA experiments were performed at several compositions in the common-ion sub-systems (Na_2CO_3 + Na_2MoO_4), (Na_2SO_4 + Na_2MoO_4), (K_2SO_4 + K_2MoO_4), (Na_2CrO_4 + Na_2MoO_4), (K_2CrO_4 + K_2MoO_4), and (Na_2MoO_4 + K_2MoO_4).

No solid solubility was introduced at low temperatures in (Na_2CO_3 + Na_2MoO_4) since our DSC thermal arrests were consistent with solid-solid transitions for the Na_2CO_3 and Na_2MoO_4 pure compounds. In (Na_2SO_4 + Na_2MoO_4), overall our DSC results for Na_2MoO_4-rich compositions agreed with the experimental data from the literature. Owing to the same crystal structure and space group of $Na_2SO_{4(S1)}$ and $Na_2CrO_{4(S1)}$, the (Na_2SO_4 + Na_2MoO_4) and (Na_2CrO_4 + Na_2MoO_4) phase diagrams were modeled simultaneously; two Na_2MoO_4-rich solid solutions ($Na_2MoO_{4(S2)}$-ss-rich and cF56) were introduced at intermediate temperatures. In (Na_2MoO_4 + K_2MoO_4), particular attention was paid to the

molybdenum-glaserite phase (hP14). Mechanical mixtures of the pre-treated reagents and an equilibrated sample (to which an excess of Na_2MoO_4 or K_2MoO_4 was added subsequently) were both studied to best characterize the compositional range of hP14 and its phase boundaries.

The Modified Quasichemical Model in the Quadruplet Approximation (MQMQA) was used to model the liquid solution and the high-temperature hexagonal solid solution hP22, while the Compound Energy Formalism (CEF) was used for all other solid solutions. All experimental data from the literature and from this study were reproduced within experimental error limits.

Using the model parameters obtained for the binary, ternary common-cation and ternary reciprocal sub-systems along with suitable interpolation methods, it is possible, from the MQMQA, to predict accurately the thermodynamic properties of the multicomponent liquid. The developed thermodynamic model is compatible with the FactSage software package [18] and can be used to calculate phase equilibria in the multicomponent system, thus permitting the investigation of high-temperature corrosion, in particular between 600 and 950° C.

Acknowledgements

Ms. Sara Benalia would like to thank the Canada Research Chair in Computational Thermodynamics for High Temperature Sustainable Processes held by Prof. Patrice Chartrand, and the Johan Gadolin Process Chemistry Centre for the 5 month-mobility grant awarded for her stay at Åbo Akademi University (Turku, Finland). The authors would like to thank Mr. Peter Backman and Ms. Jaana Paananen for operating the DSC apparatuses, and Ms. Evguenia Sokolenko for helping locate old articles and for translating them into English.

Supporting information

DSC-TGA measurements for molybdate-based common-ion binary sub-systems, SEM secondary electron images of equilibrated molybdenum-glaserite, and additional calculated isoplethal sections in the (Na_2SO_4 + Na_2CrO_4 + Na_2MoO_4) and (NaCl + KCl + Na_2MoO_4 + K_2MoO_4) systems. This information is available free of charge via the Internet at http://pubs.acs.org/.

References

(1) Eliaz, N.; Shemesh, G.; Latanision, R. Hot corrosion in gas turbine components. *Eng. Fail. Anal.* **2002**, *9*, 31-43.
(2) Stringer, J. High-temperature corrosion of superalloys. *Corros. Sci. Technol.* **1987**, *3*, 482-493.
(3) Nicholls, J. R. Designing oxidation-resistant coatings. *JOM* **2000**, *52*, 28-35. DOI: 10.1007/s11837-000-0112-2.
(4) Benalia, S.; Tesfaye, F.; Lindberg, D.; Sibarani, D.; Hupa, L.; Chartrand, P.; Robelin, C. Critical Evaluation and Calorimetric Study of the Thermodynamic Properties of Na_2CrO_4, K_2CrO_4, Na_2MoO_4, K_2MoO_4, Na_2WO_4, and K_2WO_4. *Revision submitted for publication in J. Phys. Chem. Ref. Data.* **2023**.
(5) Stringer, J. Hot Corrosion of High-Temperature Alloys. *Annu. Rev. Mater. Sci.* **1977**, *7* , 477-509. DOI: 10.1146/annurev.ms.07.080177.002401.
(6) Baxter, L. L.; Miles, T. R.; Miles, T. R.; Jenkins, B. M.; Milne, T.; Dayton, D.; Bryers, R. W.; Oden, L. L. The behavior of inorganic material in biomass-fired power boilers: field and laboratory experiences. *Fuel Process. Technol.* **1998**, *54* , 47-78. DOI: https://doi.org/10.1016/S0378-3820(97)00060-X.
(7) Nielsen, H. P.; Frandsen, F. J.; Dam-Johansen, K.; Baxter, L. L. The implications of chlorine-associated corrosion on the operation of biomass-fired boilers. *Prog. Energy Combust. Sci.* **2000**, *26*, 283-298. DOI: https://doi.org/10.1016/S0360-1285(00)00003-4.
(8) Paneru, M.; Stein-Brzozowska, G.; Maier, J. r.; Scheffknecht, G. n. Corrosion mechanism of alloy 310 austenitic steel beneath NaCl deposit under varying SO_2 concentrations in an oxy-fuel combustion atmosphere. *En. Fuels.* **2013**, *27*, 5699-5705.
(9) Lehmusto, J.; Lindberg, D.; Yrjas, P.; Skrifvars, B.-J.; Hupa, M. Studies on the partial reactions between potassium chloride and metallic chromium concerning corrosion at elevated temperatures. *Oxid. Met.* **2012**, *77*, 129-148.
(10) Fryburg, G.; Kohl, F.; Stearns, C. Chemical Reactions Involved in the Initiation of Hot Corrosion of IN-738. *J. Electrochem. Soc.* **1984**, *131*, 2985-2997.
(11) Fryburg, G. C.; Kohl, F. J.; Stearns, C. A.; Fielder, W. L. Chemical Reactions Involved in the Initiation of Hot Corrosion of B-1900 and NASA-TRW VIA. *J. Electrochem. Soc.* **1982**, *129*, 571-585. DOI: 10.1149/1.2123928.

(12) Misra, A. K. Mechanism of Na_2SO_4-Induced Corrosion of Molybdenum Containing Nickel-Base Superalloys at High Temperatures I. Corrosion in Atmospheres Containing Only. *J. Electrochem. Soc.* **1986**, *133*, 1029-1038.
(13) Peters, K.; Whittle, D.; Stringer, J. Oxidation and hot corrosion of nickel-based alloys containing molybdenum. *Corros. Sci*. **1976**, *16*, 791-804.
(14) Lindberg, D.; Backman, R.; Chartrand, P. Thermodynamic evaluation and optimization of the (Na_2SO_4+ K_2SO_4+ $Na_2S_2O_7$+ $K_2S_2O_7$) system. *J. Chem. Thermodyn.* **2006**, *38*, 1568-1583.
(15) Lindberg, D.; Backman, R.; Chartrand, P. Thermodynamic evaluation and optimization of the (NaCl+ Na_2SO_4+ Na_2CO_3+ KCl+ K_2SO_4+ K_2CO_3) system. *J. Chem. Thermodyn.* **2007**, *39*, 1001-1021.
(16) Benalia, S.; Tesfaye, F.; Lindberg, D.; Hupa, L.; Chartrand, P.; Robelin, C. Thermodynamic Evaluation and Optimization of the (NaCl+Na_2CO_3 + Na_2SO_4 + $Na_2S_2O_7$ + Na_2CrO_4+ $Na_2Cr_2O_7$ + Na_2O+KCl + K_2CO_3 + K_2SO_4 + $K_2S_2O_7$ +K_2CrO_4+$K_2Cr_2O_7$ + K_2O) System Involved in High Temperature Corrosion. *Submitted for publication in J. Therm. Anal. Calorim.* **2023**.
(17) Benalia, S.; Chartrand, P.; Robelin, C. Critical Evaluation of the Thermodynamic Properties of $Na_2Cr_2O_7$, $K_2Cr_2O_7$, $Na_2Mo_2O_7$, $K_2Mo_2O_7$, $Na_2W_2O_7$, and $K_2W_2O_7$. *Revision submitted for publication in J. Phys. Chem. Ref. Data.* **2023**.
(18) Bale, C. W.; Bélisle, E.; Chartrand, P.; Decterov, S. A.; Eriksson, G.; Gheribi, A. E.; Hack, K.; Jung, I. H.; Kang, Y. B.; Melançon, J.; et al. FactSage thermochemical software and databases, 2010–2016. *Calphad* **2016**, *54*, 35-53. DOI: https://doi.org/10.1016/j.calphad.2016.05.002.
(19) Pelton, A. D.; Chartrand, P. Thermodynamic evaluation and optimization of the LiCl-NaCl-KCl-RbCl-CsCl-$MgCl_2$-$CaCl_2$ system using the modified quasi-chemical model. *Metall. Mater. Trans. A* **2001**, *32*, 1361-1383. DOI: 10.1007/s11661-001-0227-2.
(20) Lindberg, D.; Backman, R.; Chartrand, P. Thermodynamic evaluation and optimization of the (Na_2CO_3+ Na_2SO_4+ Na_2S+ K_2CO_3+ K_2SO_4+ K_2S) system. *J. Chem. Thermodyn.* **2007**, *39*, 942-960.
(21) *γ-Na_2CO_3 (Na2[CO3] rt) Crystal Structure: Datasheet from "PAULING FILE Multinaries Edition – 2022" in SpringerMaterials (https://materials.springer.com/isp/crystallographic/docs/sd_2042290)*; Springer-Verlag Berlin Heidelberg & Material Phases Data System (MPDS), Switzerland & National Institute for Materials Science (NIMS), Japan: https://materials.springer.com/isp/crystallographic/docs/sd_2042290 (accessed.
(22) Hall, S. R.; McMahon, B. *International tables for crystallography, definition and exchange of crystallographic data*; Springer: Dordrecht, **2005**, 8, 1-904.
(23) *$Na_2S_2O_7$ (Na2[S2O7]) Crystal Structure: Datasheet from "PAULING FILE Multinaries Edition – 2022" in SpringerMaterials (https://materials.springer.com/isp/crystallographic/docs/sd_1838862)*; Springer-Verlag Berlin Heidelberg & Material Phases Data System (MPDS), Switzerland & National Institute for Materials Science (NIMS), Japan: https://materials.springer.com/isp/crystallographic/docs/sd_1838862 (accessed.
(24) *Na_2CrO_4 (Na2[CrO4] rt) Crystal Structure: Datasheet from "PAULING FILE Multinaries Edition – 2022" in SpringerMaterials (https://materials.springer.com/isp/crystallographic/docs/sd_1001365)*; Springer-Verlag

Berlin Heidelberg & Material Phases Data System (MPDS), Switzerland & National Institute for Materials Science (NIMS), Japan: https://materials.springer.com/isp/crystallographic/docs/sd_1001365 (accessed.
(25) *β-$Na_2Cr_2O_7$ (Na2[Cr2O7] rt) Crystal Structure: Datasheet from "PAULING FILE Multinaries Edition – 2022" in SpringerMaterials (https://materials.springer.com/isp/crystallographic/docs/sd_1401687)*; Springer-Verlag Berlin Heidelberg & Material Phases Data System (MPDS), Switzerland & National Institute for Materials Science (NIMS), Japan: https://materials.springer.com/isp/crystallographic/docs/sd_1401687 (accessed.
(26) *α-$Na_2Cr_2O_7$ (Na2[Cr2O7] ht) Crystal Structure: Datasheet from "PAULING FILE Multinaries Edition – 2022" in SpringerMaterials (https://materials.springer.com/isp/crystallographic/docs/sd_1100126)*; Springer-Verlag Berlin Heidelberg & Material Phases Data System (MPDS), Switzerland & National Institute for Materials Science (NIMS), Japan: https://materials.springer.com/isp/crystallographic/docs/sd_1100126 (accessed.
(27) *K_2CrO_4 (K2[CrO4] tar) Crystal Structure: Datasheet from "PAULING FILE Multinaries Edition – 2022" in SpringerMaterials (https://materials.springer.com/isp/crystallographic/docs/sd_0377606)*; Springer-Verlag Berlin Heidelberg & Material Phases Data System (MPDS), Switzerland & National Institute for Materials Science (NIMS), Japan: https://materials.springer.com/isp/crystallographic/docs/sd_0377606 (accessed.
(28) *$K_2Cr_2O_7$ (K2[Cr2O7] rt) Crystal Structure: Datasheet from "PAULING FILE Multinaries Edition – 2022" in SpringerMaterials (https://materials.springer.com/isp/crystallographic/docs/sd_1322711)*; Springer-Verlag Berlin Heidelberg & Material Phases Data System (MPDS), Switzerland & National Institute for Materials Science (NIMS), Japan: https://materials.springer.com/isp/crystallographic/docs/sd_1322711 (accessed.
(29) *Na_2MoO_4 (Na2[MoO4] rt) Crystal Structure: Datasheet from "PAULING FILE Multinaries Edition – 2022" in SpringerMaterials (https://materials.springer.com/isp/crystallographic/docs/sd_1815021)*; Springer-Verlag Berlin Heidelberg & Material Phases Data System (MPDS), Switzerland & National Institute for Materials Science (NIMS), Japan: https://materials.springer.com/isp/crystallographic/docs/sd_1815021 (accessed.
(30) *$Na_2Mo_2O_7$ rt structural transitions: Datasheet from "PAULING FILE Multinaries Edition – 2022" in SpringerMaterials (https://materials.springer.com/isp/physical-property/docs/ppp_2e7a378246c34f711dc6882c95f111c4)*; Springer-Verlag Berlin Heidelberg & Material Phases Data System (MPDS), Switzerland & National Institute for Materials Science (NIMS), Japan: https://materials.springer.com/isp/physical-property/docs/ppp_2e7a378246c34f711dc6882c95f111c4 (accessed.
(31) *K_2MoO_4 (K2[MoO4] rt) Crystal Structure: Datasheet from "PAULING FILE Multinaries Edition – 2022" in SpringerMaterials (https://materials.springer.com/isp/crystallographic/docs/sd_1220174)*; Springer-Verlag Berlin Heidelberg & Material Phases Data System (MPDS), Switzerland & National Institute for Materials Science (NIMS), Japan: https://materials.springer.com/isp/crystallographic/docs/sd_1220174 (accessed.

(32) *$K_2Mo_2O_7$ Crystal Structure: Datasheet from "PAULING FILE Multinaries Edition – 2022" in SpringerMaterials (https://materials.springer.com/isp/crystallographic/docs/sd_1610363)*; Springer-Verlag Berlin Heidelberg & Material Phases Data System (MPDS), Switzerland & National Institute for Materials Science (NIMS), Japan: https://materials.springer.com/isp/crystallographic/docs/sd_1610363 (accessed.
(33) Pelton, A. D.; Chartrand, P.; Eriksson, G. The modified quasi-chemical model: Part IV. Two-sublattice quadruplet approximation. *Metall. Mater. Trans. A* **2001**, *32*, 1409-1416.
(34) Pelton, A. D.; Chartrand, P. The modified quasi-chemical model: Part II. Multicomponent solutions. *Metall. Mater. Trans. A* **2001**, *32*, 1355-1360.
(35) Lambotte, G.; Chartrand, P. Thermodynamic optimization of the (Na_2O + SiO_2 + NaF + SiF_4) reciprocal system using the Modified Quasichemical Model in the Quadruplet Approximation. *J. Chem. Thermodyn.* **2011**, *43*, 1678-1699. DOI: 10.1016/j.jct.2011.05.038.
(36) Sundman, B.; Ågren, J. A regular solution model for phases with several components and sublattices, suitable for computer applications. *J. Phys. Chem. Solids* **1981**, *42*, 297-301.
(37) Hillert, M.; Jansson, B.; Sundman, B. Application of the Compound-Energy Model to Oxide Systems. *J. Mater. Res.* **1988**, *79*, 81-87. DOI: doi:10.1515/ijmr-1988-790203.
(38) Hillert, M. The compound energy formalism. *J. Alloys Compd.* **2001**, *320*, 161-176. DOI: https://doi.org/10.1016/S0925-8388(00)01481-X.
(39) Jin, L.; Lindberg, D.; Tsuchiyama, Y.; Robelin, C. A thermodynamic model for high temperature corrosion applications: The (Na_2SO_4 + K_2SO_4 + $ZnSO_4$ + $PbSO_4$) system. *Chem. Eng. Sci.* **2022**, *260*, 117847. DOI: https://doi.org/10.1016/j.ces.2022.117847.
(40) Fábry, J.; Petricek, V.; Vanek, P.; Cisarova, I. Phase transition in $K_3Na(MoO_4)_2$ and determination of the twinned structures of $K_3Na(MoO_4)_2$ and $K_{2.5}Na_{1.5}(MoO_4)_2$ at room temperature. *Acta Cryst. B.* **1997**, *53*, 596-603.
(41) Temkin, M. Mixtures of fused salts as ionic solutions. *Acta Physicochim. URSS* **1945**, *20*, 411.
(42) Sangster, J. M.; Pelton, A. D. Phase diagrams and thermodynamic properties of the 70 binary alkali halide systems having common ions. *J. Phys. Chem. Ref. Data.* **1987**, *16*, 509-561.
(43) Rycerz, L. Practical remarks concerning phase diagrams determination on the basis of differential scanning calorimetry measurements. *J. Therm. Anal. Calorim.* **2013**, *113*, 231-238. DOI: 10.1007/s10973-013-3097-0.
(44) Bukhalova, G. A.; Mateiko, Z. A. Complex formation and solid solutions in the adiagonal reciprocal system of the molybdates and chlorides of sodium and potassium. *Zh. Obshch. Khim.* **1955**, *25*, 851-857.
(45) Shurdumov, G. K.; Khakulov, Z. L.; Mokhosoev, M. V.; Kodzokov, K. A.; El'mesova, R. M. Thermal analysis, density, and molar volumes of melts of binary systems of sodium and potassium molybdates, tungstates, and carbonates. *Zh. Neorg. Khim.* **1984**, *29*, 2096-2101.
(46) Boeke, H. E. Die Mischkristalle von wasserfreiem Natrium-Sulfat,-Molybdat und -Wolframat. *Z. Anorg. Allg. Chem.* **1906**, *50*, 355.

(47) Belyaev, I. N.; Doroshenko, A. K. Exchange decomposition in the reciprocal system of sodium and silver sulfate and molybdate. *Zh. Obshch. Khim.* **1954**, *24*, 427-432.
(48) Mateiko, Z. A.; Bukhalova, G. A. Solid solutions in the systems: (1) Na||SO_4, CrO_4, MoO_4; (2) Na||SO_4, CrO_4, WO_4; (3) Na||SO_4, MoO_4, WO_4; (4) Na||CrO_4, MoO_4, WO_4. *Zh. Neorg. Khim.* **1959**, *4*, 2329-2334.
(49) Simoes, M. C.; Hughes, K. J.; Ingham, D. B.; Ma, L.; Pourkashanian, M. Estimation of the Thermochemical Radii and Ionic Volumes of Complex Ions. *Inorg. Chem.* **2017**, *56*, 7566-7573. DOI: 10.1021/acs.inorgchem.7b01205.
(50) Amadori, M. The Neutral Behavior of Alkaline Sulfates, Chromates, Molybdates and Tungstates at Low and High Temperatures. II. *Atti Accad. Lincei, Rend. Sci. Fis. Mat. Nat.* **1913**, *22*, 453-459.
(51) Bergman, A. G.; Kislova, A. I.; Korobka, E. I. The ternary adiagonal-belt type reciprocal system of sulfates and molybdates of lithium and potassium. *Zh. Neorg. Khim*. **1954**, *24*, 1127-1135.
(52) Mateiko, Z. A.; Bukhalova, G. A. Quaternary system K_2SO_4-K_2CrO_4-K_2MoO_4-K_2WO_4. *Zh. Neorg. Khim*. **1960**, *5*, 2071-2075.
(53) Belyaev, I. N.; Sholokhovich, M. L. Complex formation and exchange decomposition in the reciprocal system of the pyrophosphates and molybdates of sodium and potassium. *Zh. Obshch. Khim.* **1953**, *23*, 1265-1273.
(54) Amadori, M. Sulle capacità dei sali sodici e potassici di dare composti e cristalli misti. *Atti Accad. Lincei, Rend. Sci. Fis. Mat. Nat.* **1913**, *72*, 903-932.
(55) Ding, Y.; Hou, N.; Chen, N.; Xia, Y. Phase diagrams of Li_2MoO_4-Na_2MoO_4 and Na_2MoO_4-K_2MoO_4 systems. *Rare Met.* **2006**, *25*, 316-320. DOI: https://doi.org/10.1016/S1001-0521(06)60060-0.
(56) Eysel, W. CRYSTAL-CHEMISTRY OF SYSTEM Na_2SO_4-K_2SO_4-K_2CrO_4-Na_2CrO_4 AND OF GLASERITE PHASE. *Am. Mineral.* **1973**, *58*, 736-747.
(57) Chartrand, P.; Pelton, A. D. A predictive thermodynamic model for the Al-NaF-AlF_3-CaF_2-Al_2O_3 system. *Light Met. (Warrendale, PA, U. S.)* **2002**, 245-252.
(58) Saal, J. E.; Kirklin, S.; Aykol, M.; Meredig, B.; Wolverton, C. Materials Design and Discovery with High-Throughput Density Functional Theory: The Open Quantum Materials Database (OQMD). *TMS.* **2013**, *65*, 1501-1509. DOI: 10.1007/s11837-013-0755-4.
(59) Kirklin, S.; Saal, J. E.; Meredig, B.; Thompson, A.; Doak, J. W.; Aykol, M.; Rühl, S.; Wolverton, C. The Open Quantum Materials Database (OQMD): assessing the accuracy of DFT formation energies. *npj Comput. Mater.* **2015**, *1*, 15010. DOI: 10.1038/npjcompumats.2015.10.
(60) Jain, A.; Ong, S. P.; Hautier, G.; Chen, W.; Richards, W. D.; Dacek, S.; Cholia, S.; Gunter, D.; Skinner, D.; Ceder, G.; et al. Commentary: The Materials Project: A materials genome approach to accelerating materials innovation. *APL Mater.* **2013**, *1*, 011002. DOI: 10.1063/1.4812323.
(61) Shannon, R. D. Revised effective ionic radii and systematic studies of interatomic distances in halides and chalcogenides. *Acta Cryst. A.* **1976**, *32*, 751-767.
(62) Amadori, M. The Relative Behavior of Alkali Sulfates, Chromates, Molybdates and Tungstates at High and Low Temperatures. III. *Atti Accad. Lincei, Rend. Sci. Fis. Mat. Nat.* **1913**, *22*, 609-616.

(63) Groschuff, E. Über Wasserfreie Molybdate I. *Z. Anorg. Allg. Chem.* **1908**, *58*, 113-119. DOI: https://doi.org/10.1002/zaac.19080580112.
(64) Hoermann, F. Molybdates and tungstates. Binary systems: Li_2MoO_4-MoO_3, Na_2MoO_4-MoO_3, K_2MoO_4-MoO_3, Li_2WO_4-WO_3, Na_2WO_4-WO_3, K_2WO_4-WO_3, Li_2MoO_4-Na_2MoO_4, Li_2WO_4-Na_2WO_4, Li_2MoO_4-K_2MoO_4. *Z. Anorg. Allg. Chem.* **1928**, *177*, 145-186, 10.1002/zaac.19291770117. DOI: 10.1002/zaac.19291770117.
(65) Caillet, P. Anhydrous sodium or potassium polymolybdates and polytungstates. *Bull. Soc. Chim. Fr.* **1967**, (12), 4750-4755.
(66) Fedorov, P. I.; Mokhosoev, M. V. Reaction of sodium carbonate with disodium ditungstate and dimolybdate. *Zh. Neorg. Khim.* **1961**, *6*, 123-124.
(67) Amadori, M. Analisi termica dei polimolibdati e poliwolframati di potassio. *Atti Accad. Lincei, Rend. Sci. Fis. Mat. Nat.* **1913**, *72*, 893-902.

TOC Graphic (For table of contents only)